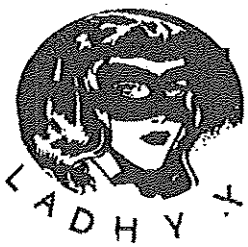

Ecole Polytechnique
Laboratoire d'Hydrodynamique

THÈSE

présentée pour obtenir
le grade de Docteur de l'Ecole Polytechnique
Spécialité: Mécanique

par

Stéphane LE DIZÈS

Sujet de la thèse :

Modes globaux dans les écoulements faiblement inhomogènes

Soutenue le **2 Mars 1994** devant le jury composé de :

J. -M. Chomaz	
D. G. Crighton	Rapporteur
J. -P. Guiraud	Président, rapporteur
P. Huerre	
P. A. Monkewitz	
J. E. Wesfreid	

REMERCIEMENTS

Le travail qui constitue cette thèse a été effectué dans les laboratoires d'Hydrodynamique du Department of Mechanical Engineering de UCLA et de l'Ecole Polytechnique.

J'ai été encadré lors de la période à Los Angeles par Peter Monkewitz. Je lui suis reconnaissant du merveilleux accueil qu'il m'a réservé, et de l'aide chaleureuse qu'il n'a pas cessé de m'apporter tout au long de mon séjour. Sa compétence scientifique et sa grande disponibilité m'ont beaucoup servi. Je l'en remercie.

Je tiens à remercier aussi les autres membres de l'équipe pour leur soutien permanent, et plus particulièrement Michael Pesenson pour toutes les références bibliographiques utiles qu'il m'a gentiment données. Je n'oublie pas non plus Jérôme, Lionel, Ramin et Thilo avec qui j'ai partagé mes loisirs, et qui ont contribué à rendre ce séjour agréable.

Patrick Huerre et Jean Marc Chomaz ont dirigé au LadHyX la deuxième période de ma thèse. J'ai beaucoup apprécié leur dynamisme, leur éternelle bonne humeur et la façon avec laquelle ils m'ont fait partager leurs expériences scientifiques. Je les remercie pour leurs conseils et le soutien constant qu'ils m'ont apporté lors de l'élaboration de ce travail, mais aussi pour tout le temps qu'ils ont consacré à "rendre lisible" une bonne partie de ce document.

J'aimerais remercier tous les autres membres du LadHyX, permanents et passagers, pour n'avoir jamais hésité à me rendre service et pour avoir contribuer à rendre l'ambiance de ce laboratoire si chaleureuse. J'ai une pensée particulière pour Olivier Pouliquen qui en tant que compagnon de bureau a du supporter mes hauts

et mes bas et me remonter le moral à de nombreuses reprises en acceptant de “parler vacances”. Merci aussi à Maurice Rossi pour avoir consacré plusieurs après-midi à écouter mes “paradoxes”.

Je tiens à remercier aussi tous mes proches que j'ai délaissés pendant la difficile période de la rédaction, Fabienne, pour m'avoir continuellement aidé et soutenu, sa famille et la mienne pour leur patience et leur compréhension.

Je remercie Jean Pierre Guiraud et David Crighton pour l'intérêt qu'ils ont manifesté pour mon travail en acceptant d'en être les rapporteurs, et Eduardo Wesfreid et Peter Monkewitz pour avoir bien voulu participer au jury de cette thèse. Je suis de plus très reconnaissant à David Crighton et Peter Monkewitz de s'être déplacé de si loin pour assister à la soutenance.

J'aimerais finir ces remerciements en rappelant les soutiens financiers que j'ai reçu tout au long de cette thèse. La SNECMA a permis d'initialiser ce travail en finançant mon Service National à Los Angeles. La Navy (ONR # N00014-90-J-1313) a apporté un complément qui a été fort apprecié lors des virées dans les Rocheuses. Enfin, les ministères de l'Education Nationale et de la Recherche m'ont accordé un salaire pendant ma période à l'ENS et cette dernière année en tant qu'AMN.

Table des matières

Chapitre 0

INTRODUCTION

L'expérience de tous les jours montre que les gaz et les liquides que l'on côtoie, évoluent de manière variée et désordonnée dans le temps et l'espace. Les études sur la *turbulence* s'attachent à décrire et à comprendre cette complexité. Deux types d'approches se distinguent nettement.

La première étudie le désordre d'un point de vue statistique et permet d'obtenir des caractéristiques moyennes globales. Elle nécessite souvent des hypothèses d'homogénéité et d'isotropie, ce qui la rend plus particulièrement adaptée à l'étude de la *turbulence développée*. Elle ne nous concernera pas dans cette thèse.

La seconde approche interprète la turbulence dans le cadre de la théorie des systèmes dynamiques comme une forme de *chaos déterministe*. Elle s'intéresse principalement à la naissance du désordre ou autrement dit, à la *transition vers la turbulence*. Elle essaye de distinguer les premiers mécanismes d'instabilité générateurs de désordre, et de décrire aussi loin que possible les *bifurcations* successives que subit le système lorsque la contrainte extérieure est augmentée. Cette approche a permis de décrire avec succès l'apparition du désordre temporel dans des *systèmes fermés* de petites tailles, tels que la convection de Rayleigh-Bénard et l'écoulement de Couette (voir Bergé *et al.* 1984). En considérant les mêmes systèmes dans une configuration plus étendue (convection dans une longue boîte, par exemple), elle a

permis d'apprécier le rôle joué par la dimension spatiale et de mettre en évidence la multiplicité des transitions possibles vers le désordre spatio-temporel (voir Manneville 1991). Elle a en revanche donné nettement moins de résultats pour les *systèmes ouverts* parmi lesquels on trouve la majorité des écoulements de fluide. Ces derniers se distinguent d'une part par le fait que les particules entrent et sortent du domaine de fluide considéré, d'autre part parce qu'ils sont généralement inhomogènes dans la direction de l'écoulement. Sous l'hypothèse WKBJ de faible inhomogénéité, une analyse linéaire d'instabilité locale peut être menée. Elle permet de savoir si après application d'une impulsion locale, les perturbations ont tendance à quitter la source impulsionnelle (*instabilité convective*), ou à croître sur place (*instabilité absolue*). Les écoulements ouverts faiblement non-parallèles peuvent ainsi être distingués par le caractère absolu ou convectif des instabilités locales (voir Huerre & Monkewitz 1990). On constate en particulier que les écoulements convectivement instables tels que les couches limites et les couches de mélange n'ont généralement pas une dynamique qui leur est propre: ils se comportent en amplificateur du bruit extérieur.

En revanche, certains écoulements absolument instables ont une dynamique intrinsèque peu sensible au bruit extérieur, ce qui les rend très proches des systèmes fermés. L'écoulement de sillage derrière un cylindre est l'exemple le plus typique. Lorsque le nombre de Reynolds dépasse la valeur critique de 45, l'écoulement laminaire stationnaire (figure 0.1a) devient *globalement* instable, et évolue vers un régime oscillatoire caractérisé par l'apparition de l'allée tourbillonnaire de Bénard-Kármán (figure 0.1b). La très faible sensibilité au bruit extérieur de la fréquence d'oscillation et de la structure spatiale de l'allée, a permis d'envisager une étude de cet écoulement dans le cadre de la théorie des systèmes dynamiques. La bifurcation globale vers le régime oscillatoire a pu ainsi être expérimentalement identifiée comme étant du type Hopf (Mathis *et al.* 1984).

FIG. 0.1 - *Sillage derrière un cylindre dans un écoulement d'huile; (a): $Re = 32$, Ecoulement laminaire, (b): $Re = 65$, Ecoulement oscillatoire. (D'après Homann 1936, tiré de Batchelor 1967).*

La modélisation théorique d'une telle transition dans un écoulement cisaillé ouvert constitue le sujet de cette thèse. L'objectif principal est de relier sous l'hypothèse WKBJ le comportement global observé aux propriétés d'instabilité locale de l'écoulement de base sous-jacent. Dans les deux premiers chapitres, les perturbations globales sont décrites à l'aide d'une équation **unidimensionnelle** de type Ginzburg-Landau avec des coefficients lentement variables. On suppose ainsi que la structure transverse des perturbations est passive dans le mécanisme de déstabilisation globale.

Le but du premier chapitre est de déterminer le mécanisme **linéaire** de sélection de fréquence du mode oscillatoire. On cherche à exprimer la fréquence du **mode global** en fonction des caractéristiques locales d'instabilité de l'écoulement, et en particulier à relier l'apparition d'un mode global instable à la présence d'une région absolument instable.

Dans le second chapitre, les modes globaux linéaires sont étudiés dans le régime non linéaire. Les conditions pour que l'évolution **faiblement non linéaire** du mode global soit régie par l'équation de Landau décrivant la bifurcation de Hopf sont obtenues. Elles sont analysées pour un mode global particulier, et interprétées à partir des caractéristiques d'instabilité locale dans un cas précis.

Le troisième chapitre est consacré à l'étude de la structure transverse des modes globaux, et plus généralement des ondes localement planes, dans les écoulements cisaillés faiblement non parallèles. Les inhomogénéités spatiales visqueuses générées par l'hypothèse WKBJ sont analysées. Nous caractérisons l'apparition des couches critiques visqueuses et des régions visqueuses, et nous donnons l'approximation de l'onde plane dans chacune de ces régions. Ce chapitre, bien qu'étant indépendant, permet de justifier dans une certaine mesure l'approche unidimensionnelle utilisée dans les deux premiers chapitres.

Nous concluons dans le dernier chapitre en résumant l'ensemble des résultats obtenus et en proposant de nouvelles études.

Chapitre 1

LINEAR GLOBAL MODES IN SPATIALLY-DEVELOPING MEDIA

Stéphane Le Dizès[#], Patrick Huerre[#], Jean Marc Chomaz[#], Peter A. Monkewitz[*]

[#] Laboratoire d'Hydrodynamique (LadHyX), Ecole polytechnique,
F-91128 Palaiseau cedex, France.

[*]Département de Mécanique, IMHEF,
Ecole Polytechnique Fédérale de Lausanne, ME-Ecublens,
CH-1015 Lausanne, Switzerland.

Submitted to the *Philosophical Transactions A of the Royal Society of London.*

October 1993

Abstract

Selection criteria for self-excited global modes in doubly infinite one-dimensional domains are examined in the context of the linearized Ginzburg-Landau equation with slowly varying coefficients. Following Lynn & Keller (1970), uniformly valid approximations are sought in the complex plane in a region containing all relevant turning points. A mapping transformation is introduced to reduce the original Ginzburg-Landau equation to an exactly solvable comparison equation which qualitatively preserves the geometry of the Stokes line network. The specific case of two turning points with counted multiplicity is analysed in detail, particular attention being paid to the allowable configurations of the Stokes line network. It is shown that all global modes are either of type 1, with two simple turning points connected by a common Stokes line, or of type 2, with a single double turning point. Explicit approximations are derived in both instances, for the global frequencies and associated eigenfunctions. It is argued, on geometrical grounds, that type 1 global modes may, in principle be more unstable than type 2 global modes. This paper is a continuation and extension of the earlier study of Chomaz, Huerre & Redekopp (1991) where only type 2 global modes were investigated via a local WKBJ approximation scheme.

1.1 Introduction

Several classes of spatially developing shear flows are known to exhibit, under certain flow conditions, self-sustained oscillations : the near field large scale dynamics become effectively tuned at a specific intrinsic frequency, the associated spatio-temporal distribution of fluctuations defining a **global mode** of the flow. The main objective of the present study is the systematic derivation of global frequency selection criteria in the context of the linearised Ginzburg-Landau model equation with varying coefficients. It should be viewed as a continuation and extension of the analysis presented in Chomaz, Huerre & Redekopp (1991) for the same model problem.

Some of the underlying physical motivation and key stability concepts are now briefly recalled. The reader is referred to the recent surveys by Huerre & Monkewitz (1990) and Monkewitz (1990) for extensive discussions on theoretical and experimental aspects of global mode evolution in shear flows. The onset of the Kármán vortex street in the flow behind a bluff cylindrical body probably constitutes the primary example of transition to a global mode régime : as the Reynolds number exceeds a critical value, the wake develops limit cycle oscillations that arise via a Hopf bifurcation, as documented extensively by Mathis, Provansal & Boyer (1984), Hannemann & Oertel (1989), Karniadakis & Triantafyllou (1989) and Strykowski & Sreenivasan (1990) among others. Current research on wake flow stability is compiled in a book of proceedings by Eckelmann, Graham, Huerre & Monkewitz (1993). As shown in the experiments of Sreenivasan, Raghu & Kyle (1989) and Monkewitz, Bechert, Lehmann & Barsikow (1990), a similar phenomenon takes place in the near field region of jets, when the jet density is gradually decreased below that of the surrounding medium. Beyond a critical density ratio, the evolution of vortical structures becomes highly repeatable in the first few diameters downstream and frequency spectra collapse into discrete peaks as one would expect in the presence of a global mode.

As a last example, one should mention the ingenious experiments of Strykowski & Niccum (1991) which conclusively demonstrate the existence of global modes in counterflow mixing layers for sufficiently high velocity ratios. The occurrence of intrinsic oscillations therefore appears to be ubiquitous in many spatially-developing shear flows.

From a stability point of view, the most elementary approach consists in entirely neglecting the spatial development of the medium : if the basic flow is assumed to be uniform in the propagation direction, the stability properties of normal modes $exp\{(i(kx - \omega t)\}$ are completely described by a dispersion relation $D[k, \omega] = 0$ between wavenumber k and frequency ω. The ability of perturbations to grow in time at the source, in response to a localized impulse, is characterized by the absolute growth rate $\omega_{0,i} \equiv \Im m\ \omega_0$, where the complex absolute frequency $\omega_0 \equiv \omega(k_0)$ is defined by the usual group velocity condition $\frac{d\omega}{dk}(k_0) = 0$. If $\omega_{0,i} < 0$, any temporally amplified perturbation leaves its source and the medium is said to be convectively unstable. If $\omega_{0,i} > 0$, there exist perturbations that will grow in situ at the source and the medium is said to be absolutely unstable. A more comprehensive account of these concepts may be found for instance in Bers (1983) as well as in the previously quoted survey articles.

Most basic flows of interest are spatially non uniform in the propagation direction x as a result of viscous diffusion or boundary effects. The previous notions can then be taken to apply locally in x, as long as the nonuniformities of the medium are small over a typical wavelength of the instability. Thus the non parallelism of the flow is characterized by a slow space scale $X = \varepsilon x$, where ε is a small parameter of the same order of magnitude as the scaled nonuniformities. Decomposition into local normal modes leads to a dispersion relation of the form

$$D[k, \omega; X] = 0 \quad . \tag{1.1}$$

The flow is then defined to be **locally** stable, convectively unstable or absolutely

unstable at a given station X in the same manner as for the uniform case. The entire medium is therefore partitioned into differents domains, according to the local nature of the instability. One can then attempt to establish a link between the experimentally observed global response of the flow and the calculated streamwise distribution of local stability properties, in particular the extent of different regions of convective and absolute instability. Such an approach has effectively been implemented for several classes of spatially developing flows, among them wakes (Koch 1985, Monkewitz 1988, Hannemann & Oertel 1989, Schär & Smith 1993), low-density jets (Monkewitz & Sohn 1988, Monkewitz *et al.* 1990) and counterflow mixing layers (Strykowski & Niccum 1991). In all three cases, there are ranges of control parameter, i.e. Reynolds number, density or velocity ratio, in which the basic state is convectively unstable everywhere. Such flows are known to behave primarily as spatial amplifiers of external noise : if forcing is turned-off they return to the basic state and are therefore globally stable. In other parameter ranges, global intrinsic oscillations are found to develop concurrently with the appearance of a sufficiently large pocket of local absolute instability.

In order to introduce global model concepts, dispersion relation (1.1) is formally rewritten in physical space as a partial differential equation

$$D(-i\frac{\partial}{\partial x}, i\frac{\partial}{\partial t}; X)\Psi(x,t;\varepsilon) = 0 \quad , \tag{1.2}$$

for the perturbation field $\Psi(x,t;\varepsilon)$. Following Huerre & Monkewitz (1990) and Chomaz *et al.* (1991), a global mode is then defined as a solution of (1.2) which is temporally harmonic of complex frequency ω_g and satisfies, say exponential decay conditions at $X = \pm\infty$. Upon making the substitution $i\dfrac{\partial}{\partial t} \rightarrow \omega_g$ in (1.2), the determination of global modes is effectively reduced to an eigenvalue problem in the propagation direction X. Our present understanding of the global mode problem has often relied on the study of the Ginzburg-Landau equation with varying coefficients as a simple model for the operator D in (1.2). Global instability concepts appear to

have first been introduced by Drazin (1974a) for a particular version of the linearized Ginzburg-Landau equation containing no advection term and with purely real coefficients. The model therefore exhibited reflectional symmetry and attention was restricted to real turning point configurations. In the purely one-dimensional context, Chomaz, Huerre & Redekopp (1988) demonstrated at an early stage, through a combined analytical and numerical approach, that a necessary condition for global instability is the existence of a region of local absolute instability of finite extent. Hunt (1993) has further shown that this condition is indeed not sufficient : for an ad-hoc Ginzburg-Landau model, the basic state can be made absolutely unstable everywhere while the medium remains globally stable. Following the seminal studies of Gent (1974), Gent & Leach (1976), Soward & Jones (1983), Pierrehumbert (1984) and Koch (1985), Chomaz *et al.* (1991) investigated global frequency selection on the Ginzburg-Landau model on a doubly infinite domain. As in the present case, the primary objective was the derivation of a criterion expressing the global frequencies ω_g solely in terms of the properties of the local dispersion relation (1.1). The global mode structure along the propagation direction was sought in the form of WKBJ expansions satisfying appropriate exponential decay conditions at $X = +\infty$ and $X = -\infty$ respectively. The ability to construct an analytic eigenfunction with such prescribed WKBJ expansions led to definite constraints on the configuration of Stokes lines associated with each turning point in the complex X plane. Thus, it was possible to prove, albeit incompletely as we shall see, that global growth rates $\omega_{g,i} \equiv \Im m\ \omega_g$ cannot exceed the maximum absolute growth rate $\omega_{0,i}^{max}$ on the real X axis. A convectively unstable medium is therefore necessarily globally stable. Furthermore, under specific assumptions regarding the nature of the turning points and the properties of the complex function $\omega_0(X)$, the WKBJ approximations near $X = +\infty$ and $X = -\infty$ could be matched to an inner turning point solution for only a discrete collection of global frequencies ω_{g_n}. At leading order in ε, all global

frequencies were found to be determined by the value $\omega_s \equiv \omega_0(X_s)$ of the absolute frequency at the saddle point X_s such that $\dfrac{d\omega_0}{dX}(X_s) = 0$. Hunt & Crighton (1991) have recently devised an elegant procedure to calculate exactly the Green function of the Ginzburg-Landau equation with varying coefficients. For quadratic variations of $\omega_0(X)$, the long-time behavior of the Green function is shown to reduce to the most unstable global mode of leading-order global mode frequency ω_s. This result fully confirms that the frequency selection criterion of Chomaz *et al.* (1991) is indeed causal and naturally emerges from the impulse response.

It should be emphasized that several real fluid flow configurations have already been analysed from the global mode point of view : the Kelvin-Helmholtz instability of a vortex sheet of varying strength in the spanwise direction (Drazin 1974b), the Taylor vortex problem between two eccentric rotating cylinders (DiPrima & Stuart 1972) or between two concentric spheres (Soward & Jones 1983), baroclinic instabilities in geophysical flows (Gent 1974, Gent & Leach 1976, Pierrehumbert 1984, Bar-Sever & Merkine 1988), unsteady viscous flow in a curved pipe (Papageorghiou 1987), thin-disc dynamo models (Soward 1992) and most recently spatially-developing shear flows (Monkewitz, Huerre & Chomaz 1993). In this regard, the combined experimental and theoretical study of Gent & Leach (1976) strikingly demonstrated that global modes can be observed in baroclinically unstable flow in an eccentrically mounted differentially heated rotating annulus. The present study is further motivated by the fact that, in many of these investigations, the Ginzburg-Landau model with varying coefficients rationally arises as the leading-order governing equation in the turning point region.

The primary goal of this work is to examine anew the global frequency selection criterion derived in Chomaz *et al.*, by resorting to a different formulation, namely the method of uniform approximations. This approach, which has been introduced and developed by Langer (1949), Mc Kelvey (1955), Lynn & Keller (1970) and Anyanwu

& Keller (1975) among others, relies on the following idea : one seeks to determine approximations to the global mode structure that remain uniformly valid in the entire domain of interest including all relevant turning points as well as the boundaries $X = \pm\infty$. Through an appropriate transformation applied to the dependent and independent variables, the original problem is reduced to a so-called comparison equation that can be solved exactly. All the art of the method resides in the careful selection of a mapping which preserves the topological properties of the initial Stokes line network. The global frequencies are directly obtained from the known solutions of the comparison equation, and the associated spatial eigenfunctions are expressed in terms of a single uniformly-valid approximation.

The paper is organised in the following manner. The global mode problem for the Ginzburg-Landau model is stated in section 1.2, together with essential definitions and properties of turning points and Stokes lines. In order for a global mode to exist, the corresponding Stokes line network should be restricted to specific configurations as demonstrated in section 1.3. Unfortunately these necessary conditions only lead to exclude a small set Δ_o of Stokes lines from consideration. The general method of uniform approximations in the version proposed by Lynn & Keller (1970) is outlined in section 1.4 for an arbitrary number of turning points. The bulk of the study is presented in section 1.5 for the specific case of two turning points. The properties of the transformation leading to the comparison equation are first analysed in detail. In particular, it is argued in section 1.5.2 that the Stokes sectors containing $X = +\infty$ and $X = -\infty$ respectively cannot be contiguous for large $|X|$ if ω is to give rise to a global frequency. Upon solving the comparison equation in the mapped domain, global modes are then shown (sections 1.5.3 and 1.5.4) to fall within only two classes : type 1 modes correspond to two simple turning points connected by a Stokes line and type 2 modes to a double turning point. The resulting extended frequency selection criteria are discussed and interpreted geometrically in section 1.5.5. In closing, we

summarize the main conclusions of the study and compare them with available numerical and experimental evidence.

1.2 Basic formulation

As in Chomaz *et al.* (1991), complex scalar fluctuations $\Psi(x,t)$ around a given basic state are assumed to be governed by the linearised Ginzburg-Landau equation

$$\left[i\frac{\partial}{\partial t}+\frac{1}{2}\omega_{kk}(X)\frac{\partial^2}{\partial x^2}-i\omega_{kk}(X)k_0(X)\frac{\partial}{\partial x}-(\frac{1}{2}\omega_{kk}(X)k_0^2(X)+\omega_0(X))\right]\Psi(x,t;\varepsilon)=0, \tag{1.3}$$

where the independent variables t and x designate time and the propagation direction, respectively. To mimic the nonparallel nature of spatially developing flows, the properties of the underlying basic state are assumed to be functions of a slow space variable $X=\varepsilon x$, where ε is a small parameter characterizing the inhomogeneities of the medium. The complex analytic functions $\omega_{kk}(X)$, $k_0(X)$ and $\omega_0(X)$ appearing in (1.3) fully specify the nature of the local dispersion relation at each station X, as discussed below following equation (1.7).

The Ginzburg-Landau equation with constant coefficients is ubiquitous in numerous analytical studies of hydrodynamic instabilities close to threshold. It is also one of the simplest generic models for the study of pattern formation in nonlinear systems, as recently reviewed by Newell *et al.* (1993). In fact, this model arises frequently in the literature on quantum mechanics (Pokrovskii & Khalatnikov 1961) to describe bound states in potential-well problems and it is well established that immersion in the complex plane is necessary to correctly handle terms that are exponentially small with respect to each other. In the present context, it can be argued that equation (1.3) displays the minimum structure necessary for the existence of a global mode on the infinite interval, namely two spatial branches $k^+(X;\omega)$ and $k^-(X;\omega)$ [see equation (1.8)]. Finally the presence of a first-order space derivative in (1.3) ensures that the local reflection symmetry $x\to -x$ has been broken, as in

most open flow configurations with a dominant advection direction.

Model equation (1.3) being invariant under arbitrary time translations $t \to t + const.$, it is legitimate to seek solutions of the form

$$\Psi(x,t;\varepsilon) = \psi(X;\omega,\varepsilon)e^{-i\omega t} \quad , \tag{1.4}$$

where ω is a complex frequency. The spatial distribution function $\psi(X;\omega,\varepsilon)$ is then governed by the second-order differential equation

$$\left[\omega + \frac{1}{2}\omega_{kk}(X)\frac{\partial^2}{\partial x^2} - i\omega_{kk}(X)k_0(X)\frac{\partial}{\partial x} - (\frac{1}{2}\omega_{kk}(X)k_0^2(X) + \omega_0(X))\right]\psi(X;\omega,\varepsilon) = 0. \tag{1.5}$$

The assumed time-harmonic fluctuation (1.4) defines a global mode solution if $\psi(X;\omega,\varepsilon)$ satisfies (1.5) subject to the boundary conditions

$$\lim_{X\to\pm\infty}\psi = 0 \quad . \tag{1.6}$$

This typically constitutes an eigenvalue problem whereby solutions are obtained only for specific complex eigenvalues, i.e. global frequencies ω_g, and associated eigenfunctions $\psi(X;\omega_g,\varepsilon)$. It is expected that, for arbitrary initial conditions, only the most unstable global mode with the largest growth rate $\omega_{g,i}$ will prevail for large time. The main objective of the present study is then the prediction of the most unstable global frequency and associated spatial distribution as given from linear stability analysis.

The local dispersion relation associated with equation (1.3) is readily derived by performing the substitutions $\dfrac{\partial}{\partial x} \to ik$, $\dfrac{\partial}{\partial t} \to -i\omega$. One obtains a single **temporal mode** given by

$$\omega = \omega_0(X) + \frac{\omega_{kk}(X)}{2}(k - k_0(X))^2 \quad . \tag{1.7}$$

The frequency ω is seen to be a simple quadratic function of wavenumber k. The form of (1.3) in physical space simply reflects the nature of the local dispersion relation in Fourier space. Note in particular that $k = k_0(X)$ satisfies $\dfrac{\partial\omega}{\partial k}(k,X) = 0$. As shown

in the next section, $k_0(X)$ is indeed the local absolute wavenumber and $\omega_0(X)$ the corresponding local absolute frequency. In order to enforce causality, we shall assume throughout that sufficiently large wavenumbers are damped, i.e. $\omega_{kk,i}(X) < 0$ for all X real, and that $\omega_{kk}(X)$ is nonzero in the entire complex X plane.

As seen from (1.7), there exist for each value of the frequency ω two local **spatial branches** given by

$$k^{\pm}(X;\omega) = k_0(X) \pm \sqrt{2\frac{\omega - \omega_0(X)}{\omega_{kk}(X)}} \quad , \tag{1.8}$$

where it is understood that a specific choice has been made for the branch cut of the square root, for instance the principal value.

In the case of a slowly varying medium, $\varepsilon \ll 1$, it is possible to directly relate the global solutions of (1.5)-(1.6) to the local dispersion relation (1.7) by means of WKBJ approximations. It is well established (see, for instance Bender & Orszag 1978, or Wasow 1985) that, at each point distinct from a turning point, the two WKBJ approximations $A^{\pm}(X;\omega,\varepsilon)e^{\frac{i}{\varepsilon}\int^X k^{\pm}(s;\omega)ds}$ are asymptotic representations when $\varepsilon \to 0$ of two independent solutions of (1.5). The amplitudes $A^{\pm}(X;\omega,\varepsilon)$ may be expanded in powers of ε and each successive term computed recursively. The global mode of frequency ω_g is then locally approximated in different regions of the complex X plane by either $A^{+}(X;\omega_g,\varepsilon)e^{\frac{i}{\varepsilon}\int^X k^{+}(s;\omega_g)ds}$ or $A^{-}(X;\omega_g,\varepsilon)e^{\frac{i}{\varepsilon}\int^X k^{-}(s;\omega_g)ds}$. We recall that a given approximation is said to be subdominant (respectively dominant) when it is exponentially small (respectively large) with respect to the other approximation. Furthermore, WKBJ approximations usually break down in the neighborhood of turning points in the complex X plane which, for each frequency ω, are defined by the relation

$$k^{+}(X;\omega) = k^{-}(X;\omega) \quad . \tag{1.9}$$

Equivalently, according to (1.8), turning points are given, for each ω, by the roots

of

$$\omega_0(X) = \omega \quad . \tag{1.10}$$

In other words, there is a direct relationship, via the transformation $\omega \mapsto X = \omega_0^{-1}(\omega)$, between the frequency ω and the location of the turning points in the complex X plane. The order m of a given turning point is, by definition, equal to the multiplicity of the corresponding root of (1.9) or (1.10). Thus, a simple turning point ($m = 1$) is a simple root of (1.10). Similarly a double turning point ($m = 2$) corresponds to a double root of (1.10) such that $\dfrac{d\omega_0}{dX} = 0$.

It is important to summarize some of the standard results pertaining to the behavior of WKBJ approximations in the vicinity of turning points. The reader is referred to Bender & Orszag (1978) for a more comprehensive presentation in a general context and to Chomaz *et al.* (1991) for more details concerning the present Ginzburg-Landau model. To each turning point X_1, one may associate a specific network of Stokes lines issuing from it and defined by

$$\Im m \left\{ \int_{X_1}^{X} [k^+(s;\omega) - k^-(s;\omega)] ds \right\} = 0 \quad , \tag{1.11}$$

equivalently, according to (1.8),

$$\Im m \left\{ \int_{X_1}^{X} \sqrt{2 \frac{\omega - \omega_0(s)}{\omega_{kk}(s)}} ds \right\} = 0 \quad . \tag{1.12}$$

The above definition implies that both WKBJ approximations become of equal order of magnitude on Stokes lines. In general, a given WKBJ approximation may change from subdominant to dominant or vice-versa as successive Stokes lines are crossed on a closed curve encircling the turning point X_1. It can readily be demonstrated that $m + 2$ Stokes lines radiate from a turning point of order m, the angle between consecutive Stokes lines at X_1 being $2\pi/(m+2)$. Thus it can be concluded that turning points and Stokes lines form a network which partitions the complex X plane into sectors as illustrated on figure 1.1. It is generally impossible to obtain

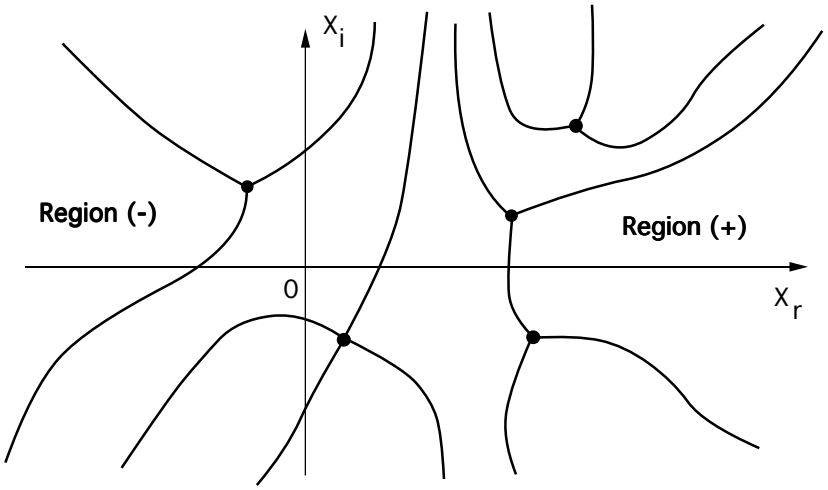

FIG. 1.1 - *Illustrative sketch of typical Stokes line network.*

a uniformly valid WKBJ approximation to a solution in a domain that is larger than a single sector delimited by consecutive Stokes lines. However there is an important exception : when a solution is asymptotic to a WKBJ approximation that is subdominant in one sector, that same approximation remains valid in the neighboring sectors where it is then dominant (Bender & Orszag 1978; Wasow 1985). In other words, a WKBJ approximation remains valid beyond the Stokes lines defining the subdominant region. This interesting property yields necessary conditions to be satisfied by the Stokes line network of a global mode, as shown by Chomaz *et al.* (1991). These conditions are examined in the next section.

1.3 Necessary conditions for the existence of global modes

It is convenient to introduce a few definitions pertaining to dispersion relation (1.7). Since we have assumed $\omega_{kk,i}(X) < 0$ for all X real, the local temporal growth rate $\omega_i(k;X)$ admits at each location X a finite maximum $\omega_i^{max}(X)$ over all real wavenumbers given by

$$\omega_i^{max}(X) \equiv \max_{k\ real} \omega_i(k;X) = \omega_{0,i}(X) - \frac{|\omega_{kk}(X)|^2}{2\omega_{kk,i}(X)} k_{0,i}^2(X) \quad . \tag{1.13}$$

As seen by inspection of (1.13), the local maximum growth rate $\omega_i^{max}(X)$ is necessarily larger than $\omega_{0,i}(X)$ at the same location :

$$\omega_{0,i}(X) \leq \omega_i^{max}(X) \quad . \tag{1.14}$$

Furthermore, let $\omega_{i,max}^{max}$ and $\omega_{0,i}^{max}$ denote the respective maxima of $\omega_i^{max}(X)$ and $\omega_{0,i}(X)$ over all X real, and $\omega_i^{max}(\infty)$ be the larger of the two limiting values taken by $\omega_i^{max}(X)$ at $X = +\infty$ and $X = -\infty$. By construction, the following inequalities hold :

$$\omega_i^{max}(\infty) \leq \omega_{i,max}^{max} \ ; \qquad \omega_{0,i}^{max} \leq \omega_{i,max}^{max} \quad .$$

According to the above definitions, when $\omega_i > \omega_{i,max}^{max}$, there is no solution ω of the dispersion relation with k real for all X real. In other words, when $\omega_i > \omega_{i,max}^{max}$, the two spatial branches $k^+(X;\omega)$ and $k^-(X;\omega)$ cannot cross the k_r axis for all X real (figure 1.2a,b). This necessarily means that the branches k^+ and k^- are either located on the same side of the k_r axis (figure 1.2a) or on opposite sides (figure 1.2b). As ω_i decreases within the range $\omega_i^{max}(\infty) < \omega_i < \omega_{i,max}^{max}$, the relative positions of $k^+(X;\omega)$ and $k^-(X;\omega)$ with respect to the real k axis are unchanged for $|X|$ sufficiently large as sketched on figures 1.2c,d. Configurations of the type shown on figures 1.2a and 1.2c are clearly not admissible : both WKBJ approximations are exponentially decaying at $X = -\infty$, as required by the boundary conditions (1.6),

but they grow exponentially at $X = \infty$. It can therefore be concluded that, **in order to obtain global solutions of growth rate larger than $\omega_i^{max}(\infty)$, the spatial branches $k^+(X;\omega)$ and $k^-(X;\omega)$ should necessarily be located on opposite sides of the k_r axis, at least for $|X|$ sufficiently large**, as illustrated on figures 1.2b and 1.2d. Note that in such a case, $k_0(X)$ is the colliding point of both branches k^+ and k^- located on opposite sides of the k_r axis for $\omega_i > \omega_{i,max}$: $k_0(X)$ is truly the local absolute wavenumber and $\omega_0(X) \equiv \omega(k_0(X);X)$ the corresponding local absolute frequency as defined in Bers (1983).

The above result has important consequences regarding the nature of the Stokes line network associated with equation (1.5). It implies that Stokes lines cannot be asymptotic to the X_r axis when $\omega_i > \omega_i^{max}(\infty)$. If they were, it would require, according to definition (1.11), that $\Im m[k^+(X;\omega) - k^-(X;\omega)] \to 0$, as $X \to \pm\infty$, but this situation has just been excluded in the previous paragraph (see also figure 1.2), which proves the statement. Since Stokes lines are not asymptotic to X_r, **regions $(+)$ and $(-)$ delimited by Stokes lines and containing the X_r axis near $+\infty$ and $-\infty$ (see figure 1.1) are unambiguously defined for any $\omega_i \geq \omega_i^{max}(\infty)$.** Furthermore, regions $(+)$ and $(-)$ cannot flip from one side of a Stokes line to the other for large $|X|$ as long as $\omega_i > \omega_i^{max}(\infty)$.

The allowable configurations of spatial branches sketched on figures 1.2b,d also imply the following property: when $\omega_i \geq \omega_i^{max}(\infty)$, one spatial branch is necessarily amplified for sufficiently large $|X|$ along the X_r axis while the other branch is damped, i.e. subdominant. Thus, in order to enforce the boundary conditions at infinity, **a global mode must be represented by subdominant WKBJ approximations in both regions $(+)$ and $(-)$.**

Since the subdominant WKBJ approximation in, say, region $(-)$ becomes dominant as a Stokes line delimiting region $(-)$ is crossed, we immediately deduce that **regions $(+)$ and $(-)$ cannot be contiguous if a global mode solution is to**

be obtained. For instance, in the single first-order turning point geometry depicted on figure 1.3, regions (+) and (−) are always neighbors and no global modes can be found. By contrast, when two simple turning points are present there exist Stokes line configurations that definitely cannot sustain a global mode, as in figure 1.4a, and others that may sustain one, as in figures 1.4b,c,d.

The Stokes line network evolves from one configuration to another as ω varies. We shall assume that the number of turning points (with counted multiplicity) remains constant in the process. The frequencies that can be excluded from consideration on the basis of the above necessary condition then constitute a set Δ_o in the complex ω plane which can be succinctly analysed. In the case of one simple turning point, we have concluded that no global modes can be found so that Δ_o coincides with the entire ω plane. In the case of two simple turning points $X_1(\omega)$ and $X_2(\omega)$, or one double turning point X_s, the set Δ_o corresponds to ω values such that a Stokes line connects $X_1(\omega)$ and $X_2(\omega)$ and separates (+) and (−) regions as in figure 1.4a. The ensemble Δ_o is then a subset of a larger set Δ defined by the single condition that $X_1(\omega)$ and $X_2(\omega)$ are connected by a Stokes line. For future reference, we call Δ_1 the complement of Δ_o in Δ. The set Δ_1 corresponds to ω values such that the Stokes line network is as illustrated on figures 1.4c,d. According to definition (1.11) for the Stokes lines, the set Δ is defined by

$$f(\omega) \equiv \Im m \left\{ \int_{X_1(\omega)}^{X_2(\omega)} [k^+(s;\omega) - k^-(s;\omega)] ds \right\} = 0 \quad . \tag{1.15}$$

The vanishing of the functional $f(\omega)$ is exceptional : it generally defines Δ as a curve or set of curves in the complex ω plane. The subset Δ_o of Δ is then even smaller. As the number of turning points increases, the dimension of Δ_o decreases since additional conditions of type (1.15) have to be enforced. In fact, the measure of Δ_o becomes zero as soon as the number of turning points exceeds two : the necessary condition based on the argument that (+) and (−) regions cannot be contiguous then becomes hopelessly inefficient in excluding regions of the complex ω plane as

possible global frequencies.

The above reasoning solely relies on the use of **local** WKBJ approximations to represent the spatial distribution of the eigenmodes and to derive necessary existence conditions. The **global** structure of the Stokes line network in the complex X plane is not incorporated in these local approximations. Such an approach is clearly adequate to reach a conclusion as long the local behavior around a single turning point provides information regarding the global behavior of the solution for all X. This is effectively the case for the single turning point configuration of figure 1.3 and the two-turning-point configuration of figure 1.4a. In both instances, $(+)$ and $(-)$ regions are connected through a single turning point and the behavior of the solutions in each of these regions is directly related to the local WKBJ approximations around only that turning point. The necessary condition for the existence of a global mode is then identical to that of a function that must be analytic at the turning point with given local subdominant WKBJ approximations in regions $(+)$ and $(-)$. Such a simple reasoning fails for other configurations, such as those in figure 1.4d, when it is necessary to relate several local WKBJ approximations pertaining to distant turning-points $X_1(\omega)$ and $X_2(\omega)$. The local analysis is even more problematic for general Stokes line networks of the kind displayed in figure 1.1 and involving many turning points.

In order to deal with distant-turning-point configurations, we prefer to resort to another method based on the derivation of approximations that are uniformly valid in a much wider domain containing all turning points and associated Stokes lines between region $(+)$ and $(-)$. The main steps of this approach are introduced in the next section.

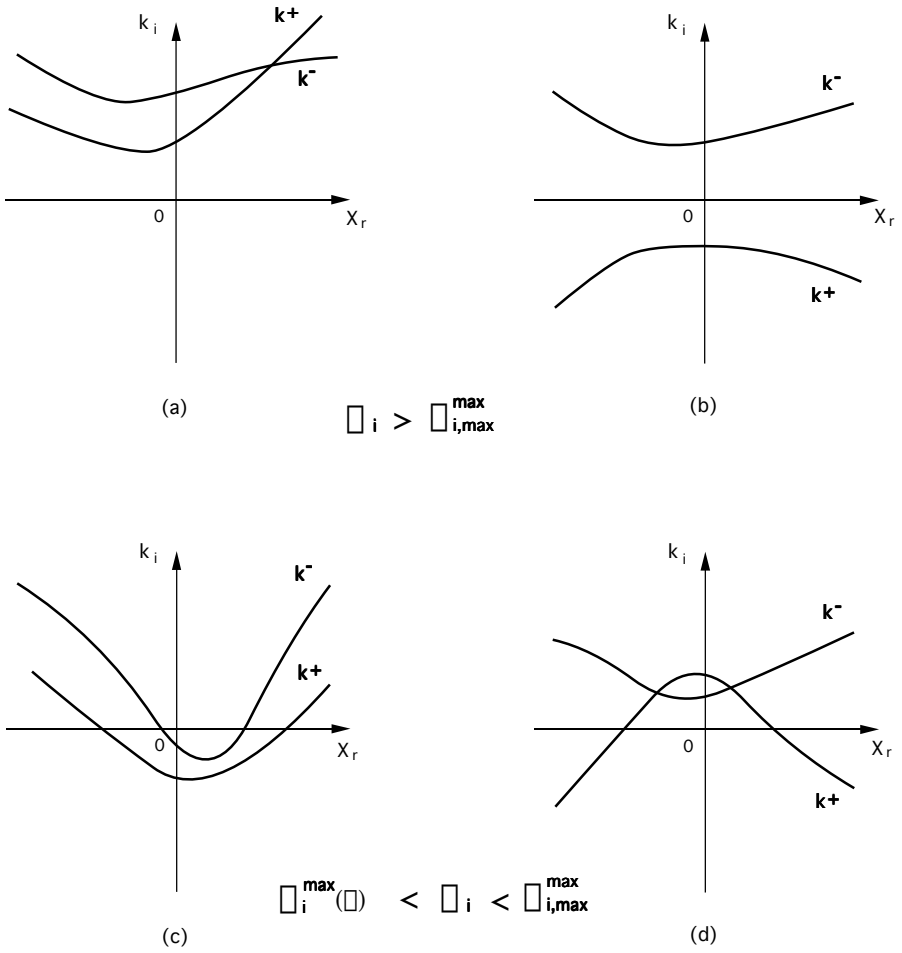

FIG. 1.2 - *Imaginary part of the spatial branches $k^+(X;\omega)$ and $k^-(X;\omega)$ versus the real location X_r at a fixed complex value of ω. (a) and (b) : $\omega_i > \omega_{i,max}^{max}$, both branches have an imaginary part of constant sign for all X_r; (c) and (d) : $\omega_i^{max}(\infty) < \omega_i < \omega_{i,max}^{max}$, both branches have an imaginary part of constant sign for $|X_r|$ sufficiently large. As shown in the text, the only permissible configurations are those sketched in (b) and (d).*

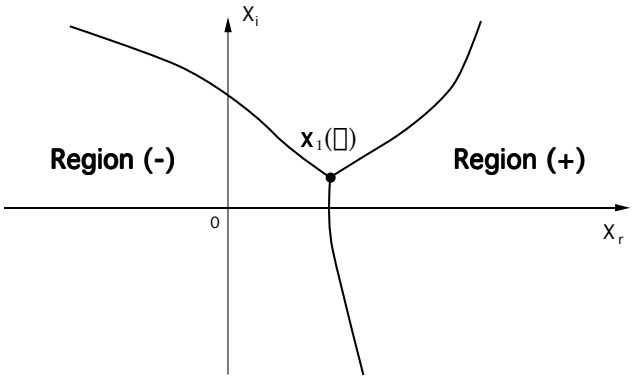

FIG. 1.3 - *Stokes line network with a single first-order turning point. No global modes.*

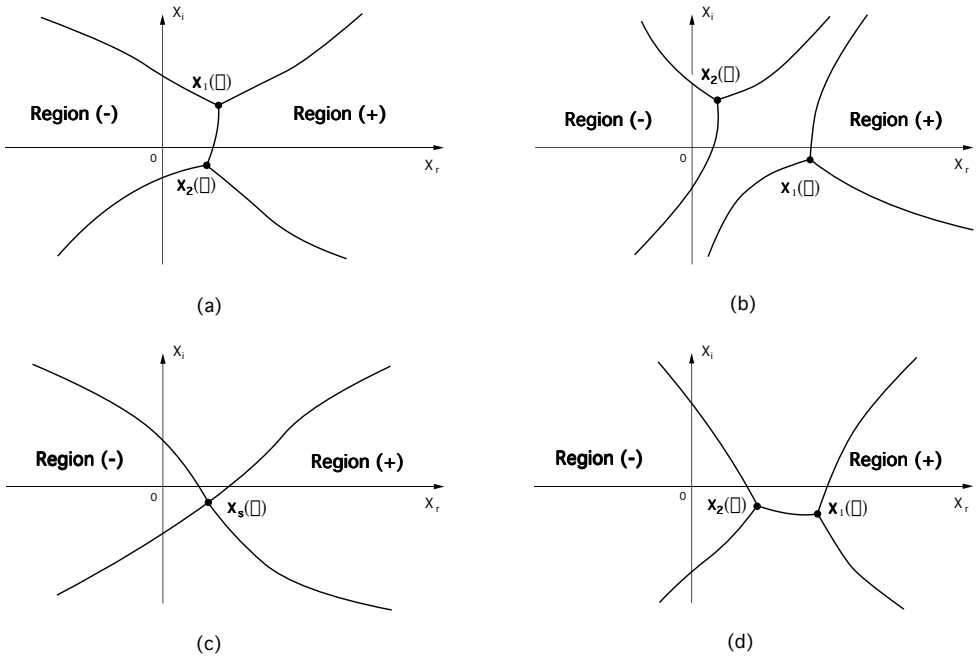

FIG. 1.4 - *Typical Stokes line networks with two turning points. (a) : two simple turning points; no global modes. (b) : two simple turning points ; global mode a-priori possible. (c) : one double turning point; global mode a-priori possible. (d) : two simple turning points; global mode a-priori possible.*

1.4 General methodology

The principle of the method of uniform approximations was first outlined by Langer (1949). Subsequent developments and refinements have been introduced by many authors including Mc Kelvey (1955) and Lynn & Keller (1970) among others. We shall follows the general treatment of Lynn & Keller (1970) for a class of second-order differential equations with μ turning points.

Under the change of dependent variable

$$\psi(X;\omega,\varepsilon) = \phi(X;\omega,\varepsilon) e^{\frac{i}{\varepsilon}\int_{X_0}^{X} k_0(s)ds} \quad , \; X_0 \; arbitrary \; constant \quad , \tag{1.16}$$

equation (1.5) is transformed into the normalized equation for ϕ

$$\varepsilon^2 \frac{\partial^2 \phi}{\partial X^2} + (R_0(X;\omega) + \varepsilon R_1(X))\phi = 0 \quad , \tag{1.17}$$

where the varying coefficients $R_0(X;\omega)$ and $R_1(X)$ introduced by Lynn & Keller (1970) take the particular form

$$R_0(X;\omega) = [k^+(X;\omega) - k^-(X;\omega)]^2 = 2\frac{\omega - \omega_0(X)}{\omega_{kk}(X)} \quad , \tag{1.18a}$$

$$R_1(X) = ik_{0X}(X) \quad . \tag{1.18b}$$

A uniform approximation to the solutions of (1.17) is given by equation (LK 1.3) of Lynn & Keller (1970). In terms of the original dependent variable ψ, this uniform approximation reduces to

$$\begin{aligned} \psi(X;\omega,\varepsilon) = \Big\{ & B(X;\omega,\varepsilon) V\left[\tfrac{\eta(X;\omega)}{\varepsilon^{2/(\mu+2)}}\right] \\ & + \varepsilon^{\mu/(\mu+2)} C(X;\omega,\varepsilon) V'\left[\tfrac{\eta(X;\omega)}{\varepsilon^{2/(\mu+2)}}\right] \Big\} e^{\frac{i}{\varepsilon}\int_{X_0}^{X} k_0(s)ds} \quad . \end{aligned} \tag{1.19}$$

The functions $B(X;\omega,\varepsilon)$ and $C(X;\omega,\varepsilon)$ admit the following expansions in powers of ε, as $\varepsilon \to 0$:

$$B(X;\omega,\varepsilon) = \sum_{l=0}^{\infty} B_l(X;\omega)\varepsilon^l \quad ; \tag{1.20a}$$

$$C(X;\omega,\varepsilon) = \sum_{l=0}^{\infty} C_l(X;\omega)\varepsilon^l \quad . \tag{1.20b}$$

Turning points of (1.17) correspond to zeroes of $R_0(X;\omega)$ given by (1.18a), i.e. to roots of (1.9) or equivalently (1.10), as discussed in section 1.2.

When μ turning points with counted multiplicity are present, the function $V(\xi)$ appearing in (1.19) satisfies the so-called comparison equation

$$V''(\xi) + (\sum_{m=0}^{\mu} \gamma_m(\omega,\varepsilon)\xi^m)V(\xi) = 0 \quad , \tag{1.21}$$

where the $(\mu+1)$ coefficients $\gamma_m(\omega,\varepsilon)$ admit expansions in powers of ε given by

$$\gamma_m(\omega,\varepsilon) = \varepsilon^{2(m-\mu)/(\mu+2)} \sum_{p=0}^{\infty} \gamma_{m_p}(\omega)\varepsilon^p \quad . \tag{1.22}$$

Note that only $(\mu-1)$ of the $(\mu+1)$ parameters γ_m are independent. For instance $\gamma_1(\omega,\varepsilon)$ and $\gamma_2(\omega,\varepsilon)$ can be assigned arbitrary values.

The conformal mapping

$$X \mapsto \eta(X;\omega)/\varepsilon^{2/(\mu+2)} \tag{1.23}$$

is chosen so as to transform the normalized equation (1.17) into the comparison equation (1.21) at leading order in ε. It is found to satisfy

$$\int_{\eta_0}^{\eta(X;\omega)} \sqrt{\sum_{m=0}^{\mu} \gamma_{m_0}(\omega)s^m}ds = \int_{X_0}^{X} \sqrt{R_0(r;\omega)}dr \quad , \tag{1.24}$$

where the arbitrarily chosen constant η_0 defines the image of X_0 under the mapping. Once the $\mu+1$ coefficients $\gamma_{m_0}(\omega)$ have been determined, the above equation implicitly defines the change of independent variable $X \mapsto \eta(X;\omega)$. Note that, according to (1.24), turning points of the original equation (1.17), given by $R_0(X;\omega) = 0$, equivalently $\omega_0(X) = \omega$, are mapped into turning points of comparison equation (1.21) given by $\sum_{m=0}^{\mu} \gamma_{m_0}(\omega)\eta^m = 0$. Furthermore, Stokes line networks issuing from each turning point in the X plane are mapped into Stokes line networks of the corresponding image turning point in the η plane. The branches of the square roots

appearing in (1.24) may be specified arbitrarily, provided that the branch cuts of the right-hand side and left-hand side square roots are mapped into each other.

The reader is referred to Lynn & Keller (1970) for a comprehensive discussion of the recursive algorithm leading to the determination of the coefficients $\gamma_{m_p}(\omega)$ and the functions $B_l(X;\omega)$ and $C_l(X;\omega)$. In the present study, we are only interested in turning points that directly influence the structure of the global mode on the real line, i.e. those with Stokes lines crossing the X_r axis. In this case, approximation (1.19) is known to be uniformly valid in a domain of the complex X plane containing these μ turning points.

There remains to specify the eigenvalue problem to be solved in the transformed η plane. Boundary conditions on $V[\eta(X;\omega)/\varepsilon^{2/(\mu+2)}]$ have to be applied in regions $\eta(+;\omega)$ and $\eta(-;\omega)$ which are the images of regions $(+)$ and $(-)$ under the mapping $X \mapsto \eta(X;\omega)$. The properties of WKBJ approximations near infinity derived in section 1.3 can be transposed from the X plane into the η plane. Recall first that, among the two branches $k^+(X;\omega)$ and $k^-(X;\omega)$ defined in (1.8), one has necessarily an imaginary part positive and the other negative as $X \to \pm\infty$. In view of relation (1.18a), $\Im m\ \sqrt{R_0(X;\omega)} = \Im m[k^+(X;\omega) - k^-(X;\omega)]$, and this behavior implies that $\Im m\ \sqrt{R_0(X;\omega)}$ does not tend to zero as $X \to \pm\infty$. Consequently, the integral on the right-hand side of (1.24) is necessarily divergent when $X \to \pm\infty$, which guarantees that $|\eta(X;\omega)| \to \infty$ as $X \to \pm\infty$. Thus, **points at infinity in the $(+)$ and $(-)$ regions are mapped into points at infinity in the $\eta(+;\omega)$ and $\eta(-;\omega)$ regions**.

According to the form of equation (1.21), two solutions $V(\xi)$ can be chosen exponentially increasing and decreasing respectively near infinity in the $\eta(+;\omega)$ and $\eta(-;\omega)$ regions. When such solutions are substituted into approximation (1.19), they have necessarily the same behaviors near $X = \infty$ as the WKBJ approximations built with the spatial branches k^+ and k^- exhibit effectively both behaviors. It follows

that the exponential factor $exp\{\frac{i}{\varepsilon}\int_{X_0}^{X} k_0(s)ds\}$ does not alter the growing or decaying nature of the solutions near infinity. It can therefore be concluded that the original eigenvalue problem is mapped into a new eigenvalue problem in the η plane whereby $V(\xi)$ **should satisfy comparison equation (1.21) and be exponentially small in regions** $\eta(+;\omega)$ **and** $\eta(-;\omega)$ **as** $|\eta| \to \infty$. This is a necessary and sufficient condition for the existence of global modes.

It should be stressed that global modes on the real X axis do not automatically map into eigenfunctions of the comparison equation for V on the **real** η axis. The regions $\eta(+;\omega)$ and $\eta(-;\omega)$ do not always contain the real η axis as $|\eta|$ tends to infinity. It is therefore essential to accurately locate the $\eta(+;\omega)$ and $\eta(-;\omega)$ domains before proceeding to a formal solution of the problem. Otherwise incorrect results might be obtained (see subsection 1.5.2 for details).

It is generally difficult to implement the method of uniform approximations when more than two turning points are involved. The solutions of the comparison equation (1.21) are then not well documented although some partial results have been derived in particular situations (Sibuya 1975). In the next section the above formulation is applied to the determination of all global modes when two turning points with counted multiplicity (two simple turning points or one double turning point) are present.

1.5 Global modes with two turning points

It is assumed that only two simple turning points $X_1(\omega)$ and $X_2(\omega)$, possibly degenerating into a single double turning point at X_s are involved in the selection of global mode frequencies.

1.5.1 Mapping and comparison equation

When $\mu = 2$, the formal solution (1.19) reduces to

$$\psi(X;\omega,\varepsilon) = \left\{ B(X;\omega,\varepsilon)V\left[\frac{\eta(X;\omega)}{\sqrt{\varepsilon}}\right] + \sqrt{\varepsilon}C(X;\omega,\varepsilon)V'\left[\frac{\eta(X;\omega)}{\sqrt{\varepsilon}}\right]\right\} e^{\frac{i}{\varepsilon}\int_{X_0}^{X} k_0(s)ds} . \tag{1.25}$$

When $\mu = 2$, comparison equation (1.21) involves only 3 coefficients γ_0, γ_1 and γ_2, only one of which is independent. According to Lynn & Keller (1970), one may, without loss of generality, set $\gamma_1(\omega,\varepsilon) = 0$ and $\gamma_2(\omega,\varepsilon) = -1/4$, the only unknown parameter being $\gamma_0(\omega,\varepsilon)$. Equation (1.21) therefore reduces to

$$V''(\xi) + [\gamma_0(\omega,\varepsilon) - \frac{\xi^2}{4}]V(\xi) = 0 \quad . \tag{1.26}$$

As in (1.22), the coefficient $\gamma_0(\omega,\varepsilon)$ can be expanded in powers of ε to read

$$\gamma_0(\omega,\varepsilon) = \varepsilon^{-1}\sum_{p=0}^{\infty}\gamma_{0_p}(\omega)\varepsilon^p \quad . \tag{1.27}$$

It is convenient to express the leading-order approximation $\gamma_{0_0}(\omega)$ in terms of a new parameter $\eta_1(\omega)$ such that

$$\gamma_{0_0}(\omega) \equiv \frac{\eta_1^2(\omega)}{4} \quad . \tag{1.28}$$

Equation (1.26), together with exponential decay conditions at infinity in the $\eta(+;\omega)$ and $\eta(-;\omega)$ regions, defines the new eigenvalue problem in the complex η plane in terms of the unknown eigenvalues $\gamma_0(\omega,\varepsilon)$ and unknown eigenfunctions $V(\xi)$.

In view of the above expressions for $\gamma_{0_0}(\omega)$, $\gamma_1(\omega,\varepsilon)$ and $\gamma_2(\omega,\varepsilon)$, and definition (1.18a) for $R_0(X;\omega)$, relation (1.24) reduces to

$$\int_{\eta_0}^{\eta(X;\omega)} \sqrt{\eta_1^2(\omega) - s^2}\, ds = 2\int_{X_0}^{X} \sqrt{2\frac{\omega - \omega_0(r)}{\omega_{kk}(r)}}\, dr \quad . \tag{1.29}$$

This relation implicitly defines the mapping $X \mapsto \eta(X;\omega)$ for each value of ω. As stated in the previous section, the turning points $X_1(\omega)$ and $X_2(\omega)$, which satisfy $\omega_0(X) = \omega$, should be transformed into turning points $\eta_1(\omega)$ and $-\eta_1(\omega)$ of comparison equation (1.26). Consequently, if one chooses $\eta_1(\omega) = \eta[X_1(\omega);\omega]$, one should also have $-\eta_1(\omega) = \eta[X_2(\omega);\omega]$. According to (1.29), these relations imply that

$$\int_{\eta_1(\omega)}^{-\eta_1(\omega)} \sqrt{\eta_1^2(\omega) - s^2}\, ds = 2\int_{X_1(\omega)}^{X_2(\omega)} \sqrt{2\frac{\omega - \omega_0(X)}{\omega_{kk}(X)}}\, dX \quad . \tag{1.30}$$

This identity remains valid when the right-hand side integral is evaluated along any path Γ joining both turning points $X_1(\omega)$ and $X_2(\omega)$, provided that the image path $\eta(\Gamma;\omega)$ is chosen to calculate the left-hand side integral. When a specific choice of branch is made for the square root on the left-hand side, the integral can readily be calculated to yield

$$\eta_1(\omega) = 2\left\{ \frac{1}{\pi}\int_{X_1(\omega)}^{X_2(\omega)} \sqrt{2\frac{\omega - \omega_0(X)}{\omega_{kk}(X)}}\, dX \right\}^{1/2} \quad . \tag{1.31}$$

It is possible to obtain a more convenient expression for $\eta_1(\omega)$ that is independent of the labeling of the turning points $X_1(\omega)$ and $X_2(\omega)$. The branch points of the square root in (1.31) satisfy $\omega_0(X) = \omega$ and therefore coincide with the turning points $X_1(\omega)$ and $X_2(\omega)$. If the branch cut is chosen to lie between $X_1(\omega)$ and $X_2(\omega)$, equation (1.31) can also be written as

$$\eta_1(\omega) = 2\left\{ \frac{1}{2\pi}\oint_C \sqrt{2\frac{\omega - \omega_0(X)}{\omega_{kk}(X)}}\, dX \right\}^{1/2} \quad , \tag{1.32}$$

where the contour C encircles both turning points. As soon as the orientation of the contour is fixed, for instance counterclockwise, the definition of $\eta_1(\omega)$ only depends

on the selected branch of the square roots. Four determinations of $\eta_1(\omega)$ are possible, which can be deduced from each other by successive multiplications [1] by $e^{ik\pi/2}$, $k = 1, 2, 3$. It is only the constraint $\eta[X_1(\omega); \omega] = \eta_1(\omega)$ which allows to obtain a unique representation of $\eta(X; \omega)$ from equation (1.29). The uniform approximation (1.25) must remain invariant when we change from one determination for $\eta_1(\omega)$ to another. Thus one should respect the following substitutions

$$\left| \begin{array}{lcl} \eta_1(\omega) & \mapsto & e^{ik\pi/2}\eta_1(\omega) \quad , \\ \eta(X;\omega) & \mapsto & e^{ik\pi/2}\eta(X;\omega) \quad , \\ \gamma_0(\omega,\varepsilon) & \mapsto & e^{ik\pi}\gamma_0(\omega,\varepsilon) \quad . \end{array} \right. \tag{1.33}$$

According to expressions (1.68a,b) listed in Appendix A, the functions $B(X; \omega, \varepsilon)$ and $C(X; \omega, \varepsilon)$ are both multiplied by the same constant factor under the above substitutions. Without loss of generality, this factor may be taken equal to unity.

The Stokes lines in the complex η plane can explicitly be obtained from the analytical form $\frac{1}{4\varepsilon}[\eta_1^2(\omega) - \eta^2]$ of the leading-order coefficient multiplying $V(\xi)$ in comparison equation (1.26). Stokes lines issuing from each turning point $\eta_1(\omega)$ and $-\eta_1(\omega)$ are respectively given by

$$\Im m \left\{ \int_{\pm\eta_1(\omega)}^{\eta} \sqrt{\eta_1^2(\omega) - s^2} ds \right\} = 0 \quad . \tag{1.34}$$

Among the four possible determinations of $\eta_1(\omega)$ solutions of (1.32), one is bound to lie in the quarter plane $3\pi/2 < arg\ \eta \leq 2\pi$. When $\eta_1(\omega)$ is restricted in this manner, Stokes lines may take one of the three characteristic configurations represented on figure 1.5. The configuration with distinct Stokes line networks for each turning point (figure 1.5a) is generic. Configurations with one Stokes line joining both turning points (figure 1.5b) or with one double turning point (figure 1.5c) are exceptional. The Stokes line networks pertaining to determinations of $\eta_1(\omega)$ falling in the other

1. Note that the branch of $\sqrt{2\frac{\omega-\omega_0(X)}{\omega_{kk}(X)}}$ in (1.32) is not necessarily the same as on the right-hand side of (1.29). The branch may change from one equation to the other depending on specific features of the mapping $X \mapsto \eta(X; \omega)$ which may or may not conserve sense of rotation.

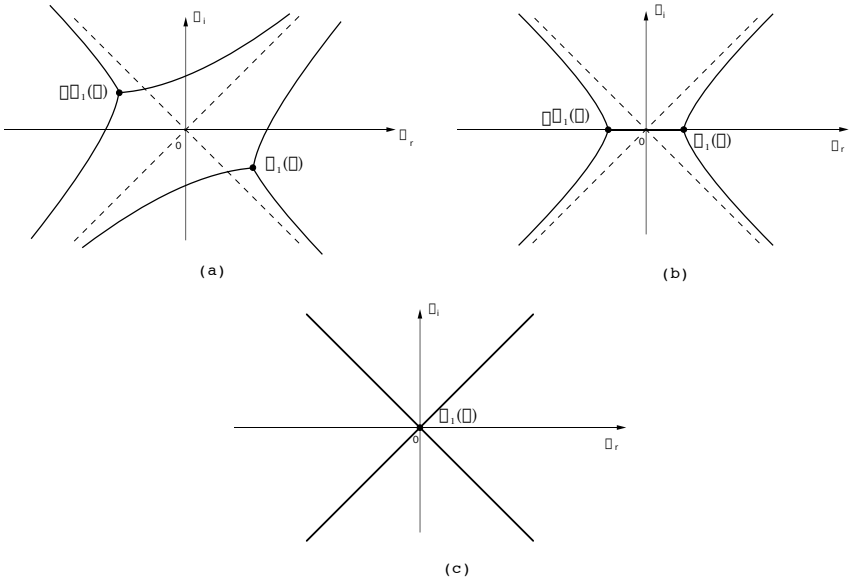

FIG. 1.5 - *Possible Stokes line networks with two turning points in the complex η plane. The parameter $\eta_1(\omega)$ is restricted to lie in the quarter plane $3\pi/2 < arg\ \eta \leq 2\pi$. (a) : generic configuration, no common Stokes line joins both turning points. (b) : $\eta_1(\omega)$ on positive η_r axis, Stokes line joins both turning points. (c) : $\eta_1(\omega) = 0$, double turning point. Other configurations are generated by rotations of angle $k\pi/2$, $k = 1, 2, 3$.*

three quadrants of the complex η plane may be generated by simple rotations of angle $k\pi/2$, $k = 1, 2, 3$. It should be emphasized that the Stokes line network in the complex η plane is solely a function of the single complex parameter $\eta_1(\omega)$ defined in (1.32), as seen from the Stokes line equation (1.34). Recall also that Stokes lines in the complex X plane and η plane are mapped into each other when $\eta(X;\omega)$ is solution of (1.29).

In order to completely define the eigenvalue problem in the complex η plane, there remains to locate the $\eta(+;\omega)$ and $\eta(-;\omega)$ regions where exponential decay boundary conditions at infinity have to be applied. This issue is examined in the next subsection.

1.5.2 "Dynamics" of the $\eta(+;\omega)$ and $\eta(-;\omega)$ regions

It has been argued in section 1.3 that regions $(+)$ and $(-)$ containing the X_r axis near $+\infty$ and $-\infty$ are well defined and cannot flip from one side of a Stokes line to the other as long as ω is maintained within the domain $\omega_i \geq \omega_i^{max}(\infty)$. This property is preserved under the conformal transformation $X \mapsto \eta(X;\omega)$: the relative positions of $\eta(+;\omega)$ and $\eta(-;\omega)$ in the complex η plane do not change when $\omega_i \geq \omega_i^{max}(\infty)$. More specifically, variations of ω should lead, in the present context, to displacements of $\eta_1(\omega)$ within the specified quarter plane $3\pi/2 < arg\ \eta \leq 2\pi$. If $\eta_1(\omega)$ happens to cross one of the boundary lines $arg\ \eta = 3\pi/2$ or $arg\ \eta = 2\pi$, a rotation of angle $k\pi/2$ must be applied to keep $\eta_1(\omega)$ within the prescribed quadrant, and $\eta(X;\omega)$ should be changed according to the rules defined in (1.33). This results in an abrupt rotation of the whole Stokes line network in the complex η plane which nonetheless preserves the relative positions of $\eta(+;\omega)$ and $\eta(-;\omega)$.

It is now possible to add on the Stokes line networks sketched on figure 1.5 all possible configurations taken by the regions $\eta(+;\omega)$ and $\eta(-;\omega)$. According to the comments following lemma 2 in Chomaz *et al.* (1991), the real axis crosses only once a single Stokes line issuing from each turning point when $\omega_i \geq \omega_{0,i}^{max}$. Thus, when $\omega_i \geq \omega_{0,i}^{max}$, permissible configurations $(+)$ and $(-)$ regions in the complex X plane are as sketched on figure 1.6. Possible locations of the corresponding regions $\eta(+;\omega)$ and $\eta(-;\omega)$ in the complex η plane are listed on figure 1.7. Note that on all configurations shown on figures 1.7c,d, $\eta(+;\omega)$ and $\eta(-;\omega)$ are contiguous regions in the limit of large $|\eta|$. This feature, initially valid for $\omega_i \geq \omega_{0,i}^{max}$, persists for all $\omega_i \geq \omega_i^{max}(\infty)$ and a solution of comparison equation (1.26) that is initially subdominant in $\eta(+;\omega)$ will become dominant in $\eta(-;\omega)$. Consequently, comparison equation (1.26) has no eigenfunctions satisfying the required boundary conditions. It can be concluded that **configurations of the η plane shown on figure 1.7c,d, together with their preimages in the X plane sketched on figures 1.6c,d,**

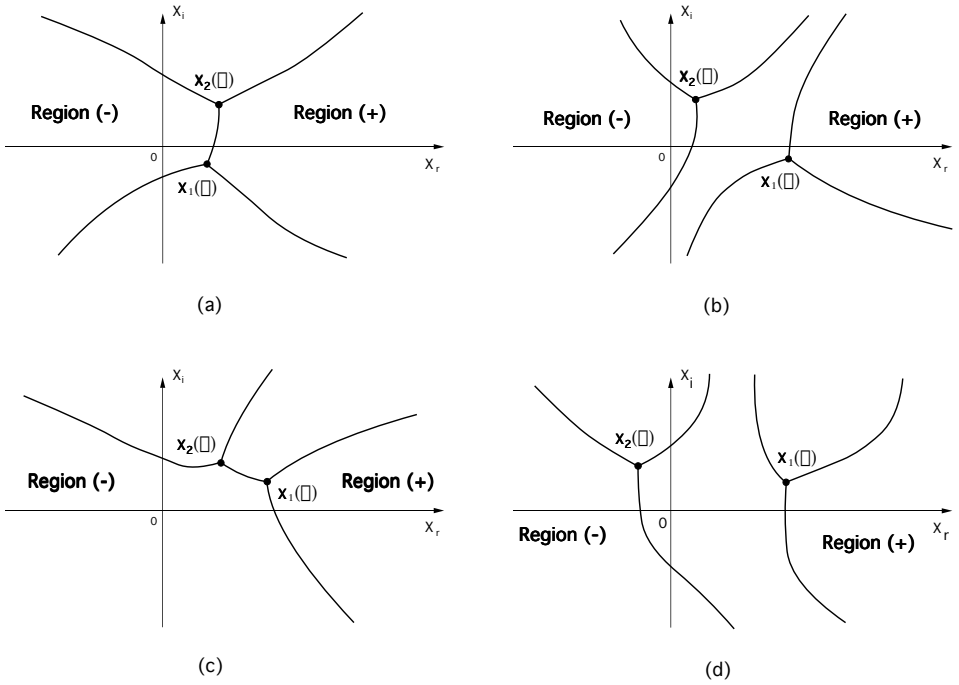

FIG. 1.6 - *Stokes line networks in the complex X plane when $\omega_i \geq \omega_{0,i}^{max}$. (a) and (b) may potentially evolve into global mode configurations with varying ω while (c) and (d) never do.*

do not give rise to global frequencies with growth rate $\omega_i \geq \omega_i^{max}(\infty)$. By contrast, in the two cases described on figures 1.7a,b, regions $\eta(+;\omega)$ and $\eta(-;\omega)$ are not contiguous for large $|\eta|$ and they will remain so as long as $\omega_i \geq \omega_{i,max}(\infty)$. Preimage configurations in the X plane illustrated on figures 1.6a,b may therefore evolve as ω varies to give rise to global modes.

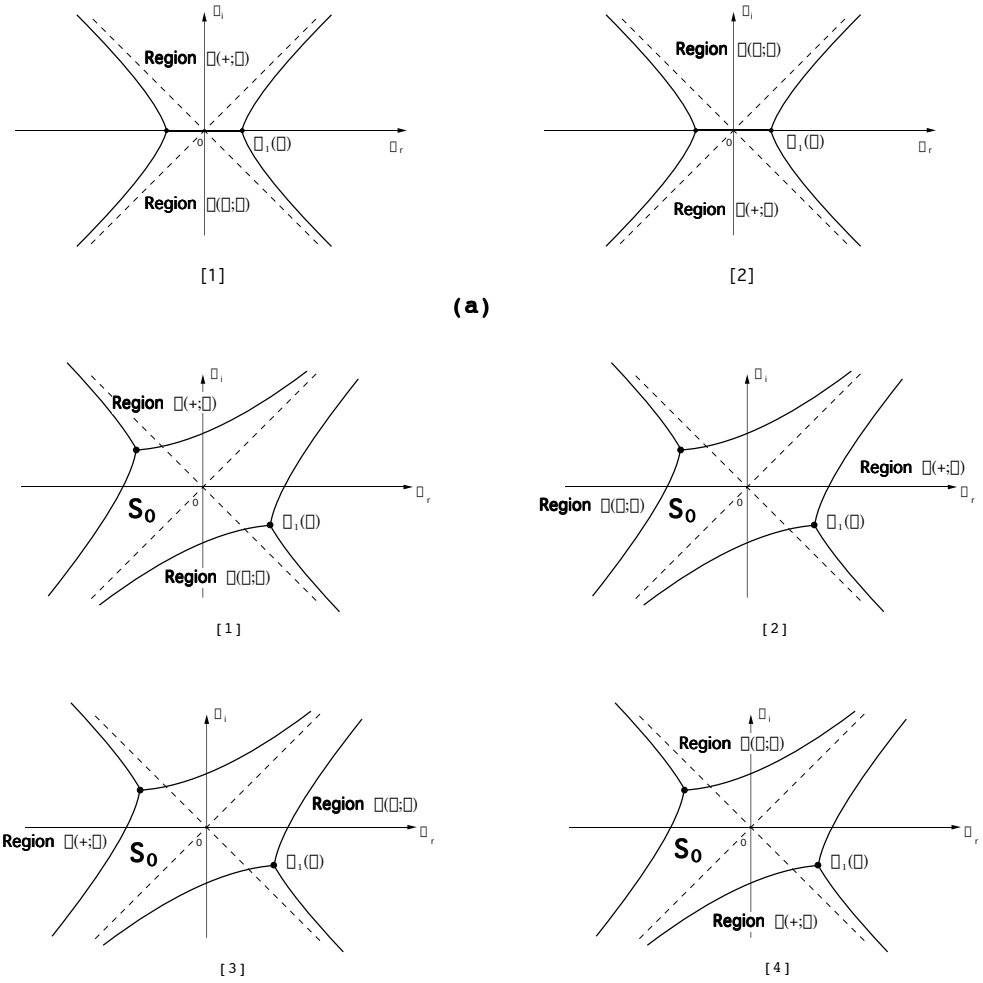

FIG. 1.7 - *Stokes line networks in the complex η plane when $\omega_i \geq \omega_{0,i}^{max}$. (a) and (b) may potentially evolve into global mode configurations with varying ω while (c) and (d) never do.*

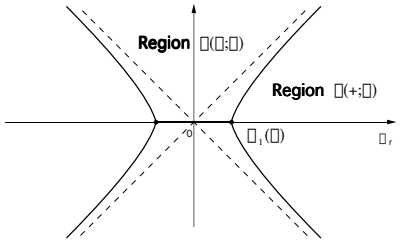
Region □(□:□)
Region □(+:□)
□1(□)
□r
0

[1]

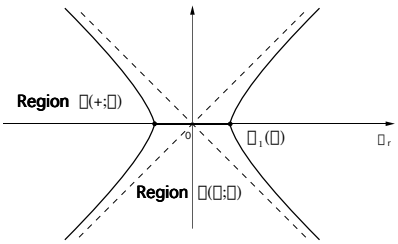
Region □(+:□)
Region □(□:□)
□1(□)
□r
0

[2]

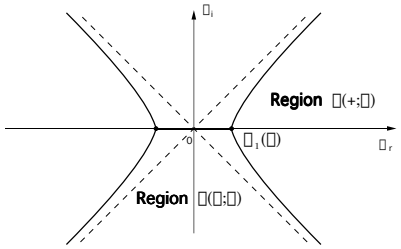
□i
Region □(+:□)
Region □(□:□)
□1(□)
□r
0

[3]

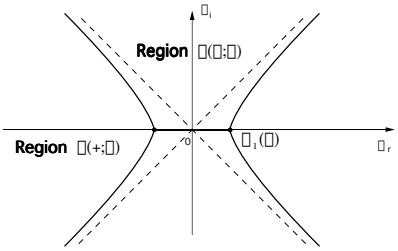
□i
Region □(□:□)
Region □(+:□)
□1(□)
□r
0

[4]

(c)

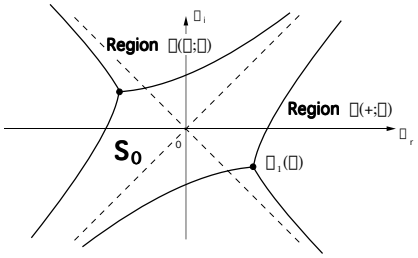
□i
Region □(□:□)
Region □(+:□)
S0
□1(□)
□r
0

[1]

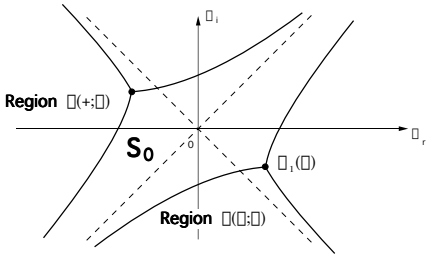
□i
Region □(+:□)
S0
□1(□)
Region □(□:□)
□r
0

[2]

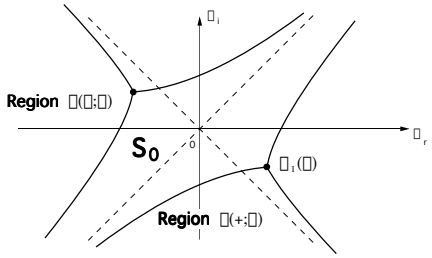
□i
Region □(□:□)
S0
□1(□)
Region □(+:□)
□r
0

[3]

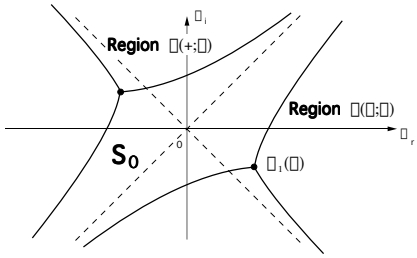
□i
Region □(+:□)
Region □(□:□)
S0
□1(□)
□r
0

[4]

(d)

1.5.3 General global mode solutions

It has proved convenient until now to restrict $\eta_1(\omega)$ to a particular quadrant of the complex η plane in order to identify all possible configurations of the Stokes line network and associated regions $\eta(+;\omega)$ and $\eta(-;\omega)$. This convention has led us to exclude some configurations but it is ill-fitted to effectively solve the eigenvalue problem pertaining to comparison equation (1.26). As observed in subsection 1.5.2, the Stokes line network as well as regions $\eta(+;\omega)$ and $\eta(-;\omega)$ evolve discontinuously with respect to ω as $\eta_1(\omega)$ reaches the quarterplane boundaries. In the following analysis, $\eta_1(\omega)$ is no longer confined to a particular sector but it is selected so that $\eta(+;\omega)$ contains[2] the real η axis for large η. In contrast with the situation

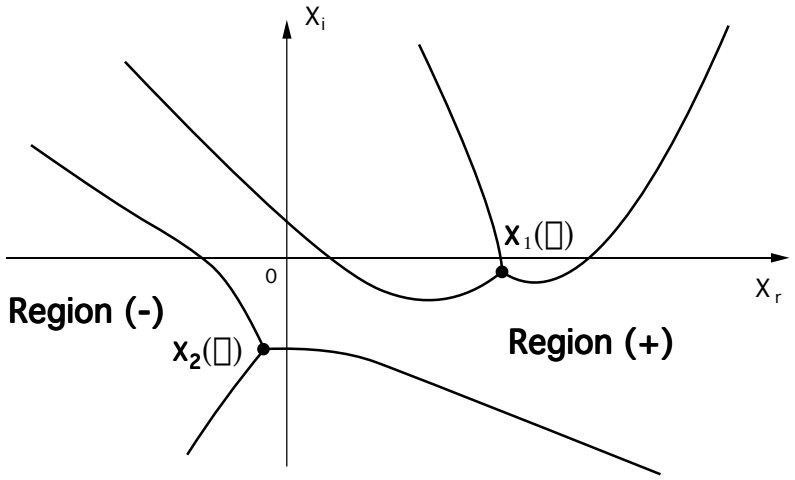

FIG. 1.8 - *Example of Stokes line network in the complex X plane such that $\eta(+;\omega)$ coincides with S_0 of figures 1.7b,d.*

prevailing in subsection 1.5.2, the determination $\eta(X;\omega)$ of the mapping remains unchanged and the Stokes line network then evolves continuously as ω varies in the

2. Note that it is always possible to do so. The region $\eta(+;\omega)$ has been shown in the previous section never to coincide with, say, the central domain S_0 between both turning points indicated on figures 1.7b,d. Hence, the preimage configuration displayed on figure 1.8 has already been excluded. Furthermore, if $\eta(+;\omega)$ does not initially contain the η_r axis for large η, a rotation of appropriate angle $k\pi/2$ will correct the situation.

domain $\omega_i \geq \omega_i^{max}(\infty)$. Finally, the eigenvalue $\gamma_0(\omega, \varepsilon)$ appearing in the comparison equation also stays continuous with respect to ω.

Recall that the only remaining configurations in the complex X plane which may evolve into global modes with varying ω are those illustrated on figures 1.6a,b. Following the procedure just outlined above, the regions $\eta(+;\omega)$ and $\eta(-;\omega)$ are always taken to correspond asymptotically for large $|\eta|$ to the sectors

$$\eta(+;\omega) \ : \ -\pi/4 < arg\ \eta < \pi/4\ ; \tag{1.35a}$$

$$\eta(-;\omega) \ : \ 3\pi/4 < arg\ \eta < 5\pi/4 \quad . \tag{1.35b}$$

Exponential decay conditions at infinity are always enforced within these sectors as long as $\omega_i \geq \omega_i^{max}(\infty)$. Solutions of comparison equation (1.26), that are exponentially small in both regions $\eta(+;\omega)$ and $\eta(-;\omega)$, are expressible in terms of Hermite polynomials of order n as follows:

$$V_n(\xi) = He_n(\xi) e^{-\frac{\xi^2}{4}} \quad , \tag{1.36}$$

and corresponding eigenvalues are given by

$$\gamma_0[\omega_{g_n}(\varepsilon), \varepsilon] = n + 1/2 \quad . \tag{1.37}$$

Any function $\omega_{g_n}(\varepsilon)$ satisfying the above functional relationship is a global frequency of the problem. Of primary interest is the derivation of a systematic approximation scheme for $\omega_{g_n}(\varepsilon)$ in the régime $\varepsilon \ll 1$. In the sequel, it is assumed that $\omega_{g_n}(\varepsilon)$ reaches a well defined limit $\omega_{g_n}^{(0)}$ as $\varepsilon \to 0$. According to expansion (1.27) and definition (1.28), the leading-order approximation to $\gamma_0[\omega_{g_n}(\varepsilon), \varepsilon]$ is then

$$\gamma_0[\omega_{g_n}(\varepsilon), \varepsilon] = \frac{\gamma_{0_0}(\omega_{g_n}^{(0)})}{\varepsilon} + O(1) = \frac{\eta_1^2(\omega_{g_n}^{(0)})}{4\varepsilon} + O(1) \quad . \tag{1.38}$$

In order for these estimates to be consistent with eigenvalue relation (1.37), the integers n should be chosen such that $n(\varepsilon) = O(1/\varepsilon)$ in the limit $\varepsilon \to 0$, i.e. $n(\varepsilon)$

should satisfy

$$\lim_{\varepsilon \to 0} \varepsilon n(\varepsilon) = m \quad , \tag{1.39}$$

with the real number m given by

$$\gamma_{0_0}(\omega_{g_n}^{(0)}) = \frac{\eta_1^2(\omega_{g_n}^{(0)})}{4} = m \ , \ m \geq 0 \quad . \tag{1.40}$$

Note that the function $\eta_1(\omega)$ has explicitly been defined in (1.32).

Higher-order approximations to the global frequencies $\omega_{g_n}(\varepsilon)$ can be sought in the form

$$\omega_{g_n} = \omega_{g_n}^{(0)} + \varepsilon \omega_{g_n}^{(1)} + \cdots \ . \tag{1.41}$$

Upon substitution into the eigenvalue relation (1.37) and identification of terms of order unity, one obtains the equation for the first-order correction $\omega_{g_n}^{(1)}$:

$$\frac{\partial \gamma_{0_0}}{\partial \omega}(\omega_{g_n}^{(0)}) \ \omega_{g_n}^{(1)} + \gamma_{0_1}(\omega_{g_n}^{(0)}) = [n + 1/2 - m/\varepsilon] \quad , \tag{1.42}$$

where the first-order term $\gamma_{0_1}(\omega_{g_n}^{(0)})$ is explicitly given in (1.66) and (1.67) of Appendix A. Relation (1.42) is valid as long as $n + 1/2 - m/\varepsilon = O(1)$ and $\dfrac{\partial \gamma_{0_0}}{\partial \omega}(\omega_{g_n}^{(0)}) \neq 0$. The procedure can readily be extended to arbitrary order to generate the entire expansion (1.41).

To the leading-order global frequencies $\omega_{g_n}^{(0)}$ correspond specific Stokes line configurations. According to eigenvalue relation (1.40), allowable parameter values $\eta_1(\omega_{g_n}^{(0)})$ are necessarily positive real or zero and the Stokes line network in the complex η plane has one of the configurations displayed on figures 1.9a,b. Since the conformal mapping $X \mapsto \eta(X; \omega_{g_n}^{(0)})$ is one to one, corresponding Stokes lines in the complex X plane are easily identified, as sketched in figures 1.10a,b. Figure 1.9a pertains to strictly positive values of m in (1.40). Such Stokes line configurations with **two simple turning points in the complex plane** are referred to as **type 1**. The eigenvalue $\omega_{g_n}^{(0)}$ is such that the two turning points in the η plane are located at $\pm\eta_1(\omega_{g_n}^{(0)}) = \pm 2\sqrt{m}$ on the real η axis, as in figure 1.9a. Note that regions $\eta(+;\omega)$

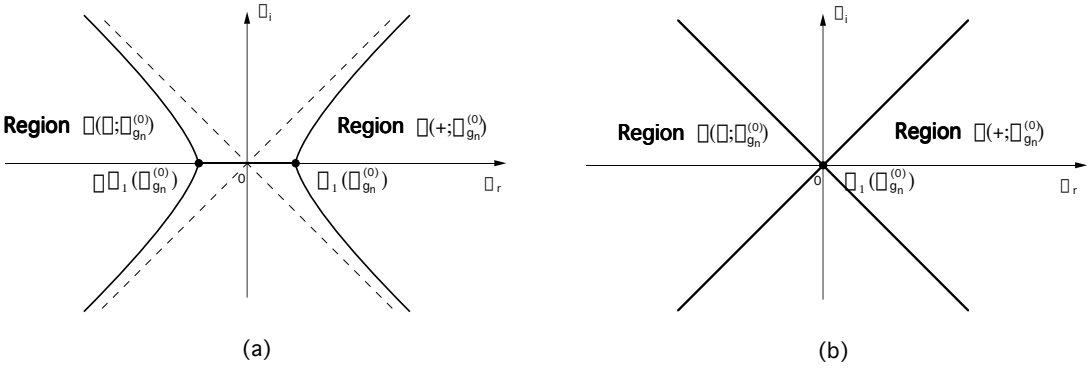

FIG. 1.9 - *Stokes line networks in the complex η plane giving rise to global frequencies satisfying (1.40). (a) : $m > 0$; two simple turning points located at $\pm\eta_1(\omega_{g_n}^{(0)}) = \pm 2\sqrt{m}$. (b) : $m = 0$; one double turning point at the origin.*

and $\eta(-;\omega)$, as well as their preimages $(+)$ and $(-)$ are necessarily not contiguous, in agreement with the necessary condition stated in section 1.3. When $m = 0$, the Stokes line network displays **a double turning point** X_s in the complex X plane, a situation referred to as **type 2** and illustrated on figure 1.10b. The image network has also a double turning point at the origin in the η plane as shown on figure 1.9b. It has therefore been demonstrated that, if $\omega_{g_n}^{(0)}$ is a global frequency, the Stokes line network in the X plane is either type 1 or type 2 as indicated in figures 1.10a,b.

The reverse proposition is also true: if, for a given value $\omega^{(0)}$, the Stokes line network is either of type 1 or type 2, $\omega^{(0)}$ is, at leading order in ε, a global frequency of the problem. To prove this statement, we simply note that, if one of the configurations depicted in figures 1.10a,b prevails in the X plane for a given frequency $\omega^{(0)}$, the transformation $X \mapsto \eta(X;\omega^{(0)})$ can be selected so as to map $(+)$ into $\eta(+;\omega^{(0)})$ containing the real η axis. The original Stokes lines in the X plane are then necessarily transformed into one of the Stokes line networks in the complex η plane shown on figures 1.9a,b. Such situations are known to give rise to eigenvalues with leading-order approximation $\omega^{(0)}$. Successive terms in the expansion (1.27) of the function $\gamma_0(\omega^{(0)}, \varepsilon)$ can be evaluated. For instance, the leading-order term $\gamma_{0_0}(\omega^{(0)})$

is calculated with the help of (1.28) and (1.32). Higher-order corrections $\gamma_{0_1}(\omega^{(0)})$, ...are given by expressions such as (1.66) or (1.67) in Appendix A. Thus, higher-order contributions to the global frequency expansion $\omega_{g_n}(\varepsilon) = \omega^{(0)} + \varepsilon\omega_{g_n}^{(1)} + \cdots$ can readily be generated by making use of recursion formulas analogous to (1.38). A global frequency has therefore been obtained.

Note that type 1 and type 2 global frequencies correspond to the set Δ_1 in the complex ω plane introduced in section 1.3 [compare type 1 and type 2 Stokes line configurations sketched in figures 1.10a,b with those displayed on figures 1.4c,d and used to define the set Δ_1]. For future reference in section 1.5.5, we recall that the set Δ_1 is by definition included in the curve or set of curves Δ defined by condition (1.15) and it is the complement in Δ of the set Δ_0 of frequencies excluded by the necessary condition invoked in section 1.3. Condition (1.15) is then satisfied by all leading-order global frequencies $\omega_{g_n}^{(0)}$ and using expressions (1.8), (1.32) and (1.40), it also reads

$$\Im m[\gamma_{0_0}(\omega_{g_n}^{(0)})] = 0 \quad . \tag{1.43}$$

Note that this relation could have been directly deduced from relation (1.40).

In closing this discussion, it should be emphasized that the present analysis is restricted to global frequencies satisfying $\omega_i \geq \omega_i^{max}(\infty)$. If $\omega_i < \omega_i^{max}(\infty)$, an essential step in the argumentation breaks down: we are unable to guarantee that regions $\eta(+;\omega)$ and $\eta(-;\omega)$ necessarily need to be noncontiguous at infinity in order to give rise to a global mode (subsection 1.5.2).

A detailed evaluation of the global mode frequencies and eigenfunctions is undertaken in the following subsection for type 1 and type 2 configurations.

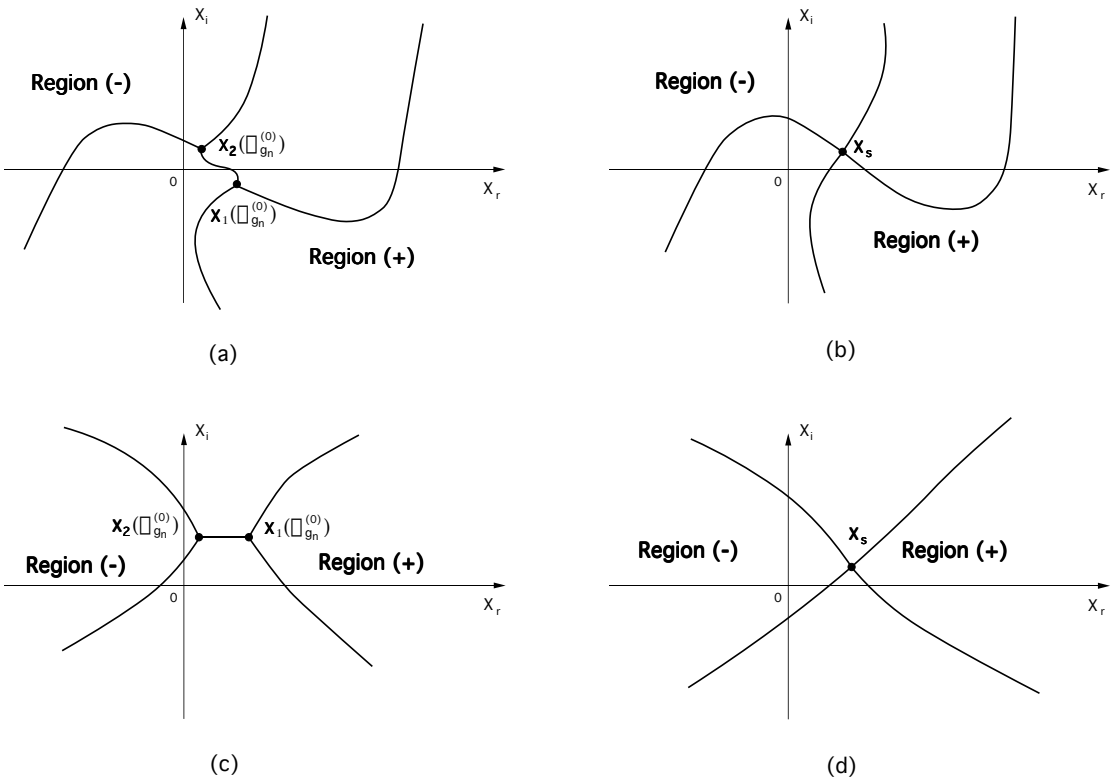

FIG. 1.10 - *Stokes line networks in the complex X plane giving rise to global frequencies satisfying (1.40). They are transformed into the networks of the η plane shown on figure 9 under the conformal mapping $X \mapsto \eta(X;\omega_{g_n}^{(0)})$. (a) : $m > 0$; two simple turning points at $X_1(\omega_{g_n}^{(0)})$ and $X_2(\omega_{g_n}^{(0)})$; type 1 configuration. (b) : $m = 0$; one double turning point at the origin; type 2 configuration. (c) : type 1 configuration with "untwisted" Stokes lines. (d) : type 2 configuration with "untwisted" Stokes lines (see discussion following equation (1.61) in the text).*

1.5.4 Global mode classification

Global modes with two simple turning points (type 1)

It is assumed that the Stokes line network is composed of two first-order turning points $X_1(\omega_{g_n}^{(0)})$ and $X_2(\omega_{g_n}^{(0)})$ connected by a common Stokes line and that regions $(+)$ and $(-)$ are not contiguous, as in figure 1.10a. According to the results of the previous subsection, the global frequencies $\omega_{g_n}(\varepsilon)$ admit expansions of the form (1.41) when $\varepsilon \ll 1$. The $O(1)$ term $\omega_{g_n}^{(0)}$ is given by (1.40) with m defined in (1.39) and $\eta_1(\omega)$ in (1.32). It can be concluded that $\omega_{g_n}^{(0)}$ is a root of the equation

$$\frac{1}{2\pi}\oint_C \sqrt{2\frac{\omega_{g_n}^{(0)} - \omega_0(X)}{\omega_{kk}(X)}}dX = m \quad , \; m > 0 \quad , \tag{1.44}$$

where the branch cut of the square root joins both turning points $X_1(\omega_{g_n}^{(0)})$ and $X_2(\omega_{g_n}^{(0)})$ as specified in the comments following (1.32). Equivalently, the eigenvalue relation for the global frequencies $\omega_{g_n}(\varepsilon)$ is, at leading order in ε given by

$$\frac{1}{2\pi\,\varepsilon}\oint_C \sqrt{2\frac{\omega_{g_n}^{(0)} - \omega_0(X)}{\omega_{kk}(X)}}dX = n + \frac{1}{2} + O(1) \quad . \tag{1.45}$$

Equation (1.44) dictates that the branch of the square root in the integrand should be the one to yield a positive value of the integral. The function $\eta_1^2(\omega_{g_n}^{(0)})$ is therefore uniquely defined. Thus, among the four determinations of the mapping function $\eta(X;\omega)$ initially possible [see (1.33)], only two remain, say $\eta(X;\omega)$ and $-\eta(X;\omega)$. Although both give the same eigenvalue relation (1.44), only one of them is such that region $\eta(+;\omega)$ contains the positive real axis as specified in subsection 1.5.3.

From the knowledge of $\omega_{g_n}^{(0)}$, one can deduce the first-order correction $\omega_{g_n}^{(1)}$ satisfying (1.42). The function $\gamma_{0_0}(\omega_{g_n}^{(0)})$ is equal to (1.44) and $\gamma_{0_1}(\omega_{g_n}^{(0)})$ is defined in

(1.67) of Appendix A so that one obtains :

$$\omega_{g_n}^{(1)} = \left(n + \frac{1}{2} - \frac{m}{\varepsilon} - \frac{\oint_C \left\{ \frac{R_1(X)}{\sqrt{R_0(X;\omega_{g_n}^{(0)})}} \right\} dX}{\oint_C \left\{ 4 \frac{\sqrt{R_0(X;\omega_{g_n}^{(0)})}}{\eta_1^2(\omega_{g_n}^{(0)}) - \eta^2(X;\omega^{(0)})} \right\} dX} \right) \left(\oint_C \frac{dX}{\sqrt{R_0(X;\omega_{g_n}^{(0)})}\omega_{kk}(X)} \right)^{-1} . \tag{1.46}$$

Recall that $R_0(X;\omega)$ and $R_1(X)$ are defined in (1.18a,b). The branch of the square root in the above integrands is the same as in (1.44).

It is worthwhile to notice the peculiar behavior of the approximation scheme for type 1 global modes, as ε tends to zero. According to (1.39), at a given real positive value of m, the expansion of $\omega_{g_n}(\varepsilon)$ refers to larger and larger values of the mode index n as $\varepsilon \to 0$. The function $n(\varepsilon)$ may for instance be defined as an integer distant by an amount n_0 from the integer part of m/ε, i.e.

$$n(\varepsilon) = I.P.(\frac{m}{\varepsilon}) + n_0 \ ; \ n_0 = 0, \pm 1, \pm 2, ... \ , \tag{1.47}$$

where I.P.$(\frac{m}{\varepsilon})$ denotes the integer part of $\frac{m}{\varepsilon}$. The integer n_0 may be seen as a local index. Each value of n_0 defines a global mode of leading order frequency $\omega_{g_n}^{(0)}$. If the variations of n are given by (1.47), condition (1.39) is satisfied, but the quantity $n(\varepsilon) - m/\varepsilon$ appearing in (1.42) and (1.46) fluctuates between n_0 and $n_0 + 1$ as $\varepsilon \to 0$. Thus, the first-order correction $\omega_{g_n}^{(1)}$ effectively oscillates between two limiting values with decreasing ε, while remaining of order unity.

As discussed in subsection 1.5.5 (see figure 1.12a, in particular), it may very well happen that the curve Δ defined by (1.43) along which all global frequencies lie, exhibits a local maximum in the complex ω plane at a particular value $\omega_{g_n}^{(0)}$ satisfying (1.44). In this case, one necessarily has $\Im m \left[\frac{\partial \gamma_{0_0}}{\partial \omega}(\omega_{g_n}^{(0)}) \right] = 0$ and, according to (1.42), the first-order correction $\omega_{g_n}^{(1)}$ has an imaginary part that is independent of n at a fixed value of ε, as long as $n \sim m/\varepsilon$. The expansion must be pursued to $O(\varepsilon^2)$ in order to catch growth rate variations $\Im m \ \omega_{g_n}^{(2)}$ between the locally most unstable

global modes. This behavior is entirely consistent with simple scaling arguments : all global frequencies along the curve Δ_1 are separated by a distance $O(\varepsilon)$ around $\omega_{g_n}^{(0)}$, as given by (1.46), but, around a locally parabolic maximum, such a configuration only leads to $O(\varepsilon^2)$ variations in the growth rate.

We now proceed to the calculation of the eigenfunctions along the real X axis. The spatial shape of type 1 global modes is given by the uniform approximation (1.25) with the expression (1.36) for $V(\xi)$. This spatial shape can be computed either for a given global frequency $\omega_{g_n}(\varepsilon)$ or for a given mode index $n(\varepsilon)$ since both are related through (1.37). Note however that the first two terms $\omega_{g_n}^{(0)}$ and $\omega_{g_n}^{(1)}$ given by relations (1.44) and (1.46) are sufficient to perfectly define the mode index $n(\varepsilon)$. Keeping only the leading-order terms in expansions (1.20a,b) for $B(X;\omega,\varepsilon)$ and $C(X;\omega,\varepsilon)$, the uniform approximation (1.25) at a given frequency $\omega_{g_n}(\varepsilon)$ can be written as :

$$\psi(X;\omega_{g_n},\varepsilon) = \left\{ \left(B_0(X;\omega_{g_n}) - 2\eta(X;\omega_{g_n})C_0(X;\omega_{g_n})\right) He_{n(\varepsilon)}\left[\frac{\eta(X;\omega_{g_n})}{\sqrt{\varepsilon}}\right] + \sqrt{\varepsilon}C_0(X;\omega_{g_n}) He'_{n(\varepsilon)}\left[\frac{\eta(X;\omega_{g_n}(\varepsilon))}{\sqrt{\varepsilon}}\right] \right\} e^{-\frac{\eta^2(X;\omega_{g_n})}{4\varepsilon}} e^{\frac{i}{\varepsilon}\int_{X_0}^{X} k_0(s)ds}, \tag{1.48}$$

where $B_0(X;\omega)$ and $C_0(X;\omega)$ are given by (1.68a,b). This approximation is valid in the entire complex X plane including both turning points $X_1(\omega_{g_n}^{(0)})$ and $X_2(\omega_{g_n}^{(0)})$.

It is also possible to deduce from (1.25) alternate expressions for the global mode eigenfunctions that remain uniformly valid only in specific subdomains of the complex X plane. We recall that the index $n(\varepsilon)$ varies as m/ε when $\varepsilon \to 0$, where m is defined in (1.40) or (1.44). Thus, the behavior of $\mathrm{He}_{n(\varepsilon)}(\eta/\sqrt{\varepsilon})$ appearing in $V_n(\eta/\sqrt{\varepsilon})$ and in (1.48) is highly singular since both the argument and the index become infinite as $\varepsilon \to 0$. As shown in Appendix B, it is possible to derive explicit asymptotic approximations for $V_{n(\varepsilon)}(\eta/\sqrt{\varepsilon})$ and $V'_{n(\varepsilon)}(\eta/\sqrt{\varepsilon})$ by applying the method of steepest descent to the integral representation of Hermite polynomials. The final

results are summarized and discussed below.

Three distinct approximations are obtained depending on the location of X with respect to both turning points $X_1(\omega_{g_n}^{(0)})$ and $X_2(\omega_{g_n}^{(0)})$ and to the Stokes line that connects them. The different subdomains are represented in the complex η plane in figure 1.11. Within disks of radius $O(\varepsilon^{2/3})$ around each turning point

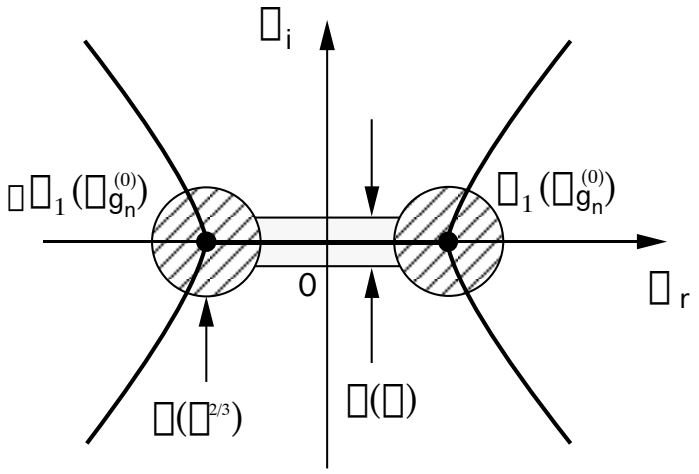

FIG. 1.11 - *Domains in the complex η plane where the uniform approximation (1.48) of type 1 global eigenfunctions can be simplified. Hatched region : near a single turning point, approximation is given by expression (1.49) or (1.80); Shaded region : near Stokes line, approximation is given by expression (1.50) or (1.81); Elsewhere : approximation is given by expression (1.51) or (1.79).*

$\pm\eta_1(\omega_{g_n}^{(0)}) = \pm 2\sqrt{m}$ in the complex η plane (hatched areas in figure 1.11), the global mode eigenfunction is approximated by

$$\psi(X;\omega_{g_n},\varepsilon) \sim \alpha_0\sqrt{2\pi}(\pm 1)^n \left(\frac{m}{\varepsilon}\right)^{\frac{n}{2}+\frac{1}{6}} Ai\left[\left(\frac{2\sqrt{2}m}{\varepsilon}\right)^{2/3}\left(\frac{\eta(X;\omega_{g_n})}{2\sqrt{m}} \mp 1\right)\right] \times e^{-\frac{m}{\varepsilon}[\frac{3}{2} \mp \frac{\eta(X;\omega_{g_n})}{\sqrt{m}} + \frac{\eta^2(X;\omega_{g_n})}{4m}]} \; e^{\frac{i}{\varepsilon}\int_{X_0}^{X} k_0(s)ds}, \tag{1.49}$$

where $Ai(x)$ denotes the usual Airy function. Correspondingly, in the complex X plane, the above result constitutes a valid approximation in circular neighborhoods of radius $O(\varepsilon^{2/3})$ around each turning point $X_1(\omega_{g_n}^{(0)})$ and $X_2(\omega_{g_n}^{(0)})$. If, for instance,

$X_1(\omega_{g_n}^{(0)})$ is mapped into $+\eta_1(\omega_{g_n}^{(0)})$ the upper sign in (1.49) pertains to the approximation near $X_1(\omega_{g_n}^{(0)})$ and the lower sign to the approximation near $X_2(\omega_{g_n}^{(0)})$.

Within a strip of width $O(\varepsilon)$ surrounding the Stokes line joining both turning points (shaded region in figure 1.11), the global mode approximation becomes :

$$\psi(X,\omega_{g_n},\varepsilon) \sim \left\{ \left[\frac{\eta+\sqrt{\eta^2-4m}}{2\sqrt{\varepsilon}}\right]^n \left[\frac{\eta+\sqrt{\eta^2-4m}}{\sqrt{\eta^2-4m}}\right]^{1/2} e^{i\Theta} e^{-\frac{1}{4\varepsilon}(2m+\eta\sqrt{\eta^2-4m})} \right.$$
$$\left. + \left[\frac{\eta-\sqrt{\eta^2-4m}}{2\sqrt{\varepsilon}}\right]^n \left[\frac{\eta-\sqrt{\eta^2-4m}}{\sqrt{\eta^2-4m}}\right]^{1/2} e^{-i\Theta} e^{-\frac{1}{4\varepsilon}(2m-\eta\sqrt{\eta^2-4m})} \right\}$$
$$\times \frac{\alpha_0}{\sqrt{2}} \left(\frac{\partial\eta}{\partial X}\right)^{-1/2} e^{\frac{i}{\varepsilon}\int_{X_0}^{X} k_0(s)ds} . \tag{1.50}$$

Elsewhere in the complex η or X plane the global mode admits a uniform expansion given by

$$\psi(X,\omega_{g_n},\varepsilon) \sim \frac{\alpha_0}{\sqrt{2}} \left[\frac{\eta+\sqrt{\eta^2-4m}}{2\sqrt{\varepsilon}}\right]^n \left[\frac{\eta+\sqrt{\eta^2-4m}}{\sqrt{\eta^2-4m}}\right]^{1/2} \left(\frac{\partial\eta}{\partial X}\right)^{-1/2}$$
$$\times e^{i\Theta} e^{-\frac{1}{4\varepsilon}(2m+\eta\sqrt{\eta^2-4m})} e^{\frac{i}{\varepsilon}\int_{X_0}^{X} k_0(s)ds} . \tag{1.51}$$

The branch cut of the square root in the above formulas is fixed on the segment joining both turning points $\pm\eta_1(\omega_{g_n}^{(0)}) = \pm 2\sqrt{m}$ and the branch is chosen such that

$$-\frac{\pi}{2} < arg(\sqrt{\eta^2-4m}) \leq \frac{\pi}{2} \quad when \quad -\frac{\pi}{2} < arg(\eta) \leq \frac{\pi}{2} \quad .$$

We recall that α_0 and X_0 are arbitrary constants which can eventually be set by a normalisation condition and that the positive number m defined as $\eta_1^2(\omega_{g_n}^{(0)})$ is also given by (1.44). The phase function $\Theta = \Theta(X;\omega_{g_n}^{(0)})$ in (1.50) and (1.51) is specified in (1.69).

Note that the uniformity of approximation (1.48) has been lost during this additional asymptotic expansion process and that the final results (1.49)-(1.51) are only local approximations. Near each turning point, the global mode approximation given

by (1.49) is an Airy type solution. This result is not surprising in view of the fact that Airy functions generally appear in local one-turning-point analysis. Far away from the turning points, the global mode is given by (1.50) or (1.51). As discussed in appendix B, these expressions are nothing but leading-order WKBJ approximations. One can indeed demonstrate that equation (1.50) is the sum of two WKBJ contributions built with the branches k^+ and k^- defined in (1.8). In the region where (1.50) is valid, i.e. near the Stokes line that connects the two turning points, both WKBJ approximations are of the same order of magnitude. It is then obvious that both must contribute to the eigenfunction. Far away from this Stokes line, approximation (1.51) consisting of a single WKBJ contribution must be used. It can readily be verified that the WKBJ approximation (1.51) is subdominant in regions (+) and (−) of the complex X plane and dominant in the other Stokes sectors. This feature is consistent with the necessary global mode existence condition obtained in section 1.3 and with the fact that WKBJ approximations defined as subdominant in the (+) and (−) subdomains remain valid in the adjacent Stokes sectors where they become dominant.

Global modes with a double turning point (type 2)

If the Stokes line network involves a double turning point X_s as in figure 1.10b, the result of Chomaz *et al.* (1991) and Monkewitz *et al.* (1993) are formally recovered. The procedure is briefly outlined below, particular attention being given to the correct choice of branches in the multiple-valued functions appearing at successive orders. Since X_s is a double turning point, one has $X_1(\omega_s) = X_2(\omega_s)$ for a particular frequency ω_s. In other words, X_s is, by definition, a double root of equation (1.10), as discussed in section 1.2. It is therefore located at a saddle point of $\omega_0(X)$ such that

$$\omega_0(X_s) = \omega_s \quad ; \tag{1.52a}$$

$$\frac{d\omega_0}{dX}(X_s) = 0 \quad . \tag{1.52b}$$

Note that the selection of type 2 global frequencies only relies on the local existence of a saddle point X_s of $\omega_0(X)$ in the complex X plane. By contrast, type 1 global frequencies are selected on the basis of an integral (1.44) involving $\omega_0(X)$ and $\omega_{kk}(X)$ over an extended domain in the complex X plane.

The image of X_s is the double turning point $\eta_1(\omega_s) = 0$ in the complex η plane as illustrated in figure 1.9b. This property leads to a simple expression for the leading-order mapping function $\eta(X;\omega_{g_n}(\varepsilon))$: when $\eta_1 = 0$, equation (1.29) reduces to

$$\eta(X;\omega_{g_n}(\varepsilon)) = \eta(X;\omega_s) + \varepsilon r(X;\omega_{g_n}(\varepsilon)) \ , \quad with \ r(X;\omega_{g_n}(\varepsilon)) = O(1) \quad , \tag{1.53}$$

where

$$\eta(X;\omega_s) = 2\left[\int_{X_s}^{X} \sqrt{2\frac{\omega_0(r)-\omega_s}{\omega_{kk}(r)}}dr\right]^{1/2} \quad . \tag{1.54}$$

In the present case, the square root function is analytic everywhere since, near X_s, $\omega_0(r) - \omega_s \sim \frac{1}{2}\omega_{0XX}(r - X_s)^2$. As before, the branch is chosen so that $\eta(+;\omega_s)$ contains the positive real η axis, i.e. $-\pi/4 < arg\ \eta < \pi/4$ when X is in region $(+)$.

Provided that $m = 0$, relation (1.40) for the leading-order global frequencies is identically satisfied since $\eta_1(\omega_s) = 0$. Higher-order approximations to $\omega_{g_n}(\varepsilon)$ are generated by assuming an expansion of the form (1.41) with $\omega_{g_n}^{(0)} = \omega_s$. The first-order correction $\omega_{g_n}^{(1)}$ is given by (1.42). When $\eta(X;\omega_s)$ takes the form (1.54), expression (1.67) for $\gamma_{0_1}(\omega_s)$ can be calculated explicitly to yield

$$\gamma_{0_1}(\omega_s) = \frac{ik_{0X}^s}{2}\sqrt{\frac{\omega_{kk}^s}{\omega_{0XX}^s}} \quad , \tag{1.55}$$

where the superscript s indicates evaluation at the saddle point X_s.

The following simple reasoning ensures that the square root appearing in (1.55) is interpreted correctly. The determination chosen for $\sqrt{\omega_{kk}^s/\omega_{0XX}^s}$ should correspond to the branch selected for the mapping $\eta(X;\omega_s)$ in (1.54). A Taylor expansion of

this relation in the immediate vicinity of X_s yields

$$\eta(X;\omega_s) \sim \left[4\frac{\omega^s_{0XX}}{\omega^s_{kk}}\right]^{1/4}(X-X_s) \quad . \tag{1.56}$$

According to the rule stated in connection with (1.54), the sector $\eta(+;\omega_s)$ in the vicinity of the origin, delimited by $-\pi/4 < arg\ \eta < \pi/4$, should map into the (+) sector close to X_s. As implied by (1.56), this sector is bounded by the straight lines

$$-\frac{\pi}{4}+\frac{1}{2}arg\sqrt{\frac{\omega^s_{kk}}{\omega^s_{0XX}}} \leq arg(X-X_s) \leq \frac{\pi}{4}+\frac{1}{2}arg\sqrt{\frac{\omega^s_{kk}}{\omega^s_{0XX}}} \quad . \tag{1.57}$$

The branch of the square root in (1.55) should therefore be such that $\frac{1}{2}arg\sqrt{\omega^s_{kk}/\omega^s_{0XX}}$ denotes a direction around X_s that points into the (+) sector of the complex X plane.

The expression for $\dfrac{\partial\gamma_{0_0}}{\partial\omega}(\omega_s)$ reduces to

$$\frac{\partial\gamma_{0_0}}{\partial\omega}(\omega_s) = \frac{\varsigma}{\omega_{kk}}\sqrt{\frac{\omega^s_{kk}}{\omega^s_{0XX}}} \quad , \tag{1.58}$$

where the square root is defined in the manner discussed above. The unknown $\varsigma = \pm 1$ has been added to account for the fact that (1.55) and (1.58) do not necessarily correspond to the same definition of the square root. Its value needs to be chosen so that the branches in $\dfrac{\partial\gamma_{0_0}}{\partial\omega}(\omega_s)$ and $\gamma_{0_0}(\omega_s)$ are the same. Unfortunately, unlike type 1 configurations, the leading-order equation for the frequency reduces to $\gamma_{0_0}(\omega_s) = 0$: it is satisfied for both branches and a conclusion cannot be reached. We therefore leave ς temporarily undetermined and appeal to a different reasoning in order to settle this point, as discussed below.

Upon substituting the expressions (1.55) and (1.58) into (1.42), the first order correction $\omega^{(1)}_{g_n}$ is found to be

$$\omega^{(1)}_{g_n} = \varsigma\left[-\frac{i}{2}k^s_{0X}\omega^s_{kk}+(n+1/2)\omega^s_{kk}\sqrt{\frac{\omega^s_{0XX}}{\omega^s_{kk}}}\right] \quad , \tag{1.59}$$

where the square root is defined as in (1.55). According to this result, $\omega_{g_n}(\varepsilon)$ moves away from ω_s as the mode index n increases, so that the type 2 Stokes line network (figure 1.10b) must gradually evolve into a type 1 configuration (figure 1.10a) with two distinct turning points $X_1[\omega_{g_n}(\varepsilon)]$ and $X_2[\omega_{g_n}(\varepsilon)]$. The expansion of the definition $\omega_0[X_j(\omega_{g_n}(\varepsilon))] = \omega_{g_n}(\varepsilon),\ j = 1, 2$, around X_s leads to the leading-order approximation

$$\frac{\omega^s_{0XX}}{2}(X_j - X_s)^2 \sim \omega^{(1)}_{g_n}\varepsilon \quad ,$$

whereby the separation distance between X_1 and X_2 can be estimated as

$$[X_2(\omega_{g_n}) - X_1(\omega_{g_n})]^2 = \frac{\omega^{(1)}_{g_n}}{\omega^s_{0XX}}\varepsilon + O(\varepsilon^2) \quad . \tag{1.60}$$

As n increases, the two turning points move away from each other along a line of angle $\frac{1}{2}arg\left[\omega^{(1)}_{g_n}/\omega^s_{0XX}\right]$, which, from (1.59), can be estimated as $\frac{1}{2}arg\left\{\varsigma\sqrt{\frac{\omega^s_{kk}}{\omega^s_{0XX}}}\right\}$ for sufficiently large n. In order to give rise to a type 1 configuration (figure 1.10a), this angle must lie within the sector (+) specified in (1.57) or the directly opposite sector (−). The value $\varsigma = 1$ must therefore be selected. It can be concluded that type 2 global frequencies form a discrete set given by

$$\omega_{g_n}(\varepsilon) \sim \omega_s + \varepsilon\left[-\frac{i}{2}k^s_{0X}\omega^s_{kk} + (n + 1/2)\omega^s_{kk}\sqrt{\frac{\omega^s_{0XX}}{\omega^s_{kk}}}\right] + O(\varepsilon^2) \quad , \tag{1.61}$$

where the branch of the square root is such that the direction around X_s of angle $\frac{1}{2}arg\sqrt{\frac{\omega^s_{0XX}}{\omega^s_{kk}}}$ points into region (+) or (−) of the complex X plane. It should be emphasized that in the configuration of figure 1.10d, this rule is equivalent to the selection of the square root satisfying $\Re e\sqrt{\frac{\omega^s_{0XX}}{\omega^s_{kk}}} > 0$. But in twisted configurations such as the one on figure 1.10b, this rule implies $\Re e\sqrt{\frac{\omega^s_{0XX}}{\omega^s_{kk}}} < 0$.

The variations of the growth rate with mode index n may now be determined in the vicinity of ω_s. If $\Im m\left[\omega^s_{kk}\sqrt{\frac{\omega^s_{0XX}}{\omega^s_{kk}}}\right] < 0$, the growth rate $\Im m\ \omega_{g_n}$ is maximum when $n = 0$, which corresponds to the most unstable type 2 global mode. If $\Im m\left[\omega^s_{kk}\sqrt{\frac{\omega^s_{0XX}}{\omega^s_{kk}}}\right] > 0$, the growth rate increases with the mode index n and type 2 global modes are not the most unstable, as discussed in subsection 1.5.5.

For any fixed n, the global mode eigenfunction of frequency ω_{g_n} admits the uniform approximation (1.25) which reduces at leading order in ε to

$$\psi(X;\omega_{g_n},\varepsilon) \sim \left\{ B_0(X;\omega_{g_n}) V_n \left[\frac{\eta(X;\omega_{g_n})}{\sqrt{\varepsilon}} \right] + \sqrt{\varepsilon} C_0(X;\omega_{g_n}) V_n' \left[\frac{\eta(X;\omega_{g_n})}{\sqrt{\varepsilon}} \right] \right\} e^{\frac{i}{\varepsilon}\int_{X_s}^{X} k_0(s)ds}, \tag{1.62}$$

where $B_0(X;\omega)$ and $C_0(X;\omega)$ are expressed in (1.68a,b) and $V_n(\xi)$ is given by (1.36). Although this approximation is of the same form as for type 1 global modes, the computation for a given X is in the present case much easier because n is fixed. As outlined in Appendix C, expression (1.62) can be further simplified by making use of eigenrelation (1.61), definition (1.29) for the transformation $X \mapsto \eta(X;\omega)$, and expressions (1.68a,b) for B_0 and C_0. According to (1.84) and (1.85), the final result can be expressed as

$$\psi(X;\omega_{g_n},\varepsilon) \sim \alpha_0 \left(\frac{\partial \eta}{\partial X}(X;\omega_s) \right)^{-1/2} H e_n \left[\frac{\eta(X;\omega_s)}{\sqrt{\varepsilon}} \right] e^{i\Theta(X;\omega_s) - \frac{\omega_{g_n}^{(1)}}{4\varepsilon} \frac{\partial(\eta^2)}{\partial \omega}(X;\omega_s)} \times e^{-\frac{\eta^2(X;\omega_s)}{4\varepsilon}} e^{\frac{i}{\varepsilon}\int_{X_0}^{X} k_0(s)ds}. \tag{1.63}$$

We recall that $\eta(X;\omega_s)$, $\Theta(X;\omega_s)$ and $\omega_{g_n}^{(1)}$ are given by (1.54), (1.69) and (1.59), respectively. The derivative $\dfrac{\partial(\eta^2)}{\partial\omega}(X;\omega_s)$ is computed in Appendix C and given by (1.87) and, as for type 1 global modes, α_0 and X_0 are constants that can be arbitrarily specified. Expression (1.63), as expression (1.62), is valid in the entire complex X plane including the double turning point X_s.

1.5.5 Frequency selection criteria

In this section, necessary and sufficient conditions for global instability are examined in succession, together with frequency selection criteria.

Necessary condition for global instability

From the previous analysis, one readily obtains an upper bound on the global mode growth rates

$$\omega_{g_n,i} \leq \omega_{0,i}^{max} \quad , \tag{1.64}$$

where we recall that $\omega_{0,i}^{max}$ is the maximum value reached by the absolute growth rate on the real X axis. The proof of this inequality directly follows from the nature of the Stokes line networks when $\omega_i > \omega_{0,i}^{max}$, as sketched in figure 1.6a,b. These configurations fall within none of the types associated with global modes, as discussed in subsections 5(c), 5(d), and illustrated in figure 1.10, which proves inequality (1.64). This result already appeared as Theorem 1 in Chomaz *et al.* (1991), but the proof was incomplete : configurations such as those of figure 1.6b were not explicitly shown not to correspond to global modes.

The following statement immediately follows from inequality (1.64) : **If $\omega_{0,i}^{max} < 0$, the medium is globally stable**. In other words, **the presence of a region of absolute instability is a necessary condition for the existence of an amplified global mode**, as already argued in Chomaz *et al.* (1991).

Sufficient conditions for global instability

By summarizing the results of subsection 1.5.4, the following sufficient condition is obtained : if there exists a global mode of positive growth rate $\omega_{g,i}$ that is associated with either two simple turning points (type 1) or a double turning point (type 2), the medium is globally unstable.

If, in particular, the absolute frequency $\omega_0(X)$ admits a saddle point X_s defined by $\dfrac{d\omega_0}{dX}(X_s) = 0$, and such that $\omega_{0,i}(X_s) > 0$, X_s is a double turning point with a Stokes line network that is necessarily type 2. According to subsection 1.5.4, the complex absolute frequency $\omega_s \equiv \omega_0(X_s)$ is then, at leading order in ε, a global frequency. The following sufficient condition therefore holds : **If the absolute fre-**

quency $\omega_0(X)$ presents a saddle point X_s with $\omega_{0,i}(X_s) > 0$, the medium is globally unstable.

However, it should be emphasized that, in such circumstances, type 2 global modes are not necessarily the most amplified. **The most unstable global mode may correspond to a double turning point type 2 configuration, in which case the dominant global frequency is given by formula (1.61) with $n = 0$. But, it may also very well correspond to a type 1 configuration with two simple turning points, in which case the global frequency is the root of equation (1.44) for a mode index $n(\varepsilon) \sim m/\varepsilon$ associated with a local maximum of $\omega_{g_n,i}$.**

In any case, **the leading-order approximation $\omega_g^{(0)}$ to the most unstable global frequency is confined to the bounds**

$$\omega_{s,i} \leq \omega_{g,i}^{(0)} \leq \omega_{0,i}^{max} \quad . \tag{1.65}$$

This result only holds when $\omega_{g,i}^{(0)} \geq \omega_i^{max}(\infty)$ as it has been pointed out in subsection 1.5.3.

Geometrical interpretation

It has been shown that Stokes line configurations giving rise to global modes present either a double turning point (figures 1.10b,d) or two simple turning points connected by a common Stokes line (figures 1.10a,c). This property has enabled us to prove that all global modes frequencies lie on the curve Δ in the complex ω plane defined by the single condition (1.43) that both turning points are connected by a Stokes line. Furthermore, as mentioned in subsection 1.5.3, if we partition the curve Δ into "no global mode" and "global mode" sections (dashed lines and solid lines on figure 1.12, respectively), the "no global mode" and "global mode" sections correspond respectively to the sets Δ_o and Δ_1 introduced in section 1.3. All frequencies on the "no global mode" section are then such that regions (+) and

$(-)$ are contiguous, as illustrated on figure 1.12c. By contrast, all frequencies on the "global mode" section are such that regions $(+)$ and $(-)$ are not contiguous. In such situations, we have demonstrated the existence of a denumerable set of type 1 global frequencies that are spaced within $O(\varepsilon)$ of each other. It can further be shown that "global mode" and " no global mode" sections are separated by a type 2 global frequency ω_s. Qualitative changes in the Stokes line network can easily be traced in the complex η plane (figure 1.12c). When ω travels along the curve Δ from the "global mode" to the "no global mode" sides, the two turning points $\eta_1(\omega)$ and $-\eta_1(\omega)$ collide at the origin and reemerge on the vertical η axis in a "no global mode" configuration. Finally, for frequencies lying outside the curve Δ, the Stokes line connection between both turning points is broken, as sketched in figure 1.12c.

Two distinct situations (figure 1.12a,b) may now be envisioned for the shape of the curve Δ. If the "global mode" section of Δ exhibits a local maximum sufficiently far away from ω_s, at a complex frequency $\omega^{(0)}$ such that $\omega_i^{(0)} > \omega_{s,i}$ (figure 1.12a), the most unstable global mode is necessarily type 1. If that local maximum is lower that $\omega_{s,i}$ or is absent, the most unstable global frequency is then type 2 (figure 1.12b).

Note that, near a type 1 local maximum, unstable global modes exhibit growth rates differing by $O(\varepsilon^2)$, in agreement with the analysis of subsection 1.5.4. If the most unstable global mode is type 2, the growth rates of neighboring modes are separated by $O(\varepsilon)$, as can be observed from (1.61).

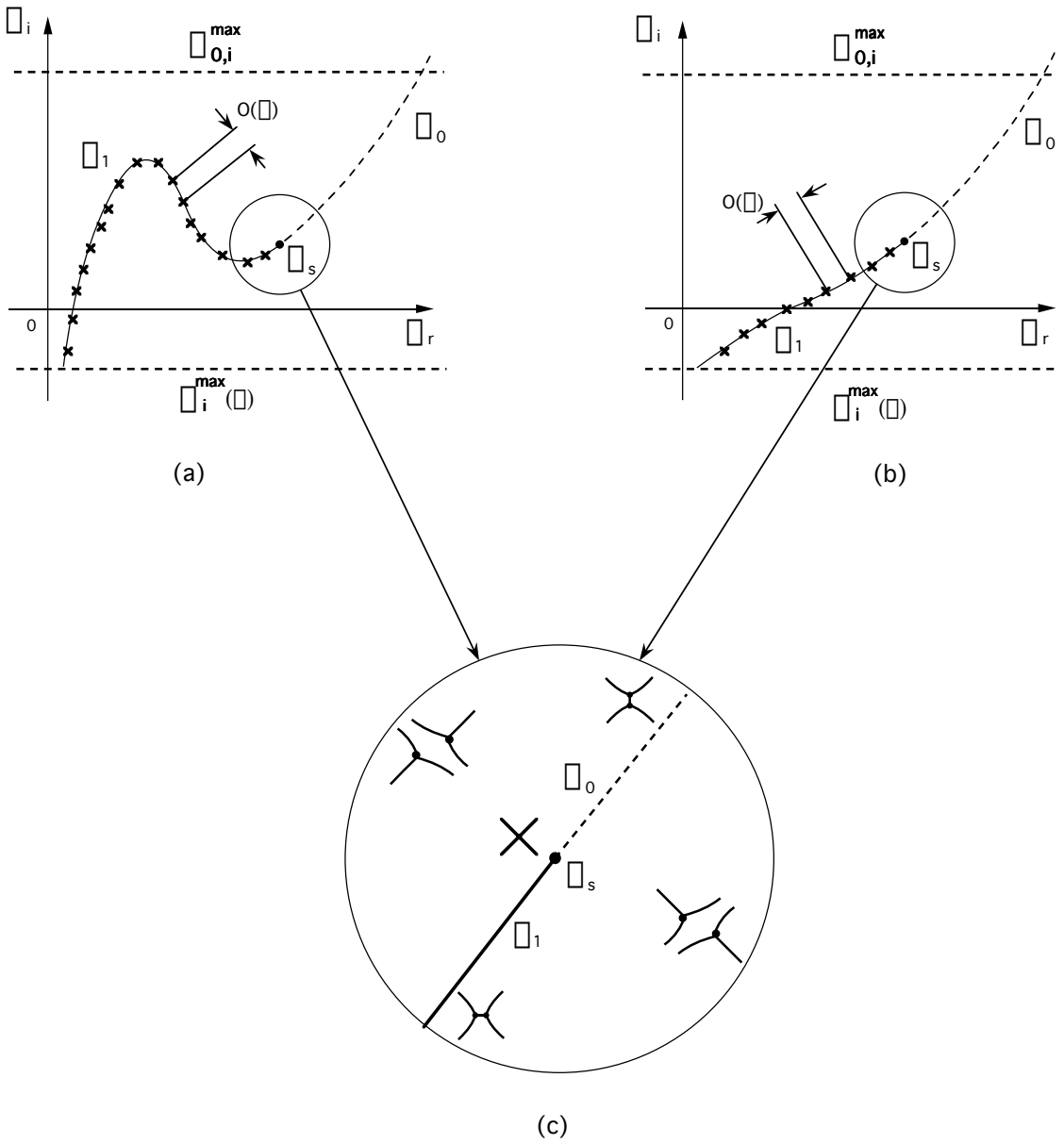

FIG. 1.12 - *Sketches of possible global frequency distributions in complex ω plane. Curve Δ is defined by equation (1.15) in the text. – – –: Δ_o, "no global mode" section of Δ. ——: Δ_1, "global mode" section of Δ. $\times$: location of type 1 global mode. $\bullet$: type 2 global mode. (a) : most unstable global mode is type 1. (b) : most unstable global mode is type 2. (c) : Qualitative changes in Stokes line network of the complex η plane as ω is displaced around ω_s.*

1.6 Discussion and conclusions

The main results of this investigation may be summarized in the following way. Global frequency selection criteria have been established for a class of systems governed by the linearised Ginzburg-Landau equation with slowly varying coefficients, when at most two turning points influence the spatial structure of perturbations in physical space. The complex frequencies of unstable global modes fall within two broad classes, according to the nature of the Stokes line network in the complex X plane. Type 1 global modes are associated with two simple turning points connected by a common Stokes line with no contiguous $(+)$ and $(-)$ regions. Corresponding frequencies are the roots of eigenvalue relation (1.45) with $n = O(1/\varepsilon)$. Type 2 global modes arise when both turning points merge into a double turning point X_s. Selected frequencies are then given by (1.61) where $\omega_s = \omega_0(X_s)$ is defined by the saddle point condition (1.52b). The most unstable global mode may either be type 1 (figure 1.12a) or type 2 (figure 1.12b), depending on the shape of the curve(s) supporting the eigenvalues in the complex ω plane. Finally, by reducing the Ginzburg-Landau equation to a single comparison equation, uniformly valid approximations to the spatial eigenfunctions have been derived, in a domain containing both turning points.

The analysis of Chomaz *et al.* (1991) has been extended significantly in several respects. First, Chomaz *et al.* limited their study to type 2 global modes. More specifically, the Stokes line network was explicitly assumed to be of the "untwisted" kind (Assumption 2 and figure 5 of Chomaz *et al.* 1991), which allowed to prove that the most unstable global frequency is necessarily type 2 and given by ω_s. This restriction has been lifted here (compare figure 1.10b and figure 5 of Chomaz *et al.* 1991), and, as a result, it can be concluded that, in all generality, **the most unstable global mode may be type 1 or type 2**. Note that type 2 global frequencies (1.61) are identical to those calculated in Chomaz *et al.* Second, the leading-order approximation to the largest global growth rate is bounded from above

by the maximum absolute growth rate $\omega_{0,i}^{max}$ and from below by the growth rate $\omega_{s,i}$ at the saddle point X_s. The proof for the validity of the upper bound presented in Chomaz *et al.* (1991) has been completed. Third, instead of matching separate outer WKBJ expansion to inner expansions close to the turning points, we have obtained a single uniformly valid approximation for both type 1 and type 2 global mode eigenfunctions.

The present work has been restricted to the Ginzburg-Landau model equation with varying coefficients in a single space dimension. In order to be directly applicable to real flow situations, the cross-stream structure of the perturbations should be included within the setting of a linearised two-dimensional instability analysis around a slowly-diverging basis flow. Such a formulation has recently been presented by Monkewitz *et al.* (1993) for type 2 global modes in a streamwise domain that is doubly infinite. It is then found that type 2 global frequencies remain formally given by (1.61), the cross-stream structure being "slaved" to the streamwise evolution of the fluctuations. No comparable two-dimensional study of type 1 global modes has yet been undertaken and it remains to be determined whether type 1 eigenrelation (1.45) stays unchanged.

Experimental and numerical validations of the above global frequency selection criteria have been scarce and, for the most part, limited to testing the type 2 saddle point criterion of Chomaz *et al.* (1991). There is so far no evidence that type 1 global modes might dominate the dynamics of a specific spatially developing shear flow, but such structures have not actively been looked for. We therefore restrict the discussion to the validation of the type 2 criterion with the underlying provisional assumption that type 1 global modes are less unstable (figure 1.12b).

The numerical simulations of Hannemann & Oertel (1989) clearly demonstrate that, in the case of the wake behind a plate of thickness h, the computed global frequency is nearly equal to the absolute frequency taken at the location $x/h = 1$. As

discussed in Monkewitz *et al.* (1993), the absolute frequency $\omega_0(X)$ exhibits a saddle point close to that location and the present type 2 saddle point criterion is then in good agreement with numerical observations. Note also that the computed global frequency is very close to the absolute frequency at the transition point between absolute and convective instability [Koch (1985)'s criterion]. More recently, Schär & Smith (1993) have numerically investigated the flow behind a vertical circular cylinder in the shallow-water wave régime. At a critical value of the Froude number, the wake is observed to undergo a transition to large scale Kármán vortex shedding. When all nonlinear terms in the numerical code are turned off, the wake beats at a global frequency $\omega_g \approx 0.17 + 0.045\ i$. Local stability calculations performed on the unstable basic state then indicate the presence of a broad region of absolute instability behind the obstacle. The function $\omega_0(X)$ can be estimated from a parabolic fit near the maximum absolute growth rate and application of the criterion (1.52a,b) leads to the prediction $\omega_g \approx 0.19 + 0.040\ i$, which compares very favourably with the computed value. Note, however, that, when all nonlinearities are restored, the observed Strouhal frequency becomes $\omega_g \approx 0.27$, which is noticeably different from the predicted value. A similar approach has been applied by Huerre & Monkewitz (1990) to estimate the frequency of the preferred mode in two-dimensional jets from experimental data. As in the preceding case, the reconstruction of $\omega_0(X)$ from a parabolic fit leads to $\omega_g \approx 0.225$ to be compared with the measured value $\omega_g \approx 0.25$.

The above validation procedure can only be viewed as preliminary. A more thorough implementation of the frequency selection criteria requires a careful analytic continuation of the local quantities $\omega_0(X)$, $k_0(X)$, etc. from the real X axis into the complex X plane. Unfortunately, the number, location and structure of turning points are very sensitive to slight changes in the numerical or experimental data on the real X axis. This sensitivity becomes particularly acute when turning points

that are implicated in the global mode structure, i.e. those with at least one Stokes line crossing the real X axis, are located far into the complex X plane. It is then practically impossible to determine how many turning points are involved and their respective locations. In the favourable case where a saddle point X_s lies close to the real axis, one might envision reducing the physical domain of interest on the real axis to a finite segment around X_s, say $|X| < A$ as shown on figure 1.13. The (+)

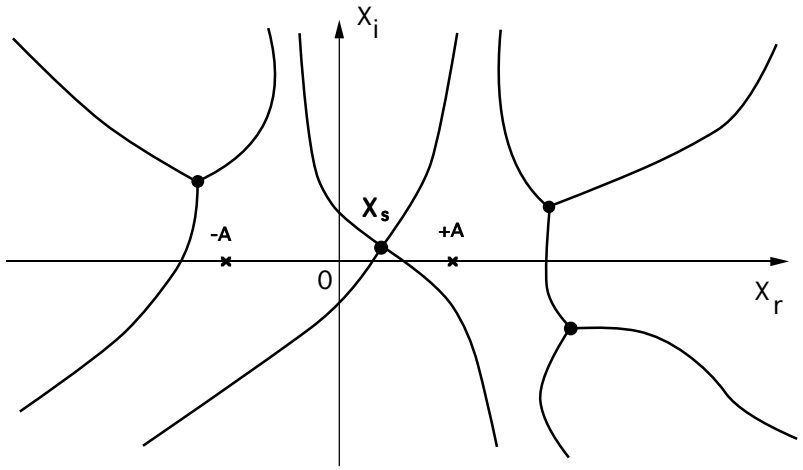

FIG. 1.13 - *Example of domain reduction to a two-turning-point problem. The regions* (+) *and* (−) *are transferred in the neighborhood of the saddle point* X_s *of* $\omega_0(X)$ *to the regions delimited by Stokes lines containing the points* $-A$ *and* $+A$*, respectively.*

and (−) regions could then be defined as those containing $X = A$ and $X = -A$ respectively and a subdominant solution could be built on the finite interval as long as no other turning point is involved.

In the experiments on wakes, low-density jets and counterflow mixing layers alluded to in the introduction, global modes are isolated and seem to set in via a Hopf bifurcation, the modal amplitude being governed by a Landau equation close to onset, to a very good degree of approximation. Preliminary studies of weakly nonlinear effects for type 2 global modes have been undertaken by Chomaz, Huerre & Redekopp (1990) and Le Dizès, Huerre, Chomaz & Monkewitz (1993) in the context of

the present Ginzburg-Landau model. The results indicate that the Landau equation has a severely restricted range of validity in the limit of weak spatial nonuniformities, unless restrictive assumptions are made concerning the location of the saddle point X_s. In such a case, one may further include the cross-stream structure and extend the weakly nonlinear analysis to two-dimensional spatially-developing flows in the viscous critical layer régime (Le Dizès, Monkewitz & Huerre, 1991).

The authors wish to thank P. G. Drazin for drawing their attention to early pertinent work on global modes. They are grateful to M. Pesenson for many helpful discussions. They are also indebted to Colonel Buck Danny and Major Sonny Tucson for their useful comments on the final manuscript.

This investigation was supported by the Direction des Recherches, Etudes et Techniques of the French Ministry of Defense under Grants # 90-040 and 92-098 (SLD, PH, JMC), by SNECMA (SLD), by the US Office of Naval Research under Grant # N00014-90-J-1313 (SLD, PAM) and by AFOSR under Grant # F49620-92-J-0471 (PAM). The Laboratoire d'Hydrodynamique (LadHyX) is part of URA 317 of the CNRS.

Appendix A: some analytical results for the two-turning-point problem.

In the following, a few analytical results pertaining to the two-turning-point problem are extracted from the earlier study by Lynn & Keller (1970). The functions $R_0(X;\omega)$ and $R_1(X)$ that repeatedly appear in the expressions below, have been defined in (1.18a,b) in terms of the local dispersion relation characteristics.

The first-order term $\gamma_{0_1}(\omega)$ in expansion (1.27) is given by (LK 6.21) as follows

$$\gamma_{0_1}(\omega) = \frac{\int_{X_1(\omega)}^{X_2(\omega)} R_1(X)/\sqrt{R_0(X;\omega)}dX}{\int_{X_1(\omega)}^{X_2(\omega)} 4\sqrt{R_0(X;\omega)}/[\eta_1^2(\omega)-\eta^2(X;\omega)]dX} \quad , \tag{1.66}$$

where the integration path joining $X_1(\omega)$ to $X_2(\omega)$ should avoid crossing the branch cut of the square root and be identical for both integrals. With the use of a closed contour C encircling both turning points, this expression can be rewritten as

$$\gamma_{0_1}(\omega) = \frac{\oint_C R_1(X)/\sqrt{R_0(X;\omega)}dX}{\oint_C 4\sqrt{R_0(X;\omega)}/[\eta_1^2(\omega)-\eta^2(X;\omega)]dX} \quad . \tag{1.67}$$

The leading-order terms $B_0(X;\omega)$ and $C_0(X;\omega)$ in expansions (1.20a,b) for $B(X;\omega,\varepsilon)$ and $C(X;\omega,\varepsilon)$ are given by expressions (LK 3.10) and (LK 3.11) as

$$B_0(X;\omega) = \alpha_0[\frac{\partial\eta}{\partial X}(X;\omega)]^{-1/2}\cos\Theta(X;\omega) \quad , \tag{1.68a}$$

$$C_0(X;\omega) = \alpha_0[\frac{\partial\eta}{\partial X}(X;\omega)]^{1/2}[R_0(X;\omega)]^{-1/2}\sin\Theta(X;\omega) \quad , \tag{1.68b}$$

with $\Theta(X;\omega)$ defined by (LK 6.20) as

$$\Theta(X;\omega) = \frac{1}{2}\int_{X_1(\omega)}^{X}\left[\frac{R_1(X)}{R_0^{1/2}(X;\omega)} - \frac{4\gamma_{0_1}(\omega)R_0^{1/2}(X;\omega)}{\eta_1^2(\omega)-\eta^2(X;\omega)}\right]dX \quad . \tag{1.69}$$

Note that function $\Theta(X;\omega)$ satisfies $\Theta(X_1(\omega),\omega) = \Theta(X_2(\omega),\omega) = 0$ by definition of $\gamma_{0_1}(\omega)$.

Appendix B : Type 1 global eigenfunctions.

In this appendix, the uniform approximation (1.48) for type 1 global modes is reduced by deriving when $\varepsilon \to 0$ appropriate asymptotic expansions of $He_{n(\varepsilon)}(\eta/\sqrt{\varepsilon})$ and $He'_{n(\varepsilon)}(\eta/\sqrt{\varepsilon})$. The underlying idea is to seek further approximations for the functions $V_{n(\varepsilon)}(\eta/\sqrt{\varepsilon})$ and $V'_{n(\varepsilon)}(\eta/\sqrt{\varepsilon})$ defined in (1.36), in the limit $\varepsilon \to 0$, bearing in mind that $n(\varepsilon) \sim m/\varepsilon$. For this purpose, it is convenient to evaluate the Hermite polynomials $He_{n(\varepsilon)}(\eta/\sqrt{\varepsilon})$ by applying the method of the steepest descent to their integral representation. The results are then substituted into (1.25) to generate local approximations for the global mode eigenfunctions in different regions of the complex X plane.

The integral representation of $\mathrm{He}_n(x)$ given in Bender & Orszag (1978), p 574, reads

$$He_n(x) = \sqrt{\frac{2}{\pi}} e^{\frac{x^2}{2}} \int_0^{+\infty} e^{-\frac{r^2}{2}} r^n \cos(rx - n\pi/2) dr \quad ,$$

equivalently

$$He_n(x) = \frac{1}{2}\sqrt{\frac{2}{\pi}} e^{\frac{x^2}{2}} \int_{-\infty}^{+\infty} e^{-\frac{r^2}{2}} r^n e^{irx - in\pi/2} dr \quad . \tag{1.70}$$

Upon substituting (1.70) into (1.36), one obtains :

$$V_{n(\varepsilon)}(\eta/\sqrt{\varepsilon}) = \frac{1}{2}\sqrt{\frac{2}{\pi}} e^{\frac{-in\pi}{2}} \left[\frac{2m}{\varepsilon}\right]^{(n+1)/2} e^{-\frac{\eta^2}{4\varepsilon}} \int_{-\infty}^{+\infty} r^{n-\frac{m}{\varepsilon}} e^{-\frac{m}{\varepsilon}\left[(r-\frac{i\eta}{\sqrt{2m}})^2 - \ln r\right]} dr \ ,$$

$$V'_{n(\varepsilon)}(\eta/\sqrt{\varepsilon}) = \frac{1}{2}\sqrt{\frac{2}{\pi}} e^{\frac{-i(n-1)\pi}{2}} \left[\frac{2m}{\varepsilon}\right]^{(n+2)/2} e^{-\frac{\eta^2}{4\varepsilon}} \int_{-\infty}^{+\infty} r^{n-\frac{m}{\varepsilon}} e^{-\frac{m}{\varepsilon}\left[(r-\frac{i\eta}{\sqrt{2m}})^2 - \ln r\right]} dr \ .$$

These expressions can be recast into the following compact form :

$$V_{n(\varepsilon)}(\eta/\sqrt{\varepsilon}) = C_\varepsilon I_\varepsilon(\eta) e^{-\frac{\eta^2}{4\varepsilon}} \quad , \tag{1.71a}$$

$$V'_{n(\varepsilon)}(\eta/\sqrt{\varepsilon}) = e^{\frac{i\pi}{2}} \sqrt{\frac{2m}{\varepsilon}} C_\varepsilon J_\varepsilon(\eta) e^{-\frac{\eta^2}{4\varepsilon}} \quad , \tag{1.71b}$$

with

$$I_\varepsilon(\eta) = \int_{-\infty}^{+\infty} r^{n-m/\varepsilon} e^{-\frac{m}{\varepsilon} f(r;\eta)} dr \quad , \tag{1.72a}$$

$$J_\varepsilon(\eta) = \int_{-\infty}^{+\infty} r^{n+1-m/\varepsilon} e^{-\frac{m}{\varepsilon} f(r;\eta)} dr \quad , \tag{1.72b}$$

$$C_\varepsilon = \frac{1}{2}\sqrt{\frac{2}{\pi}} e^{\frac{-in\pi}{2}} \left[\frac{2m}{\varepsilon}\right]^{(n+1)/2} \quad , \tag{1.72c}$$

$$f(r;\eta) = (r - \frac{i\eta}{\sqrt{2m}})^2 - \ln r \quad . \tag{1.72d}$$

The behavior of both integrals $I_\varepsilon(\eta)$ and $J_\varepsilon(\eta)$ when $\varepsilon \to 0$ can be determined by applying the method of steepest descent to the function $f(r;\eta)$, the variations of the factors appearing in front of the exponentials being negligible when $n - m/\varepsilon \ll m/\varepsilon$. As explained in standard text books (Bender & Orszag 1978, chapter 6), the principle of the method consists in deforming the contour of integration into lines $\Im m[f(r;\eta)] = const$ which are also steepest-descent paths of $\Re e[f(r;\eta)]$, and searching for the saddle point(s) $r(\eta)$ where $\Re e[f(r;\eta)]$ reaches a minimum on that path. The main contribution to the integral as $\varepsilon \to 0$ is then found to arise from the neighborhood of the saddle points $r(\eta)$ satisfying the condition $\dfrac{\partial f}{\partial r}(r(\eta);\eta) = 0$. In the present case, expression (1.72d) tells us that the function $f(r;\eta)$ admits only 2 saddle points given by

$$r^\pm(\eta) = \frac{i\eta \pm i\sqrt{\eta^2 - 4m}}{2\sqrt{2m}} \quad . \tag{1.73}$$

When $r^+(\eta)$ and $r^-(\eta)$ are distinct, there exist two possible candidates for the leading-order approximations to $I_\varepsilon(\eta)$ and $J_\varepsilon(\eta)$ as $\varepsilon \to 0$:

$$I_\varepsilon^\pm(\eta) = \left[r^\pm(\eta)\right]^{n-m/\varepsilon} e^{-\frac{m}{\varepsilon} f(r^\pm(\eta);\eta)} \sqrt{\frac{2\pi\varepsilon}{m\partial_r^2 f(r^\pm(\eta);\eta)}} \quad , \tag{1.74a}$$

$$J_\varepsilon^\pm(\eta) = r^\pm(\eta) I_\varepsilon^\pm(\eta) \quad . \tag{1.74b}$$

These expressions have been obtained by expanding the function $f(r,\eta)$ near each saddle point $r^\pm(\eta)$ according to $f(r;\eta) = f(r^\pm(\eta),\eta) + \frac{(r-r^\pm(\eta))^2}{2}\partial_r^2 f(r^\pm(\eta),\eta) + \cdots$,

the contribution to the integrals $I_\varepsilon(\eta)$ and $J_\varepsilon(\eta)$ from each saddle point being then a trivial Gaussian integral.

If one proceeds to a detailed analysis of the topography of the $\Im m[f(r,\eta)] = const$ contours, one can in fact show that the leading-order contribution to the integrals $I_\varepsilon(\eta)$ and $J_\varepsilon(\eta)$ always arises from the neighborhood of the same saddle point $r^+(\eta)$, if the branch cut and branch of the square root in (1.73) are chosen to be the interval $[-2\sqrt{m}, 2\sqrt{m}]$ of the real η_r axis and such that

$$-\frac{\pi}{2} < arg(\sqrt{\eta^2 - 4m}) \leq \frac{\pi}{2} \; when \; -\frac{\pi}{2} < arg(\eta) \leq \frac{\pi}{2} \quad . \tag{1.75}$$

Thus, for that particular determination, we obtain

$$I_\varepsilon(\eta) \sim I_\varepsilon^+(\eta) \quad , \tag{1.76a}$$

$$J_\varepsilon(\eta) \sim r^+(\eta) I_\varepsilon^+(\eta) \quad . \tag{1.76b}$$

Nevertheless, there are two localized regions in the complex η plane where these approximations are not valid (see figure 1.11).

The first region is for η values close to the turning points $\pm 2\sqrt{m} = \pm\eta_1(\omega_{g_n}^{(0)})$. At turning points, both saddle points $r^+(\eta)$ and $r^-(\eta)$ collide at a single point $r_o(\pm 2\sqrt{m}) = \pm i/\sqrt{2}$ to create a zero of $f(r;\eta)$ of order two such that
$\partial_r f(r_o(\pm 2\sqrt{m}), \pm 2\sqrt{m}) = 0$ and $\partial_r^2 f(r_o(\pm 2\sqrt{m}), \pm 2\sqrt{m}) = 0$.
Note in particular that the function $1/\partial_r^2 f(r^+(\eta), \eta)$ being infinite at $\eta = \pm 2\sqrt{m}$, the approximation (1.74a) for $I_\varepsilon(\eta)$ could not possibly remain valid. In disks of radius $O(\varepsilon^{2/3})$ around each turning point $\pm 2\sqrt{m}$, $I_\varepsilon(\eta)$ and $J_\varepsilon(\eta)$ are found to be of the form

$$I_\varepsilon(\eta) \sim 2\pi \left(\frac{\varepsilon}{2\sqrt{2}m}\right)^{1/3} \left(\frac{\pm i}{\sqrt{2}}\right)^n e^{\frac{m(-3\pm 2\eta/\sqrt{m})}{2\varepsilon}} Ai\left[\left(\frac{2\sqrt{2}m}{\varepsilon}\right)^{2/3} \left(\frac{\eta}{2\sqrt{m}} \mp 1\right)\right], \tag{1.77a}$$

$$J_\varepsilon(\eta) \sim \pm\frac{i}{\sqrt{2}} I_\varepsilon(\eta) \; , \tag{1.77b}$$

where the upper and lower signs refer to approximations near $+2\sqrt{m}$ and $-2\sqrt{m}$, respectively. To derive approximations (1.77a,b), $f(r;\eta)$ is expanded around the

second-order saddle point $r_0(\pm 2\sqrt{m}) = \pm i/\sqrt{2}$ that gives the dominant contribution to the integrals as done in order to obtain (1.74a,b). The expressions (1.77a,b) are then easily generated from (1.72a,b) if one further recalls the following integral representation for Ai (Bender & Orszag 1978, p. 313):

$$Ai(x) = \frac{1}{2\pi i} \int_{\infty e^{-2\pi i/3}}^{\infty e^{2\pi i/3}} e^{xs - s^3/3} ds \quad .$$

The approximations (1.76a,b) are also not valid in a strip of width $O(\varepsilon)$ along the Stokes line connecting both turning points $\pm 2\sqrt{m} = \pm \eta_1(\omega_{g_n}^{(0)})$. For values of η in that region, the contour of integration deformed along the lines $\Im m[f(r;\eta)] = const$ goes through both saddle points $r^+(\eta)$ and $r^-(\eta)$ and the contributions from each to the integrals (1.72a,b) are found to be of the same order. Approximations to $I_\varepsilon(\eta)$ and $J_\varepsilon(\eta)$ then do not reduce to a single contribution from the saddle point $r^+(\eta)$ but to the sum of both contributions from $r^+(\eta)$ and $r^-(\eta)$:

$$I_\varepsilon(\eta) \sim I_\varepsilon^+(\eta) + I_\varepsilon^-(\eta) \quad , \tag{1.78a}$$

$$J_\varepsilon(\eta) \sim r^+(\eta) I_\varepsilon^+(\eta) + r^-(\eta) I_\varepsilon^-(\eta) \quad . \tag{1.78b}$$

Everywhere in the complex η plane, except close to both turning points $\pm 2\sqrt{m}$ and close to the Stokes line that connects them (hatched and shaded regions in figure 1.11, respectively), $I_\varepsilon(\eta)$ and $J_\varepsilon(\eta)$ are given by (1.76a,b). The functions $V_{n(\varepsilon)}(\eta/\sqrt{\varepsilon})$ and $V'_{n(\varepsilon)}(\eta/\sqrt{\varepsilon})$ can then be computed using (1.71a,b) and the uniform approximation (1.48) for the global mode reduces to

$$\psi \sim C_\varepsilon I_\varepsilon^+(\eta) \left[B_0 + e^{-i\pi/2} \sqrt{2m} r^+(\eta) C_0 \right] e^{-\frac{\eta^2}{4\varepsilon}} e^{\frac{i}{\varepsilon} \int_{X_0}^{X} k_0(s) ds} \quad .$$

From expressions (1.68a,b) for B_0 and C_0 and the relation $\frac{\partial \eta}{\partial X} \sqrt{\eta^2 - 4m} = 2i\sqrt{R_0}$ obtained by differentiating (1.29) with respect to X, the expression within brackets can be simplified as:

$$\left[B_0 + e^{-i\pi/2} r^+(\eta) C_0 \right] = \alpha_0 \left(\frac{\partial \eta}{\partial X} \right)^{-1/2} e^{i\Theta} \quad .$$

It immediately follows that

$$\psi(X;\omega_{g_n},\varepsilon) \sim \frac{\alpha_0}{\sqrt{2}}\left[\frac{\eta+\sqrt{\eta^2-4m}}{2\sqrt{\varepsilon}}\right]^n \left[\frac{\eta+\sqrt{\eta^2-4m}}{\sqrt{\eta^2-4m}}\right]^{1/2}\left(\frac{\partial\eta}{\partial X}\right)^{-1/2} \times e^{i\Theta} e^{-\frac{1}{4\varepsilon}(2m+\eta\sqrt{\eta^2-4m})}\, e^{\frac{i}{\varepsilon}\int_{X_0}^{X} k_0(s)ds} \quad . \tag{1.79}$$

In the vicinity of the turning points $\pm 2\sqrt{m}$, using the expression (1.77a,b) for $I_\varepsilon(\eta)$ and $J_\varepsilon(\eta)$, the uniform approximation reduces to

$$\psi(X;\omega_{g_n},\varepsilon) \sim \alpha_0\sqrt{2\pi}(\pm 1)^n \left(\frac{m}{\varepsilon}\right)^{\frac{n}{2}+\frac{1}{6}} Ai\left[\left(\frac{2\sqrt{2}m}{\varepsilon}\right)^{2/3}\left(\frac{\eta}{2\sqrt{m}}\mp 1\right)\right] \times e^{-\frac{m}{\varepsilon}[\frac{3}{2}\mp\frac{\eta}{\sqrt{m}}+\frac{\eta^2}{4m}]}\, e^{\frac{i}{\varepsilon}\int_{X_0}^{X} k_0(s)ds} \quad . \tag{1.80}$$

Finally, near the Stokes line connecting $\pm 2\sqrt{m}$, by making use of (1.78a,b), the uniform approximation is obtained as :

$$\psi(X,\omega_{g_n},\varepsilon) \sim \left\{\left[\frac{\eta+\sqrt{\eta^2-4m}}{2\sqrt{\varepsilon}}\right]^n \left[\frac{\eta+\sqrt{\eta^2-4m}}{\sqrt{\eta^2-4m}}\right]^{1/2} e^{i\Theta} e^{-\frac{1}{4\varepsilon}(2m+\eta\sqrt{\eta^2-4m})} + \left[\frac{\eta-\sqrt{\eta^2-4m}}{2\sqrt{\varepsilon}}\right]^n \left[\frac{\eta-\sqrt{\eta^2-4m}}{\sqrt{\eta^2-4m}}\right]^{1/2} e^{-i\Theta} e^{-\frac{1}{4\varepsilon}(2m-\eta\sqrt{\eta^2-4m})}\right\} \times \frac{\alpha_0}{\sqrt{2}}\left(\frac{\partial\eta}{\partial X}\right)^{-1/2} e^{\frac{i}{\varepsilon}\int_{X_0}^{X} k_0(s)ds} \quad . \tag{1.81}$$

We note that equation (1.81) can be written as the superposition $\psi^+ + \psi^-$ of two distinct contributions ψ^+ and ψ^- which can be constructed from (1.25) by substituting $I_\varepsilon^+(\eta)$ and $I_\varepsilon^-(\eta)$ defined in (1.74a,b) into the expressions (1.71a,b) for V and V'. The resulting functions $\psi^+(X;\omega_{g_n},\varepsilon)$ and $\psi^-(X;\omega_{g_n},\varepsilon)$ take the form of local WKBJ approximations pertaining to spatial branches $k^+(X;\omega_{g_n})$ and $k^-(X;\omega_{g_n})$, respectively. When the condition $I_\varepsilon^+(\eta)/I_\varepsilon^-(\eta) = O(1)$, equivalently

$$\Re e\left\{f(r^+(\eta),\eta) - f(r^-(\eta),\eta)\right\} = \Im m\left[\int_{2\sqrt{m}}^{\eta}\sqrt{4m-s^2}ds\right] = 0 \quad ,$$

is fulfilled, both approximations ψ^+ and ψ^- become of the same order of magnitude, as one would expect on a Stokes line. Furthermore, one can easily show that $\Re e[f(r^+(\eta),\eta)] - \Re e[f(r^-(\eta),\eta)] > 0$ in regions $\eta(+;\omega_{g_n})$ and $\eta(-;\omega_{g_n})$, provided that the square root is defined according to (1.75). Approximation (1.79) for $\psi(X;\omega_{g_n},\varepsilon)$ then coincides with $\psi^+(X;\omega_{g_n},\varepsilon)$ in regions $\eta(+;\omega_{g_n})$ and $\eta(-;\omega_{g_n})$ and it is therefore subdominant. Following classical properties of the Stokes phenomenon, this subdominant WKBJ approximation remains valid in neighboring sectors of the complex η plane where it now becomes dominant.

Appendix C: type 2 global eigenfunctions.

This appendix is concerned with the reduction of uniform approximation (1.62) obtained for type 2 global modes.

Note first that when $\eta(X;\omega_{g_n}) = O(\sqrt{\varepsilon})$, i.e. when X is close to the double turning point X_s and satisfies $|X - X_s| = O(\sqrt{\varepsilon})$, two simplifications immediately occur : the second term in (1.62) becomes negligible with respect to the first one and expression (1.68a,b) for $B_0(X;\omega_{g_n})$ reduces to

$$B_0(X,\omega_{g_n}) \sim \alpha_0 \left(\frac{\partial \eta}{\partial X}(X;\omega_{g_s})\right)^{-1/2} \quad ,$$

Θ being $O(\sqrt{\varepsilon})$ when $|X - X_s| = O(\sqrt{\varepsilon})$. If, in addition, (1.53) is used to replace $\eta(X;\omega_{g_n})$ by its leading-order approximation $\eta(X;\omega_s)$, expression (1.62) may be written as

$$\psi(X;\omega_{g_n},\varepsilon) \sim \alpha_0 \left(\frac{\partial \eta}{\partial X}(X;\omega_s)\right)^{-1/2} He_n\left[\frac{\eta(X;\omega_s)}{\sqrt{\varepsilon}}\right] e^{-\frac{\eta^2(X;\omega_{g_n})}{4\varepsilon}} e^{\frac{i}{\varepsilon}\int_{X_s}^{X} k_0(s)ds} \quad . \tag{1.82}$$

Note that $\eta(X;\omega_{g_n})$ has not be replaced by $\eta(X;\omega_s)$ in the exponent of (1.82) because the $O(\varepsilon)$ correction induces an $O(1)$ amplitude correction as shown below.

When $\eta(X;\omega_{g_n}) \gg \sqrt{\varepsilon}$, i.e. when X is at a distance larger than $O(\sqrt{\varepsilon})$ from the double turning point X_s, the second term in (1.62) is no longer negligible but nevertheless the expression of $V_n'(\eta/\sqrt{\varepsilon})$ can be simplified. When $\eta(X;\omega_{g_n}) \gg \sqrt{\varepsilon}$, using again (1.53), one immediately shows that

$$V_n'\left[\frac{\eta(X;\omega_{g_n})}{\sqrt{\varepsilon}}\right] \sim -2\frac{\eta(X;\omega_s)}{\sqrt{\varepsilon}} He_n\left[\frac{\eta(X;\omega_s)}{\sqrt{\varepsilon}}\right] e^{-\frac{\eta^2(X;\omega_{g_n})}{4\varepsilon}} \quad .$$

Expression (1.62) is then written as

$$\psi(X;\omega_{g_n},\varepsilon) \sim He_n\left[\frac{\eta(X;\omega_s)}{\sqrt{\varepsilon}}\right] \{B_0(X;\omega_s) - 2\eta(X;\omega_s)C_0(X;\omega_s)\} \times e^{-\frac{\eta^2(X;\omega_{g_n})}{4\varepsilon}} e^{\frac{i}{\varepsilon}\int_{X_0}^{X} k_0(s)ds} \quad . \tag{1.83}$$

The expression within braces takes a simpler form if one appeals to the relation

$$\eta(X;\omega_s)\frac{\partial\eta}{\partial X}(X;\omega_s) = 2\sqrt{-R_0(X;\omega_s)} \quad ,$$

obtained by differentiating (1.54) with respect to X, and if expressions (1.68a,b) for $B_0(X;\omega)$ and $C_0(X;\omega)$ are invoked. The intermediate result then reads

$$\{B_0(X;\omega_s) - 2\eta(X;\omega_s)C_0(X;\omega_s)\} = \alpha_0\left(\frac{\partial\eta}{\partial X}(X;\omega_s)\right)^{-1/2} e^{i\Theta(X;\omega_s)} \quad .$$

It therefore follows that

$$\psi(X;\omega_{g_n},\varepsilon) \sim \alpha_0\left(\frac{\partial\eta}{\partial X}(X;\omega_s)\right)^{-1/2} He_n\left[\frac{\eta(X;\omega_s)}{\sqrt{\varepsilon}}\right] e^{i\Theta(X;\omega_s)} e^{-\frac{\eta^2(X;\omega_{g_n})}{4\varepsilon}} e^{\frac{i}{\varepsilon}\int_{X_0}^{X} k_0(s)ds} \quad . \tag{1.84}$$

Recall that $\Theta(X;\omega_s)$ is given by (1.69) in Appendix A and satisfies $\Theta(X_s;\omega_s) = 0$. Approximation (1.84) expanded near X_s then gives exactly the same result as (1.82) for the global mode in the region $|X - X_s| = O(\sqrt{\varepsilon})$. Thus, (1.84) remains valid for all X and can be considered as a uniform leading-order approximation.

These remains to evaluate the exponential factor of $e^{-\frac{\eta^2(X;\omega_{g_n})}{4\varepsilon}}$ when $\varepsilon \to 0$. Using expansion (1.41) for ω_{g_n}, $\eta^2(X;\omega_{g_n})$ can be approximated by its Taylor expansion around ω_s to give

$$e^{-\frac{\eta^2(X;\omega_{g_n})}{4\varepsilon}} \sim e^{-\frac{\eta^2(X;\omega_s)}{4\varepsilon}} e^{-\frac{\omega_{g_n}^{(1)}}{4\varepsilon}\frac{\partial(\eta^2)}{\partial\omega}(X;\omega_s)} \quad . \tag{1.85}$$

Both $\eta(X;\omega_s)$ and $\omega_{g_n}^{(1)}$ have already been calculated as (1.54) and (1.59) respectively. An expression for $\dfrac{\partial(\eta^2)}{\partial\omega}(X;\omega_s)$ has not yet been obtained and its computation requires a little algebra, as outlined in the rest of this appendix.

An expression involving $\dfrac{\partial\eta}{\partial\omega}(X;\omega)$ is generated by differentiating (1.29) with respect to ω :

$$\begin{aligned}\frac{\partial\eta}{\partial\omega}(X;\omega)\sqrt{\eta^2(X;\omega) - \eta_1^2(\omega)} + \frac{\partial(\eta_1^2)}{\partial\omega}(\omega)\int_{\eta_0}^{\eta(X;\omega)} \frac{ds}{\sqrt{s^2 - \eta_1^2(\omega)}} \\ = 2\int_{X_0}^{X} \frac{1}{\omega_{kk}(r)}\sqrt{\frac{\omega_{kk}(r)}{2(\omega_0(r) - \omega)}}dr \quad .\end{aligned} \tag{1.86}$$

This functional equation is independent of the definitions chosen for the various square roots, provided that the branches of the square roots appearing on the left-hand side of (1.86) are the images of those on the right-hand side through the mapping $X \mapsto \eta(X;\omega)$. However, the contour of integration should not cross any branch cut. A convenient selection of X_0 and of the integration path may have to be made in order to have that property satisfied. At the value $\omega = \omega_s$, the first term of (1.86) reduces to $\frac{1}{2}\frac{\partial(\eta^2)}{\partial\omega}(X;\omega_s)$. In addition, $\eta_1(\omega_s)$ is zero and, according to relations (1.32) and (1.58) with $\varsigma = 1$, $\frac{\partial(\eta_1^2)}{\partial\omega}(\omega_s)$ is equal to $\frac{1}{4\omega^s_{kk}}\sqrt{\frac{\omega^s_{kk}}{\omega^s_{0XX}}}$. One may then obtain from (1.86) the following expression :

$$\frac{\partial(\eta^2)}{\partial\omega}(X;\omega_s) = \int_{X_0}^{X} \frac{1}{\omega_{kk}(r)}\sqrt{\frac{\omega_{kk}(r)}{2(\omega_0(r)-\omega_s)}}dr - \frac{1}{8\omega^s_{kk}}\sqrt{\frac{\omega^s_{kk}}{\omega^s_{0XX}}}\int_{\eta_0}^{\eta(X;\omega_s)}\frac{ds}{s} \quad . \quad (1.87)$$

The second integral has voluntarily not been replaced by a logarithmic function because its value varies according to the number of complete 2π rotations made by the contour of integration around the origin[3]. The first integral taken separately, is also multiple-valued and it depends on the number of rotations completed around X_s. Since the integration path from η_0 to η in the second integral is the image by $X \mapsto \eta(X;\omega_s)$ of the integration path from X_0 to X in the first integral, the sum of both integrals is however single-valued. Finally, in view of the relation

$$\frac{\partial(\eta_1^2)}{\partial\omega}(\omega)\int_{\eta_0}^{\eta_1(\omega)}\frac{1}{\sqrt{\eta_1^2(\omega)-s^2}}ds = 2\int_{X_0}^{X_1(\omega)}\frac{1}{\omega_{kk}(r)}\sqrt{\frac{\omega_{kk}(r)}{2(\omega_0(r)-\omega)}}dr \quad ,$$

valid for any ω including ω_s, the function $\frac{\partial(\eta^2)}{\partial X}(X;\omega_s)$ defined by (1.87) can be continuously extended to X_s as

$$\frac{\partial(\eta^2)}{\partial X}(X_s;\omega_s) = 0 \quad .$$

3. To get a single-valued expression for that integral, a branch cut issuing from the origin should be selected in the η plane, the contour of integration in the η plane being required not to cross it. The contour of integration in the X plane for the first integral in (1.87) is the preimage of the previous contour through the mapping $X \mapsto \eta(X;\omega_s)$ and it suffers from similar restrictions.

Chapitre 2

MODES GLOBAUX FAIBLEMENT NON LINEAIRES

2.1 Introduction

Ce chapitre est consacré à l'extension dans le domaine non linéaire de la théorie des modes globaux développée dans le chapitre 1. Le principal objectif est d'étudier sous quelles conditions le mode global linéairement instable peut avoir une amplitude décrite par une équation de Landau.

Les motivations physiques de cette étude sont nombreuses. Pour le sillage derrière un cylindre, il est maintenant bien établi que le régime oscillatoire qui apparaît pour des valeurs du nombre de Reynolds supérieures à 45 correspond à la déstabilisation d'un mode global. Il a été expérimentalement prouvé que la bifurcation est du type Hopf (Mathis *et al.* 1984) et que l'équation de Landau décrit de manière satisfaisante l'amplitude des oscillations (Strykowski & Sreenivasan 1990). Le seuil d'apparition de l'allée de von Kármán a de plus été relié avec succès à la présence d'une région absolument instable suffisamment grande (Triantafyllou *et al.* 1986, Monkewitz 1988, Hannemann & Oertel 1989). Des résultats similaires ont pu être obtenus pour d'autres écoulements. On trouvera une bibliographie extensive sur ce sujet dans Huerre & Monkewitz (1990).

D'un point de vue théorique, Landau (1944) a été le premier à décrire l'évolution non linéaire de l'amplitude des ondes d'instabilité à l'aide de l'équation qui porte son nom. Stuart (1960) et Watson (1960) ont ensuite montré comment effectivement l'obtenir à partir des équations fondamentales de l'hydrodynamique pour des écoulements plans parallèles. La méthode, basée sur l'analyse faiblement non linéaire a été depuis mise en oeuvre dans de nombreux contextes. Son principe consiste à se placer au voisinage du seuil d'instabilité linéaire et à remplacer l'équation aux dérivées partielles non linéaire décrivant l'évolution des perturbations par une succession d'équations linéaires inhomogènes calculées au seuil d'instabilité. Pour un bon choix d'échelles caractéristiques, l'équation de Landau apparaît alors comme la première condition de solvabilité à imposer sur l'amplitude du mode linéaire déstabilisé pour garantir l'existence de solutions des équations inhomogènes.

L'équation de Landau est la forme normale associée à une bifurcation de Hopf. Elle peut donc aussi s'obtenir de manière systématique à partir du théorème de la variété centrale (Guckenheimer & Holmes 1983) dès qu'un seul mode linéaire de fréquence complexe est déstabilisé. L'étude réalisée au chapitre 1 montre que l'on est effectivement dans ce cas : les fréquences globales étant discrètes, un seul mode est généralement déstabilisé au voisinage du seuil. Cependant, les modes globaux dépendent de manière singulière du paramètre ε caractérisant l'inhomogénéité du milieu : les coefficients de l'équation de Landau sont donc des fonctions de ε.

Le but est ici d'obtenir explicitement l'équation de Landau par une analyse faiblement non linéaire du mode global de type 2 (double point tournant) d'indice $n = 0$ étudié au chapitre 1 et de déterminer ensuite l'ensemble des conditions garantissant sa validité lorsque le paramètre WKBJ ε tend vers zéro.

Le chapitre est organisé de la manière suivante. Dans la section 2.2, l'analyse faiblement non linéaire classique de type Landau-Stuart est conduite de façon formelle et l'ensemble des conditions de validité du modèle de Landau est obtenu. Ces

conditions sont ensuite explicitées en section 2.3 dans la limite de l'approximation WKBJ, pour le cas d'un mode global avec un double point tournant (type 2). Les corrections successives de la fonction propre générées par le schéma perturbatif sont également évaluées dans la limite WKBJ. On montre que le domaine d'applicabilité de l'analyse faiblement non linéaire ainsi que l'écart au seuil d'instabilité admissible est considérablement restreint. Des hypothèses supplémentaires sont introduites en section 2.3.4 pour assurer la validité physique du modèle de Landau-Stuart. Ces hypothèses sont interprétées dans la section 2.3.5 sur un exemple simple, en terme de caractéristiques d'instabilité locale.

2.2 Etude du modèle de Landau-Stuart : conditions formelles de validité

2.2.1 Position du problème

Les perturbations $\Psi(x,t)$ d'un état de base donné sont supposées vérifier l'équation suivante :

$$[i\frac{\partial}{\partial t} + \mathcal{L}(-i\frac{\partial}{\partial x}, X; R)]\Psi = \gamma(X)|\Psi|^2\Psi \quad , \tag{2.1}$$

où l'opérateur $\mathcal{L}(k, X; R)$ est donné par

$$\mathcal{L}(k, X; R) = -\omega_0(X; R) - \frac{\omega_{kk}(X; R)}{2}[k - k_0(X; R)]^2 \quad . \tag{2.2}$$

Les fonctions apparaissant dans l'opérateur $\mathcal{L}$ ainsi que la fonction γ sont supposées analytiques dans le plan complexe par rapport à la variable X et suffisamment dérivables par rapport au paramètre de contrôle R. La variable lente X est reliée à la variable spatiale x par la relation

$$X = \varepsilon x \quad , \tag{2.3}$$

où ε est un paramètre tendant vers 0 qui caractérise l'inhomogénéité du milieu dans la direction x. Les perturbations sont soumises aux conditions aux limites suivantes :

$$\lim_{X\to\pm\infty} \Psi = 0 \ . \tag{2.4}$$

Si l'on supprime le terme non linéaire, l'équation (2.1) soumise aux conditions aux limites (2.4), a été étudiée dans le chapitre 1. Sous des conditions spécifiques, en particulier, la présence de deux points tournants uniquement, l'ensemble des modes globaux a pu être obtenu. Ces solutions de la forme

$$\Psi_g = \phi_g(X,\varepsilon;R)e^{-i\omega_g t} \quad , \tag{2.5}$$

où $\phi_g(X,\varepsilon;R)$ et ω_g vérifient

$$[\omega_g + \mathcal{L}(-i\frac{\partial}{\partial x}, X; R)]\phi_g = 0 \quad , \tag{2.6a}$$

$$\lim_{X\to\pm\infty} \phi_g = 0 \quad , \tag{2.6b}$$

n'existent que pour des valeurs discrètes, indicées par l'entier n, de la fréquence ω_g, séparées les unes des autres par une contribution d'ordre ε. Deux types de modes globaux ont pu être obtenus, correspondant soit à des valeurs de n fixées (type 2), soit à des valeurs de n d'ordre $1/\varepsilon$ (type 1).

Nous supposons que la fonction propre la plus instable est le mode global de type 2, correspondant à la valeur $n = 0$. La fréquence ω_{g_0} et la distribution spatiale ϕ_{g_0} de ce mode ont été calculées dans le chapitre 1 : elles sont données respectivement par les expressions (1.41) et (1.63). Le seuil d'instabilité correspond à la déstabilisation du mode global le plus instable. Il est associé à la valeur critique $R_c(\varepsilon)$ du paramètre de contrôle, définie par $\Im m[\omega_{g_0}] = 0$. Dès que le paramètre de contrôle est supérieur[1] à $R_c(\varepsilon)$, tout en étant suffisamment proche de $R_c(\varepsilon)$, le mode global Ψ_{g_0} est le seul mode temporellement amplifié, les autres étant tous atténués. L'amplitude de

1. On suppose ici qu'il y a une direction de déstabilisation bien définie à la limite $\varepsilon \to 0$. Nous vérifierons à postériori cette hypothèse physiquement indispensable.

ce mode augmente exponentiellement avec un taux de croissance linéaire $\Im m[\omega_{g_0}]$, jusqu'à ce que les effets non linéaires deviennent trop importants pour être négligés. Il s'agit d'étudier ces effets pour l'équation modèle (2.1), dans le cadre de l'analyse faiblement non linéaire.

2.2.2 Analyse faiblement non linéaire "à la Landau-Stuart"

La méthode classique utilisée pour l'analyse faiblement non linéaire est présentée dans de nombreux livres. Nous renvoyons le lecteur qui désire plus de détails à Nayfeh (1973). Le point de départ consiste à introduire un petit paramètre μ, qui mesure l'écart au seuil d'instabilité

$$R = R_c(\varepsilon) + \mu \quad ; \qquad \mu \ll 1 \ . \tag{2.7}$$

Une solution non linéaire est alors cherchée sous la forme d'un développement asymptotique en puissance de μ :

$$\Psi(X,t;\mu,\varepsilon) = \sqrt{\mu}[\Psi_0(X,T_1,T_2,..;\varepsilon) + \mu\Psi_1(X,T_1,T_2,..;\varepsilon) + \cdots]e^{-i\omega^c_{g_0}t} \quad , \tag{2.8}$$

où $\omega^c_{g_0}$ est la fréquence globale du mode neutre en $R_c(\varepsilon)$, et T_k sont des variables de temps lentes définies par

$$T_k = \mu^k t \ , \ k = 0,1,2,... \ . \tag{2.9}$$

Elles sont introduites afin d'obtenir une solution (2.8) uniformément valable dans le temps. La dérivée temporelle de l'équation (2.1) est transformée suivant la règle habituelle du formalisme multi-échelle :

$$\frac{\partial}{\partial t} = \frac{\partial}{\partial T_0} + \mu\frac{\partial}{\partial T_1} + \mu^2\frac{\partial}{\partial T_2} + \cdots \quad . \tag{2.10}$$

Le choix de $\sqrt{\mu}$ pour la normalisation de l'amplitude s'effectue en général à postériori et de façon à ce que les effets de croissance linéaires et les effets non linéaires apparaissent au même ordre.

Pour définir la solution Ψ de manière unique, il est nécessaire d'imposer une condition de normalisation à un instant et à une position donnée. Sans réduire la généralité, on peut choisir l'instant t et la position X_M sur l'axe réel, où l'amplitude spatiale $|\phi^c_{g_0}|$ du mode global Ψ_{g_0} à $R_c(\varepsilon)$ atteint son maximum. On écrit ainsi

$$\Psi(X_M, 0, \varepsilon, \mu) = \sqrt{\mu}\ \delta(\varepsilon) \quad , \tag{2.11}$$

où $\delta(\varepsilon)$ est une fonction de jauge quelconque. Cette condition se traduit sur les fonctions Ψ_m du développement (2.8) de la manière suivante :

$$\Psi_0(X_M, 0, \varepsilon) = \delta(\varepsilon) \quad , \tag{2.12a}$$

$$\Psi_m(X_M, 0, \varepsilon) = 0 \ ; \quad m = 1, 2 \cdots . \tag{2.12b}$$

Si les expressions (2.7), (2.8) et (2.10) sont introduites dans l'équation (2.1) et l'opérateur $\mathcal{L}$ développé en série de Taylor, on obtient une équation de la forme :

$$[\omega^c_{g_0} + \mathcal{L}^c]\Psi_0$$

$$= \sum_{r=1}^{\infty} \left\{ -\sum_{p=0}^{r} \left(i \frac{\partial \Psi_p}{\partial T_{r-p}} + \frac{1}{(r-p)!} \mathcal{L}^c_{R^{r-p}}[\Psi_p] \right) + \sum_{m_1+m_2+m_3=r-1} \gamma \Psi_{m_1} \Psi_{m_2} \Psi^*_{m_3} \right\} \mu^r \quad , \tag{2.13}$$

où

- l'opérateur $\mathcal{L}^c_{R^k}$ désigne la $k$ième dérivée de l'opérateur $\mathcal{L}(-i\partial/\partial x, X; R)$ par rapport au paramètre de contrôle R, prise en $R_c(\varepsilon)$;
- l'opérateur $\mathcal{L}^c_{R^0}$ (ou $\mathcal{L}^c$) est l'opérateur $\mathcal{L}(-i\partial/\partial x, X; R_c)$.

Les deux premiers ordres de l'expression (2.13) fournissent une équation linéaire pour Ψ_0, et une équation inhomogène pour Ψ_1.

A **l'ordre** μ^0, l'équation (2.13) se réduit à

$$\left[\omega^c_{g_0} + \mathcal{L}^c\right] \Psi_0 = 0 \quad . \tag{2.14}$$

Comme attendu, on retrouve l'équation linéaire vérifiée par la distribution spatiale $\phi^c_{g_0}$ du mode global neutre à $R_c(\varepsilon)$. En normalisant cette solution particulière à son maximum X_M, la solution générale de (2.14) qui vérifie la condition de normalisation (2.12a) et les conditions aux limites à l'infini, est donc

$$\Psi_0 = \delta(\varepsilon) A_0(T_1, T_2, ..; \varepsilon) \phi^c_{g_0}(X, \varepsilon) \quad , \tag{2.15}$$

où l'amplitude inconnue $A_0(T_1, T_2, ..; \varepsilon)$ doit satisfaire la condition

$$A_0(0, 0, ..; \varepsilon) = 1 \quad . \tag{2.16}$$

A **l'ordre** μ^1, on obtient

$$\left[\omega^c_{g_0} + \mathcal{L}^c\right] \Psi_1 = -\left[i\frac{\partial}{\partial T_1} + \mathcal{L}^c_R\right] \Psi_0 + \gamma |\Psi_0|^2 \Psi_0 \quad . \tag{2.17}$$

Cette équation admet des solutions qui satisfont aux conditions aux limites (2.4), uniquement si le terme de droite est orthogonal à la solution du problème homogène adjoint. Ceci se traduit par une condition sur l'amplitude A_0 qui s'écrit selon la familière équation de Landau :

$$i\frac{\partial A_0}{\partial T_1} = L^{(0)}_1(\varepsilon) A_0 + L^{(1)}_1(\varepsilon) |\delta(\varepsilon)|^2 |A_0|^2 A_0 \quad , \tag{2.18}$$

avec

$$L^{(0)}_1(\varepsilon) = -\frac{< \phi^A_{g_0} | \mathcal{L}^c_R[\phi^c_{g_0}] >}{< \phi^A_{g_0} | \phi^c_{g_0} >} \quad , \tag{2.19a}$$

$$L^{(1)}_1(\varepsilon) = \frac{< \phi^A_{g_0} | \gamma | \phi^c_{g_0} |^2 \phi^c_{g_0} >}{< \phi^A_{g_0} | \phi^c_{g_0} >} \quad . \tag{2.19b}$$

- $< f | g >$ représente ici le produit scalaire $\int_{-\infty}^{+\infty} f^* g dx$, où $*$ désigne le complexe conjugué;

- la fonction propre adjointe $\phi^A_{g_0}$ est la solution du problème adjoint défini par

$$[\omega^c_{g_0} + \mathcal{L}^A(-i\frac{\partial}{\partial x}, X; R_c)] \phi^A_{g_0} = 0 \quad , \tag{2.20a}$$

$$\lim_{X \to \pm\infty} \phi^A_{g_0} = 0 \quad , \qquad \phi^A_{g_0}(X_M) = 1 \quad ; \tag{2.20b}$$

– $\mathcal{L}^A$ est l'opérateur adjoint de $\mathcal{L}^c$ défini par $< f|\mathcal{L}(g) >=< \mathcal{L}^A(f)|g >$ pour des fonctions f, g s'annulant à l'infini ainsi que leurs dérivées.

Dès que l'équation (2.18) est vérifiée, la solution de (2.17) qui tend vers 0 à l'infini, et qui vaut zéro en X_M, s'écrit sous la forme

$$\Psi_1 = \delta(\varepsilon)\Big[A_1(T_1,T_2,..;\varepsilon)\phi^c_{g_0}(X,\varepsilon) \quad + A_0\phi^{(0)}_1(X,\varepsilon) \\ + |\delta(\varepsilon)|^2|A_0|^2A_0\phi^{(1)}_1(X,\varepsilon)\Big]\, e^{-i\omega^c_{g_0}T_0} \quad , \tag{2.21}$$

où les fonctions $\phi^{(0)}_1$ et $\phi^{(1)}_1$ vérifient les conditions aux limites (2.4) et les équations

$$[\omega^c_{g_0} + \mathcal{L}^c]\phi^{(0)}_1 = -L^{(0)}_1\phi^c_{g_0} - \mathcal{L}^c_R[\phi^c_{g_0}] \quad , \tag{2.22a}$$

$$[\omega^c_{g_0} + \mathcal{L}^c]\phi^{(1)}_1 = -L^{(1)}_1\phi^c_{g_0} + \gamma|\phi^c_{g_0}|^2\phi^c_{g_0} \quad , \tag{2.22b}$$

$$\phi^{(0)}_1(X_M,\varepsilon) = \phi^{(1)}_1(X_M,\varepsilon) = 0 \quad . \tag{2.22c}$$

A cet ordre, l'amplitude $A_1(T_1,T_2,..;\varepsilon)$ de la solution homogène est uniquement soumise à la condition $A_1(0,0,..;\varepsilon) = 0$. A l'ordre suivant, on montre que A_1 peut être prise nulle pour tout t, si A_0 satisfait une condition de solvabilité par rapport à la variable lente T_2. Ainsi Ψ_1 est une somme de termes proportionnels à $|A_0|^{2k}A_0$ (k =0 ou 1). Ce résultat se généralise à tous les ordres: si A_0 satisfait une condition de solvabilité par rapport à chacune des variables T_k, Ψ_m est une somme de termes proportionels à $|A_0|^{2k}A_0$ ($k \leq m$). Les conditions de solvabilité et les expressions de Ψ_m s'obtiennent facilement par un raisonnement par récurrence.

A **l'ordre** μ^m, la condition de solvabilité et la $m$ième correction Ψ_m du développement (2.8) s'écrivent respectivement

$$i\frac{\partial A_0}{\partial T_m} = \sum_{k\leq m} L^{(k)}_m(\varepsilon)|\delta(\varepsilon)|^{2k}|A_0|^{2k}A_0 \quad , \tag{2.23}$$

$$\Psi_m = \delta(\varepsilon)\left[\sum_{0\leq k\leq m} |\delta(\varepsilon)|^{2k}|A_0|^{2k}A_0\phi^{(k)}_m(X,\varepsilon)\right] e^{-i\omega^c_{g_0}T_0} \quad , \tag{2.24}$$

où les coefficients $L_m^{(k)}(\varepsilon)$ et les distributions spatiales $\phi_m^{(k)}$ sont définis pour tout $m \geq 1$ et $0 \leq k \leq m$, par

$$L_m^{(k)}(\varepsilon) = \frac{< \phi_{g_0}^A | F_m^{(k)} >}{< \phi_{g_0}^A | \phi_{g_0}^c >} \quad , \tag{2.25}$$

$$[\omega_{g_0}^c + \mathcal{L}^c]\phi_m^{(k)} = F_m^{(k)}(X, \varepsilon) - L_m^{(k)}(\varepsilon)\phi_{g_0}^c \quad , \tag{2.26a}$$

$$\phi_m^{(k)}(X_M, \varepsilon) = 0 \quad , \tag{2.26b}$$

$$\lim_{X \to \pm\infty} \phi_m^{(k)} = 0 \ , \tag{2.26c}$$

avec l'expression suivante de $F_m^{(k)}$:

$$F_m^{(k)} = -\sum_{p=1}^{m-1} \left[\sum_{s=max\{0,k+p-m\}}^{min\{k,p\}} \left\{ 2(k-s)\Re e(L_p^{(s)}) + L_p^{(s)} \right\} \phi_{m-p}^{(k-s)} \right]$$

$$- \sum_{p=1}^{min(m,m-k)} \mathcal{L}_{R^p}^c \left[\phi_{m-p}^{(k)} \right] + \gamma \sum_{m_1+m_2+m_3=m-1} \sum_{\substack{k_1+k_2+k_3=k-1 \\ 0 \leq k_i \leq m_i}} \phi_{m_1}^{(k_1)} \phi_{m_2}^{(k_2)} (\phi_{m_3}^{(k_3)})^* \quad , \tag{2.27}$$

où l'on convient de poser $\phi_0^{(0)} = \phi_{g_0}^c$.

L'ensemble des équations (2.8), (2.9), (2.15)-(2.27) définit entièrement le développement asymptotique de la solution Ψ pour μ tendant vers zéro.

2.2.3 Conditions physiques d'interprétation du modèle de Landau-Stuart

La particularité du problème considéré est la présence simultanée de deux petits paramètres μ et ε. Tant que μ est incommensurablement petit par rapport à ε, l'ordre des termes du développement asymptotique en μ reste inchangé, mais les échelles choisies pour l'amplitude, et les variables temporelles lentes peuvent devenir mal adaptées à la limite $\varepsilon \to 0$. En effet, les équations d'amplitude (2.18) et (2.23) présupposent que tous les termes sont d'ordre unité dans chacune des équations. Ceci

n'est plus nécessairement vérifié quand $\varepsilon \to 0$ et certains termes peuvent tendre vers l'infini alors que d'autres tendent vers zéro.

Dans l'équation (2.23), on peut associer à chaque terme $|\delta(\varepsilon)|^{2k}|L_m^{(k)}(\varepsilon)||A_0|^{2k}A_0$, une échelle de temps caractéristique

$$T_m^{(k)} = |\delta(\varepsilon)|^{2k}|L_m^{(k)}(\varepsilon)|T_m = |\delta(\varepsilon)|^{2k}|L_m^{(k)}(\varepsilon)|\mu^m t \quad . \tag{2.28}$$

Ainsi, l'échelle caractéristique associée aux premiers effets non linéaires est $T_1^{(1)} = |\delta(\varepsilon)|^2|L_1^{(1)}(\varepsilon)|\mu t$ et celle associée aux effets de croissance linéaires est $T_1^{(0)} = |L_1^{(0)}(\varepsilon)|\mu t$. Si l'on désire que les premiers effets non linéaires et les premiers effets linéaires apparaissent au même ordre, les deux échelles de temps $T_1^{(0)}$ et $T_1^{(1)}$ doivent rester identiques. Ceci est possible en choisissant $\delta(\varepsilon)$ de la manière suivante

$$\delta(\varepsilon) = \left| \frac{L_1^{(0)}(\varepsilon)}{\mathrm{L}_1^{(1)}(\varepsilon)} \right|^{1/2} \quad . \tag{2.29}$$

L'équation de Landau (2.18) peut alors s'écrire avec l'échelle de temps $T_1^{(1)}$:

$$i\frac{\partial A_0}{\partial T_1^{(1)}} = e^{iarg(L_1^{(0)})}A_0 + e^{iarg(L_1^{(1)})}|A_0|^2A_0 \quad , \tag{2.30}$$

Les autres échelles de temps $T_m^{(k)}$ calculées avec l'expression (2.29) de $\delta(\varepsilon)$, peuvent à priori être toutes différentes. Dans ce cas, l'équation (2.23) doit être partagée en $(m+1)$ équations qui peuvent s'écrire sous la forme

$$i\frac{\partial A_0}{\partial T_m^{(k)}} = e^{iarg(L_m^{(k)})}|A_0|^{2k}A_0 \quad ; \quad 0 \le k \le m \quad . \tag{2.31}$$

Dans les autres cas, on décompose l'équation (2.23) en autant d'équations qu'il y a de termes d'ordres différents, ou de manière équivalente d'échelles de temps différentes. On obtient ainsi des équations pour l'amplitude A_0 dont les coefficients sont tous de même ordre. L'évolution temporelle de l'amplitude A_0 est ainsi définie de manière uniforme à la limite $\varepsilon \to 0$.

Notez, néanmoins, que les coefficients des équations obtenues après ces changements d'échelles, quoique d'ordre unité, n'ont pas nécessairement une limite quand $\varepsilon \to 0$. Cette particularité est de plus indépendante de la normalisation choisie[2] : elle ne concerne que la phase des coefficients $|\delta(\varepsilon)|^{2k} L_m^{(k)}$, qui reste indépendante de la fonction de jauge $\delta(\varepsilon)$. Elle ne préjuge pas de la validité de la solution formelle obtenue, mais elle peut en revanche lui faire perdre son sens physique.

Pour cette raison, nous ne considérons que des solutions pour lesquelles

$$arg[L_1^{(0)}] \ \ et \ \ arg[L_1^{(1)}] \ \ ont \ \ une \ \ limite \ \ lorsque \ \ \varepsilon \to 0 \ \ . \qquad (2.32)$$

La première condition est nécessaire pour pouvoir définir la stabilité du mode global neutre vis-à-vis de perturbations du paramètre de contrôle au voisinage de $R_c(\varepsilon)$. Le taux de croissance linéaire du mode global pour un paramètre de contrôle (2.7) est en effet donné au premier ordre par $\Im m[L_1^{(0)}]\mu$. Si $arg[L_1^{(0)}]$ n'a pas de limite quand $\varepsilon \to 0$, le taux d'amplification oscille entre des valeurs positives et négatives quand $\varepsilon \to 0$, contredisant ainsi l'hypothèse d'instabilité linéaire pour des paramètres de contrôle supérieurs à $R_c(\varepsilon)$.

De même, le signe de $\Im m[L_1^{(1)}]$ définit le rôle des premiers effets non linéaires (stabilisateur si positif, et déstabilisateur si négatif) ou encore la nature de la bifurcation (super-critique et sous-critique, respectivement). Si $arg[L_1^{(1)}(\varepsilon)]$ n'a pas de limite quand $\varepsilon \to 0$, les premiers effets non linéaires ne sont donc pas définis, ce qui n'est pas concevable d'un point de vue physique.

Finalement, sous les conditions (2.32), l'équation de Landau (2.30) a un sens à la limite $\varepsilon \to 0$. Sous l'hypothèse que μ est incommensurablement petit par rapport à ε, elle décrit les premiers effets non linéaires et d'amplification linéaire sur l'amplitude A_0 du mode global neutre déstabilisé.

Cette équation peut facilement s'intégrer. L'amplitude A_0 présente deux types

2. On pourrait d'ailleurs montrer ce dernier point en utilisant le fait que la phase de chaque coefficient $L_m^{(k)}$ définit une propriété physique qui est indépendante des choix d'échelles.

de comportement distincts, suivant que les effets non linéaires sont stabilisants ou déstabilisants. Dans le premier cas, $\arg[L_1^{(1)}]$ est compris entre π et 2π, et la bifurcation est supercritique. L'amplitude A_0 tend vers une valeur limite lorsque $T_1^{(1)}$ tend vers l'infini. Dand le second cas, $\arg[L_1^{(1)}]$ est compris entre 0 et π et la bifurcation est souscritique. L'amplitude A_0 explose alors en temps fini, ce qui veut dire que l'échelle de l'amplitude de la solution Ψ doit alors être modifiée pour des valeurs du temps supérieures.

Nous retiendrons que dans tous les cas, pour des valeurs finies de $T_1^{(1)}$, c'est-à-dire pour des temps t de l'ordre de $[|L_1^{(0)}|\mu]^{-1}$, la solution non linéaire Ψ admet, lorsque μ est **incommensurablement petit** par rapport à ε, **l'approximation de Landau-Stuart**

$$\Psi \underset{\varepsilon\to 0}{\sim} \sqrt{\mu}\left|\frac{L_1^{(0)}}{L_1^{(1)}}\right|^{1/2} A_0(T_1^{(1)})\phi_{g_0}^c(X,\varepsilon)e^{-i\omega_{g_0}^c t} \quad , \tag{2.33}$$

en tout point où $\phi_{g_0}^c(X,\varepsilon)$ est non nul avec A_0 vérifiant (2.30).

Une question naturelle se pose alors: jusqu'à quelle valeur $\mu_l(\varepsilon)$ du paramètre μ un tel résultat reste t'il valable? Nous allons y répondre d'un point de vue formel dans la section suivante.

2.2.4 Conditions de validité de l'approximation de Landau-Stuart

Une première condition évidente sur μ s'obtient à partir de l'expression (2.33) elle-même. La distribution spatiale de la solution non linéaire ne peut être celle du mode global neutre **linéaire** que si son amplitude est plus petite que l'unité. Cette condition implique en particulier $|\Psi(X_M,0,\varepsilon,\mu)| \ll 1$ qui se réduit au vu de (2.33) à

$$\mu \ll \left|\frac{L_1^{(1)}(\varepsilon)}{L_1^{(0)}(\varepsilon)}\right| \quad . \tag{2.34}$$

Par ailleurs, l'expression (2.33) est le terme dominant de Ψ uniquement si toutes les corrections Ψ_m données par (2.24) sont négligeables. Cette condition s'écrit

$$\forall m \geq 1, \forall k \text{ tel que } 0 \leq k \leq m, \qquad \mu^m |\delta(\varepsilon)|^{2k} |\phi_m^{(k)}(X,\varepsilon)| \ll |\phi_{g_0}(X,\varepsilon)| \ ,$$

ou encore en utilisant (2.29),

$$\forall m \geq 1, \forall k \text{ tel que } 0 \leq k \leq m, \qquad \mu \ll \left[\left| \frac{L_1^{(1)}(\varepsilon)}{L_1^{(0)}(\varepsilon)} \right|^k \left| \frac{\phi_{g_0}^c}{\phi_m^{(k)}} \right| \right]^{1/m} \ . \tag{2.35}$$

Enfin, l'équation de Landau (2.30) ne peut décrire l'évolution de l'amplitude A_0 jusqu'à des valeurs finies de $T_1^{(1)}$ que si les autres échelles $T_m^{(k)}$ de variation de A_0 sont plus lentes. En utilisant l'expression (2.28), cette condition conduit à

$$\forall m \geq 2, \forall k \text{ tel que } 0 \leq k \leq m, \qquad \mu^m |\delta(\varepsilon)|^{2k} |L_m^{(k)}(\varepsilon)| \ll \mu \ ,$$

qui s'écrit aussi

$$\forall m \geq 2, \forall k \text{ tel que } 0 \leq k \leq m, \qquad \mu \ll \left[\frac{|L_1^{(1)}(\varepsilon)|^k}{|L_1^{(0)}(\varepsilon)|^k |L_m^{(k)}(\varepsilon)|} \right]^{1/(m-1)} \ . \tag{2.36}$$

Les conditions (2.34) (2.35) et (2.36) sont des conditions que doit nécessairement vérifier le paramètre limite $\mu_l(\varepsilon)$. On peut facilement montrer qu'elles sont aussi suffisantes. En conclusion, l'ensemble des conditions (2.32), (2.34)-(2.36) garantit la validité et le sens de l'approximation (2.33) du mode global non linéaire.

Considérons maintenant une perturbation quelconque. Si celle-ci peut initialement se décomposer sur l'ensemble des modes globaux linéaires avec une composante non nulle sur le mode global Ψ_{g_0}, on ne peut espérer déduire l'évolution post-critique de cette perturbation à partir du comportement de Ψ_{g_0} que si

$$\mu \ll [R_2(\varepsilon) - R_c(\varepsilon)] \ , \tag{2.37}$$

où $R_2(\varepsilon)$ est le paramètre critique associé à la déstabilisation éventuelle d'un deuxième mode global. Cette condition est nécessaire. Elle n'est probablement pas suffisante. On peut dès à présent expliciter cette dernière condition pour le cas considéré.

Lorsque le second mode le plus instable est aussi un mode avec un double point tournant (type 2), l'expression (1.41) des fréquences globales garantit que celui-ci est nécessairement le mode global correspondant à la valeur $n = 1$. Sa fréquence ne diffère alors de la fréquence globale ω_{g_0} que par une quantité d'ordre $O(\varepsilon)$. Dans le cas non dégénéré[3] le paramètre critique $R_2(\varepsilon)$ vérifie donc $R_2 - R_c \sim \Delta R\ \varepsilon$ avec $\Delta R \neq 0$ et la condition (2.37) s'écrit $\mu \ll \varepsilon$.

2.3 Mode global non linéaire avec un double point tournant (type 2)

Nous allons maintenant étudier la signification des conditions nécessaires et suffisantes pour assurer la validité de l'approximation (2.33) :

$$\left\{\begin{array}{ll}
(2.32) & arg[L_1^{(0)}]\ et\ arg[L_1^{(1)}]\ ont\ une\ limite\ lorsque\ \varepsilon \to 0\ , \\
(2.34) & \mu \ll \left|\frac{L_1^{(1)}(\varepsilon)}{L_1^{(0)}(\varepsilon)}\right|\ , \\
(2.35) & \forall m \geq 1, \forall k \text{ tel que } 0 \leq k \leq m, \qquad \mu \ll \left[\left|\frac{L_1^{(1)}(\varepsilon)}{L_1^{(0)}(\varepsilon)}\right|^k \left|\frac{\phi^c_{g_0}}{\phi_m^{(k)}}\right|\right]^{1/m}\ , \\
(2.36) & \forall m \geq 2, \forall k \text{ tel que } 0 \leq k \leq m, \qquad \mu \ll \left[\frac{|L_1^{(1)}(\varepsilon)|^k}{|L_1^{(0)}(\varepsilon)|^k |L_m^{(k)}(\varepsilon)|}\right]^{1/(m-1)}\ ,
\end{array}\right.$$

Dans ce but, nous allons examiner le comportement asymptotique des fonctions $\phi^c_{g_0}$, $\phi^A_{g_0}$ (section 2.3.1), puis des coefficients $L_1^{(0)}$ et $L_1^{(1)}$ (section 2.3.2). Nous nous placerons ensuite dans un cas particulier permettant d'obtenir le comportement asymptotique des coefficients $L_m^{(k)}$ et des fonctions $\phi_m^{(k)}$, pour tout X réel, et d'expliciter l'ensemble des conditions. Nous étudierons finalement sur un modèle simple les conditions à imposer sur les caractéristiques d'instabilité locales.

3. Ce cas correspond à $(\partial_R \omega_s)(R_c)$ et $\omega^s_{kk}\sqrt{\frac{\omega^s_{0XX}}{\omega^s_{kk}}}(R_c)$ non nuls à la limite $\varepsilon \to 0$.

2.3.1 Développements asymptotiques uniformes des fonctions propres $\phi^c_{g_0}$ et $\phi^A_{g_0}$

Un développement asymptotique uniforme de la distribution spatiale $\phi^c_{g_0}(X,\varepsilon)$ a été obtenu au chapitre 1. Le premier ordre du développement est donné par l'approximation (1.63) pour la valeur $n=0$. Pour obtenir les ordres suivants, on peut revenir à l'expression générale (1.25) du développement asymptotique. La distribution spatiale $\phi^c_{g_0}$ est associée à la fréquence $\omega^c_{g_0}$ donnée par (1.61) et la fonction V_0 donnée par (1.36). Si l'on introduit ces expressions dans (1.25) et si l'on utilise l'expression (1.53) de $\eta(X;\omega^c_{g_0})$, on obtient finalement un développement de la forme

$$\phi^c_{g_0} = [\alpha_0(X) + \varepsilon\alpha_1(X) + \cdots] e^{\dfrac{i}{\varepsilon}\displaystyle\int_{X_M}^{X} k^+(r,\omega^c_s)dr} \quad , \tag{2.38}$$

où la branche spatiale $k^+(X,\omega^c_s)$ est la branche sous-dominante à l'infini parmi les 2 branches k^+ et k^- définies en (1.8). Le point X_M est la position où $|\phi^c_{g_0}|$ atteint son maximum. Ainsi, il vérifie

$$\Im m[k^+(X_M,\omega^c_s)] = 0 \quad . \tag{2.39}$$

On a supposé que la fonction $\phi^c_{g_0}$ est normalisée en X_M. Cette condition implique que

$$\alpha_0(X_M) = 1 \quad . \tag{2.40}$$

L'expression exacte de $\alpha_0(X)$ peut de plus être obtenue en comparant le premier ordre de (2.38) et l'approximation (1.63) du chapitre 1.

Il est intéressant de remarquer que le développement asymptotique (2.38) n'est rien d'autre qu'un développement WKBJ, et que celui-ci reste valable au voisinage du double point tournant X_s, contrairement au comportement habituel. L'unicité d'un tel développement le rend de plus égal à celui obtenu par Chomaz *et al.* (1991) dans les régions (+) et (−).

La fonction propre adjointe $\phi^A_{g_0}$ apparaît systématiquement dans l'analyse faiblement non linéaire pour le calcul des coefficients $L^{(k)}_m$. Ce mode vérifie le problème adjoint défini par les équations (2.20a,b). L'équation adjointe (2.20a) s'explicite sous la forme :

$$\left[\frac{\omega^*_{kk}}{2}\frac{\partial^2}{\partial x^2} - i\omega^*_{kk}k^*_0\frac{\partial}{\partial x} + \varepsilon\frac{\partial\omega^*_{kk}}{\partial X}\frac{\partial}{\partial x} - \left(\frac{\omega^*_{kk}k^{*2}_0}{2} + \omega^*_0 - \omega^c_{g_0}\right) - i\frac{\partial\omega^*_{kk}k^*_0}{\partial X}\varepsilon + \frac{1}{2}\frac{\partial^2\omega^*_{kk}}{\partial X^2}\varepsilon^2\right]\phi^A_{g_0} = 0 \quad . \tag{2.41}$$

Par le changement de fonction

$$\phi^A_{g_0} = \psi^A\frac{\omega^*_{kk}(X_M)}{\omega^*_{kk}(X)}e^{\frac{i}{\varepsilon}\int_{X_M}^{X} k^*_0(r)dr} \quad , \tag{2.42}$$

elle se transforme en

$$\left[\frac{\partial^2}{\partial x^2} + R^*_0(X,\omega^c_{g_0}) + \varepsilon R^*_1(X,\omega^c_{g_0})\right]\psi^A = 0 \quad , \tag{2.43}$$

où $R_0(X,\omega)$ et $R_1(X,\omega)$ sont donnés par les expressions (1.18a,b) du chapitre 1. Cette dernière équation est le conjugué de l'équation (1.17) obtenue à partir de l'équation (1.5) par la transformation (1.16) pour la valeur particulière $\omega^c_{g_0}$ de la fréquence. Ainsi, la fonction ψ^A se déduit immédiatement de $\phi^c_{g_0}$ par le conjugué de la transformation inverse:

$$\psi^A = [\phi^c_{g_0}]^* e^{\frac{i}{\varepsilon}\int_{X_M}^{X} k^*_0(r)dr} \quad . \tag{2.44}$$

Par suite, en utilisant (2.42), la fonction $\phi^A_{g_0}$ s'écrit

$$\phi^A_{g_0} = [\phi^c_{g_0}]^*\frac{\omega^*_{kk}(X_M)}{\omega^*_{kk}(X)}e^{\frac{2i}{\varepsilon}\int_{X_M}^{X} k^*_0(r)dr} \quad , \tag{2.45}$$

Elle admet donc un développement asymptotique uniforme de la même forme que (2.38) à savoir :

$$\phi^A_{g_0} = \frac{\omega^*_{kk}(X_M)}{\omega^*_{kk}(X)}[\alpha^*_0(X) + \varepsilon\alpha^*_1(X) + \cdots]e^{\frac{i}{\varepsilon}\int_{X_M}^{X}[k^-(r,\omega_s)]^* dr} \quad , \tag{2.46}$$

où $[k^-(r,\omega_s)]^*$ est bien la branche sous-dominante à l'infini [voir expression (1.8)].

2.3.2 Evaluation des coefficients $L_1^{(0)}(\varepsilon)$ et $L_1^{(1)}(\varepsilon)$ par la méthode du col

Les développements asymptotiques de $\phi^c_{g_0}$ et $\phi^A_{g_0}$ permettent d'évaluer les expressions (2.19a,b) des coefficients $L_1^{(0)}(\varepsilon)$ et $L_1^{(1)}(\varepsilon)$. Si l'on introduit formellement ces développements dans les expressions $< \phi^A_{g_0}|\phi^c_{g_0} >$ et $< \phi^A_{g_0}|\mathcal{L}^c_R(\phi^c_{g_0}) >$, celles-ci s'écrivent sous la forme d'un développement en puissance de ε d'intégrales du type[4]

$$I = \int_{-\infty}^{+\infty} D(X) e^{\frac{p_0(X)}{\varepsilon}} dX \quad , \tag{2.47}$$

avec

$$p_0(X) = i \int_{X_M}^{X} (k^+(r) - k^-(r)) dr \quad . \tag{2.48}$$

Cette même procédure appliquée à $< \phi^A_{g_0}|\gamma|\phi^c_{g_0}|^2\phi^c_{g_0} >$ conduit à un développement en puissance de ε d'intégrales du type

$$J = \int_{-\infty}^{+\infty} D(X) e^{\frac{p_1(X)}{\varepsilon}} dX \quad , \tag{2.49}$$

avec

$$p_1(X) = i \int_{X_M}^{X} (k^+(r) - k^-(r) + 2i\Im m[k^+(r)]) dr \quad . \tag{2.50}$$

La forme de ces intégrales est bien adaptée pour une évaluation par la méthode du col. Cette technique consiste à déformer le chemin d'intégration le long des contours qui rendent la phase du facteur exponentiel stationnaire; la partie principale provient alors des régions sur ce contour où l'amplitude de ce même facteur exponentiel est maximale; ces régions correspondent aussi, grâce à la propriété d'analycité, aux

4. Noter tout de même qu'une telle procédure nécessite que les intégrales aient un sens. On peut faire deux types d'hypothèses: soit supposer que les développements WKBJ sont uniformément valables à l'infini de sorte que la convergence de toutes les intégrales est garantie, soit supposer que les intégrales entre $-\infty$ et $+\infty$ faisant intervenir $\phi^c_{g_0}$ et $\phi^A_{g_0}$, et de manière générale les fonctions $\phi^{(k)}_m$, peuvent être remplacées lorsque $\varepsilon \to \infty$, à des termes exponentiellement petit près par une intégrale entre $-A$ et $+A$ avec A fixé suffisament grand. On retiendra par la suite par soucis de simplicité la première hypothèse.

voisinages de points selles de la phase. Nous renvoyons le lecteur à Bender & Orszag (1978) pour plus de détails sur cette méthode classique.

Les contours de phase constante du facteur $\exp[p_0(X)/\varepsilon]$ sont définis par $\Im m[p_0(X)] = Cte$ ou de manière équivalente par $\Re e[\int_{X_M}^{X}\{k^+(r) - k^-(r)\}dr] = Cte$. Ces courbes sont perpendiculaires aux contours d'amplitude constante de $\exp[p_0(X)/\varepsilon]$ définis par $\Im m[\int_{X_M}^{X}(k^+(r) - k^-(r))dr] = Cte$. Les points selles de $p_0(X)$ vérifient $k^+(X) - k^-(X) = 0$. Vu la définition (1.9) du chapitre 1, ce sont aussi des points tournants de la relation de dispersion (1.7)! Pour le mode global de type 2 que l'on considère, il n'y a qu'un point tournant double en X_s. Les lignes d'amplitude constante passant par X_s sont alors les lignes de Stokes associées au problème linéaire pour la fréquence particulière $\omega_{g_0}^c$! La géométrie de ces dernières dans le plan complexe a été étudiée au chapitre 1: elle correspond à une des configurations illustrées sur les figures 1.10b et 1.10d du chapitre 1. Comme indiqué sur la figure 2.1, on peut déformer le chemin d'intégration en un contour en restant dans les régions $(+)$ et $(-)$, passant par X_s, et suivant les lignes de phase constante au voisinage de X_s. Grâce à des résultats classiques (Bender & Orszag 1978), on sait alors que la

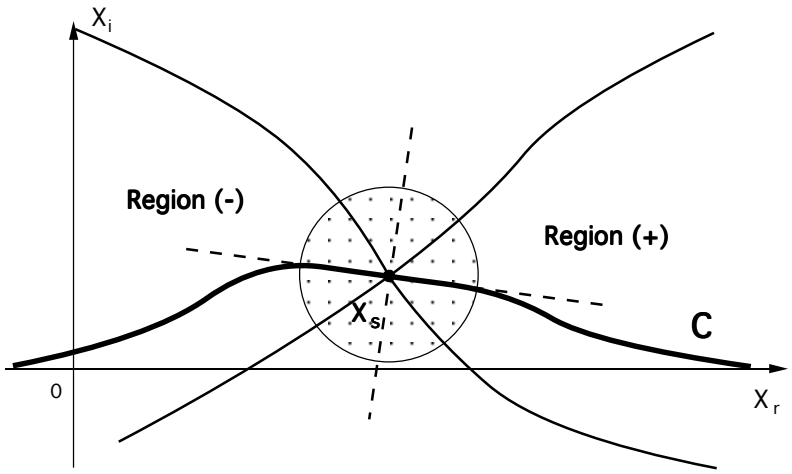

FIG. 2.1 - *Contour d'intégation utilisé pour le calcul des intégrales du type I.*

contribution dominante à l'intégrale I vient effectivement du point selle X_s, lorsque

ε tend vers zéro. Un équivalent est donné lorsque $D(X_s) \neq 0$, par

$$I(\varepsilon) \underset{\varepsilon \to 0}{\sim} D(X_s)\sqrt{\frac{\pi\,\varepsilon}{-p_0''(X_s)}}e^{\frac{p_0(X_s)}{\varepsilon}} \quad . \tag{2.51}$$

Lorsque $D(X_s)$ est nul, le comportement dominant reste du type $e^{\frac{p_0(X_s)}{\varepsilon}}$, mais il est multiplié par une puissance plus grande de ε.

Les contours de phase stationnaire associés à l'intégrale J sont définis par $\Im m[p_1(X)] = Cte$, ou de manière équivalente par $\Re e[\int_{X_M}^{X}(k^+(r) - k^-(r) + 2i\Im m[k^+](r))dr] = Cte$, où $\Im m[k^+](X)$ désigne le prolongement analytique[5] de la fonction de la variable réelle $\Im m[k^+(X)]$. Malheureusement, la géométrie de ces courbes dans le plan complexe n'est pas connue. Contrairement au cas précédent, l'existence d'un point selle unique vérifiant

$$k^+(X_1) - k^-(X_1) + 2i\Im m[k^+](X_1) = 0 \quad , \tag{2.52}$$

n'est pas garantie par les hypothèses effectuées au chapitre 1 sur la relation de dispersion locale. Il peut exister plusieurs point tournants, ou éventuellement aucun. Nous étudierons dans ce chapitre uniquement le cas où la contribution dominante de l'intégrale J vient effectivement d'un point selle X_1 défini par (2.52). Cette hypothèse sera étudiée plus précisément dans la prochaine section. On montrera en particulier qu'elle s'interprète sur le réseau de lignes de Stokes associé à une onde WKBJ linéaire et une onde WKBJ engendrée par les intéractions non linéaires. Sous cette hypothèse, on obtient un équivalent de l'intégrale J de la forme

$$J(\varepsilon) \underset{\varepsilon \to 0}{\sim} D(X_1)\sqrt{\frac{\pi\,\varepsilon}{-p_1''(X_1)}}e^{\frac{p_1(X_1)}{\varepsilon}} \quad . \tag{2.53}$$

5. Notons bien que le prolongement analytique de la partie imaginaire de k^+ est différent de la partie imaginaire du prolongement analytique de k^+: la première fonction est analytique par définition, la seconde ne l'est pas!

Chaque terme des développements de $< \phi^A_{g_0} | \phi^c_{g_0} >$, $< \phi^A_{g_0} | \mathcal{L}^c_R(\phi^c_{g_0}) >$ et $< \phi^A_{g_0} | \gamma | \phi^c_{g_0} |^2 \phi^c_{g_0} >$ admet ainsi le même type d'équivalent. L'expression $< \phi^A_{g_0} | \phi^c_{g_0} >$ peut donc être évaluée par son premier terme, c'est-à-dire par l'expression (2.51) avec $D(X) = \omega_{kk}(X_M)\alpha_0^2(X)/\omega_{kk}(X)$. De manière similaire, $< \phi^A_{g_0} | \mathcal{L}^c_R(\phi^c_{g_0}) >$ est donné par (2.51) avec $D(X) = \omega_{kk}(X_M)\mathcal{L}_R(k^+, X; R_c)\alpha_0^2(X)/\omega_{kk}(X)$; et $< \phi^A_{g_0} | \gamma | \phi^c_{g_0} |^2 \phi^c_{g_0} >$ par (2.53) avec $D(X) = \gamma(X)\omega_{kk}(X_M)|\alpha_0(X)|^2\alpha_0^2(X)/\omega_{kk}(X)$, si ces fonctions sont non nulles respectivement en X_s et X_1.

Finalement, on obtient des équivalents pour $L_1^{(0)}(\varepsilon)$ et $L_1^{(1)}(\varepsilon)$ de la forme

$$L_1^{(0)}(\varepsilon) \underset{\varepsilon \to 0}{\sim} - \mathcal{L}_R(k^+(X_s), X_s; R_c) \quad , \tag{2.54a}$$

$$L_1^{(1)}(\varepsilon) \underset{\varepsilon \to 0}{\sim} K e^{\frac{\Theta}{\varepsilon}} \quad , \tag{2.54b}$$

où dans la seconde expression, les nombres complexes K and Θ sont donnés par

$$\Theta = i \int_{X_M}^{X_1} (k^+(r) - k^-(r) + 2i\Im m[k^+](r))dr - i \int_{X_M}^{X_s} (k^+(r) - k^-(r))dr \quad , \tag{2.55a}$$

$$K = \gamma(X_1) \frac{\alpha_0^2(X_1)|\alpha_0(X_1)|^2 \omega_{kk}(X_s)}{\alpha_0^2(X_s)\omega_{kk}(X_1)} \sqrt{\frac{\partial_X \left[k^+ - k^-\right](X_s)}{\partial_X \left[k^+ - k^- + 2i\Im m[k^+]\right](X_1)}} \; . \tag{2.55b}$$

Sous la condition qu'on puisse utiliser les estimations (2.51), le premier coefficient a donc une limite finie non nulle[6] lorsque $\varepsilon \to 0$. L'hypothèse de déstabilisation du mode global Ψ_{g_0} pour $R > R_c(\varepsilon)$ est ainsi satisfaite dès que $\arg(L_1^{(0)})$ a une limite comprise entre 0 et π.

En revanche, la forme de l'expression (2.54b) ne garantit pas que $\arg(L_1^{(1)})$ a une limite quand $\varepsilon \to 0$. Si l'on suppose que les fonctions impliquées dans l'opérateur $\mathcal{L}$ défini en (2.2) sont continues en $\varepsilon = 0$ par rapport à ε, la condition de définition de $arg(L_1^{(1)}(\varepsilon))$ à la limite $\varepsilon \to 0$ est donc

$$\Im m(\Theta) = O(\varepsilon) \quad . \tag{2.56}$$

6. Noter que dans les autres cas, l'équivalent demeure proportionnel à une puissance de ε; son argument a donc toujours une limite lorsque $\varepsilon \to 0$.

Etant donné que Θ peut a priori prendre n'importe quelle valeur complexe, cette dernière condition réduit considérablement le domaine de validité de l'analyse faiblement non linéaire. Plus précisément, la nature de la bifurcation associée à la déstabilisation du mode global $n = 0$ n'est finalement définie qu'exceptionnellement.

Les expressions (2.54a,b) permettent aussi d'expliciter la condition (2.34). Cette condition s'écrit

$$\mu \ll e^{\frac{\Re e(\Theta)}{\varepsilon}} \quad . \tag{2.57}$$

Lorsque $\Re e(\Theta) < 0$, cette condition est relativement surprenante : même lorsque l'équation de Landau a un sens physique, cette équation n'est valable que pour des écarts au seuil μ exponentiellement petits. La condition (2.34) n'étant de plus qu'une condition nécessaire, on peut raisonnablement penser que l'ensemble des conditions (2.34), (2.35) et (2.36) est encore plus contraignant.

L'évaluation des deux premiers coefficients $L_1^{(0)}(\varepsilon)$ et $L_1^{(1)}(\varepsilon)$, nous a permis de tirer les conclusions importantes suivantes :

- **L'équation de Landau n'a un sens physique que pour des cas exceptionnels.**

- **Il est possible que l'équation de Landau ne soit valable que pour des écarts au seuil exponentiellement petits.**

On peut remarquer que l'évaluation des intégrales I et J intervenant dans la constante de Landau $L_1^{(1)}$ admet une interprétation physique intéressante. Les contributions dominantes des intégrales I et J proviennent des points tournants X_s et X_1, c'est-à-dire des **points de résonance** dans le plan complexe où deux nombres d'ondes coincident. Les ondes impliquées dans cette résonance apparaîtront dans la section suivante.

2.3.3 Points tournants et phénomène de Stokes de la correction $\phi_1^{(1)}$

Dans le but d'obtenir une condition suffisante qui garantit que l'ensemble des conditions nécessaires et suffisantes obtenues dans les sections 2.2.2 et 2.2.4 est satisfait, nous devons obtenir une majoration de toutes les distributions spatiales $\phi_m^{(k)}$ ainsi que de toutes les constantes $L_m^{(k)}$. Ce programme est trop ambitieux sans hypothèses supplémentaires, comme on va pouvoir le constater par l'analyse de la première distribution spatiale $\phi_1^{(1)}$.

La fonction $\phi_1^{(1)}$ est solution de l'équation (2.22b), et doit vérifier les conditions aux limites (2.4). L'existence d'une telle solution est garantie par le choix de $L_1^{(1)}$. En utilisant le développement asymptotique (2.38) de $\phi_{g_0}^c$, (2.22b) s'écrit

$$\begin{aligned}[\omega_{g_0}^c + \mathcal{L}^c]\phi_1^{(1)} = [\alpha_0^{(1)}(X) + \varepsilon\alpha_1^{(1)}(X) + \cdots]e^{i\varphi_1^+(X,\varepsilon)} \\ -L_1^{(1)}(\varepsilon)[\alpha_0(X) + \varepsilon\alpha_1(X) + \cdots]e^{i\varphi_0^+(X,\varepsilon)} \quad ,\end{aligned} \tag{2.58}$$

où

$$\varphi_l^+(X,\varepsilon) \equiv \frac{\int_{X_M}^X (k^+(r) + 2il\Im m[k^+](r))dr}{\varepsilon} \quad , \quad l = 0,1,2,\ldots , \tag{2.59}$$

et

$$[\alpha_0^{(1)}(X) + \varepsilon\alpha_1^{(1)}(X) + \cdots] \equiv \gamma(X)[\alpha_0(X) + \varepsilon\alpha_1(X) + \cdots]|\alpha_0(X) + \varepsilon\alpha_1(X) + \cdots|^2 \quad .$$

Cette équation peut s'intégrer par la méthode WKBJ. La solution admet ainsi un développement formel de la forme :

$$\begin{aligned}\phi_1^{(1)} = [a_0(X) + \varepsilon a_1(X) + \cdots]e^{i\varphi_1^+(X,\varepsilon)} - \frac{L_1^{(1)}(\varepsilon)}{\varepsilon}[b_0(X) + \varepsilon b_1(X) + \cdots]e^{i\varphi_0^+(X,\varepsilon)} \\ +\nu(\varepsilon)[\alpha_0(X) + \varepsilon\alpha_1(X) + \cdots]e^{i\varphi_0^+(X,\varepsilon)} + \lambda(\varepsilon)[\beta_0(X) + \varepsilon\beta_1(X) + \cdots]e^{i\varphi_0^-(X,\varepsilon)} \quad .\end{aligned} \tag{2.60}$$

Les deux premiers développements représentent une solution inhomogène particulière; les deux derniers, deux solutions homogènes indépendantes affectées de coefficients quelconques $\nu(\varepsilon)$ et $\lambda(\varepsilon)$. La première de ces solutions homogènes est le

développement WKBJ de la distribution spatiale $\phi^c_{g_0}$ [voir expression (2.38)], alors que la seconde est le développement WKBJ associé à la branche dominante k^-, la phase φ^-_0 étant définie par

$$\varphi^-_0(X,\varepsilon) = \frac{\int_{X_M}^{X} k^-(r)dr}{\varepsilon} \quad . \tag{2.61}$$

Les coefficients $a_r(X)$ et $b_r(X)$ sont calculés en introduisant le développement (2.60) dans l'équation (2.58) et en identifiant terme à terme les puissances de ε facteurs de $e^{i\varphi^+_1}$ et $e^{i\varphi^+_0}$. Nous avons reporté ce calcul en annexe A. En annexe B, on montre que les coefficients $a_r(X)$ et $b_r(X)$ sont singuliers respectivement aux zéros de $\omega^c_s + \mathcal{L}(k^+ + 2i\Im m[k^+], X, R_c)$ et aux zéros de $\partial_k \mathcal{L}(k^+, X, R_c)$.

Ce résultat n'est pas surprenant car, comme indiqué en annexe B, ces zéros définissent les points tournants associés aux ondes WKBJ composant la solution $\phi^{(1)}_1$ et les développements WKBJ présentent généralement des singularités aux points tournants. La détermination des régions du plan complexe en X où le développement (2.60) peut représenter asymptotiquement une solution de l'équation (2.58), repose comme on a déjà pu le signaler dans le chapitre 1, sur l'analyse des réseaux de lignes de Stokes associées à chaque couple d'ondes WKBJ. La solution inhomogène étant une somme de 3 ondes WKBJ, trois réseaux de lignes de Stokes doivent donc être impliqués. Ils sont examinés ci-dessous.

Le réseau de lignes de Stokes associé aux ondes WKBJ de phase φ^+_0 et φ^-_0 a déjà été étudié au chapitre 1; les points tournants et les lignes de Stokes sont définis respectivement par les équations (1.9) et (1.11) du chapitre 1 pour la valeur particulière ω^c_s de la fréquence. Il est représenté dans le plan complexe sur la figure 1.10b ou 1.10d.

D'aprés (2.59), le réseau associé aux ondes WKBJ de phase φ^+_1 et φ^+_0 est défini par

$$\Re e\left(\int_{X_\infty}^{X} \Im m[k^+](r)dr\right) = 0 \quad , \tag{2.62}$$

où X_∞ est un point tournant vérifiant

$$\Im m[k^+](X_\infty) = 0 \quad . \tag{2.63}$$

Cette relation permet ainsi d'identifier un certain nombre de points tournants : le point X_M sur l'axe réel où l'amplitude spatiale $|\phi^c_{g_0}|$ atteint son maximum, ainsi que tous les extréma locaux de l'amplitude du facteur de phase $e^{i\varphi_0^+}$ sur l'axe réel. Dans le cas le plus simple qu'on considérera par la suite, le point X_M est le **seul** point tournant, et c'est une raçine simple de (2.63). Le réseau de lignes de Stokes peut alors être esquissé : il est composé de quatre lignes de Stokes distinctes issues de X_M avec un angle égal à $\pi/4 + l\pi/2$, $l = 0, 1, 2, 3$. Ces lignes ne recoupent pas l'axe réel car dans le cas contraire, le point d'intersection X_R vérifierait $\int_{X_M}^{X_R} \Im m[k^+](r)dr = 0$, ce qui voudrait dire que $\Im m[k^+]$ change de signe, ou est nulle sur l'intervalle réel (X_M, X_R); et donc qu'il existe nécessairement un deuxième point tournant. Le réseau de lignes de Stokes obtenu est donc du type illustré sur la figure 2.2.

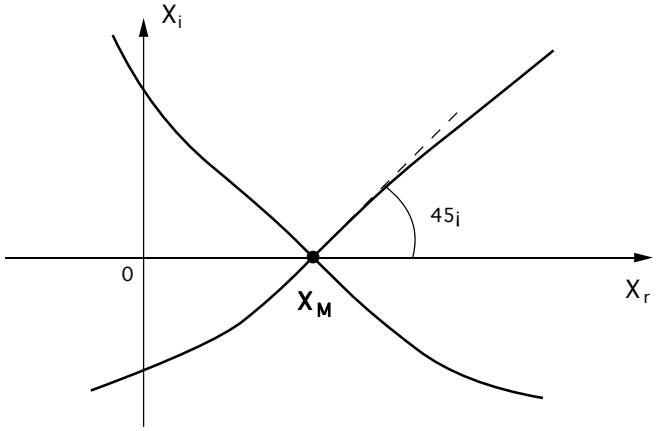

FIG. 2.2 - *Réseau de lignes de Stokes associées aux ondes WKBJ de phase φ_1^+ et φ_0^+ lorsque le point X_M est l'unique point tournant.*

Le réseau de lignes de Stokes associé aux ondes φ_1^+ et φ_0^- intervient lors de l'estimation par la méthode du col de l'intégrale J donnée en (2.49). Les points tournants sont en particulier définis par l'équation (2.52) et les lignes de Stokes sont

les contours d'amplitude constante du facteur de phase $e^{i(\varphi_1^+ - \varphi_0^-)}$ dans l'intégrale J. On a supposé qu'il existe au moins un point tournant dont le voisinage donne la partie dominante (2.53) de J. Dans le cas le plus simple, ce point tournant X_1 est unique et non dégénéré, et le réseau de lignes de Stokes partage alors le plan complexe en 4 régions issues de X_1, comme c'est le cas pour les deux autres réseaux de lignes de Stokes.

La superposition des 3 réseaux de lignes de Stokes conduit à une partition du plan complexe illustrée sur la figure 2.3. Généralement, la solution formelle (2.60)

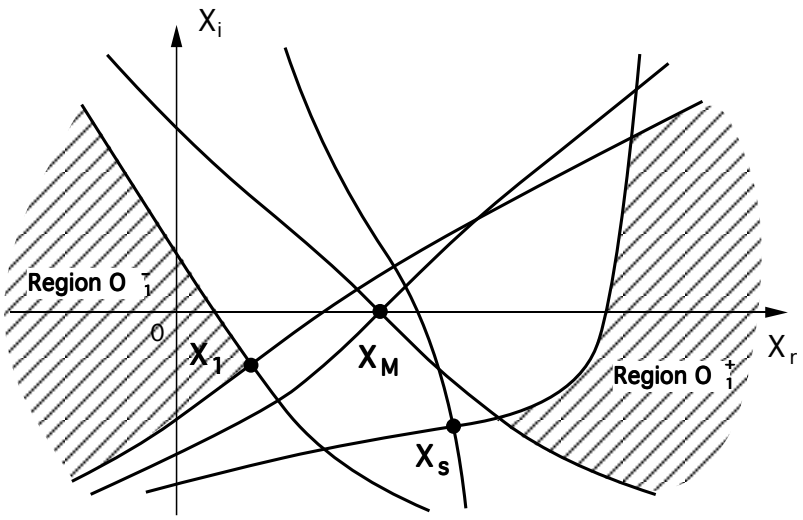

FIG. 2.3 - *Exemple de réseau de lignes de Stokes obtenu par la superposition des trois réseaux de lignes de Stokes associées aux couples d'ondes WKBJ de phases φ_1^+, φ_0^+ et φ_0^-. Les régions O_1^+ et O_1^- sont les régions, délimitées par les lignes de Stokes, contenant respectivement l'axe réel à $+\infty$ et $-\infty$, respectivement.*

n'est alors valable que dans une seule région délimitée par des lignes de Stokes. Cela signifie que lorsqu'une ligne de Stokes est traversée, les coefficients $\nu(\varepsilon)$ et $\lambda(\varepsilon)$ facteurs des solutions homogènes changent dans l'expression (2.60)[7]. Même dans le cas extrêmement simple considéré, dès que les trois points tournants X_s, X_M et X_1

7. Ce phénomène est communément appelé phénomène de Stokes. Pour plus de détails nous renvoyons le lecteur à Bender & Orszag (1978).

sont distincts, le nombre de régions obtenues est très important (voir figure 2.3).

Comme pour le problème linéaire étudié au chapitre 1, les régions délimitées par les lignes de Stokes contenant l'axe réel au voisinage de l'infini jouent un rôle particulier : c'est en effet dans ces domaines que l'on appellera région O_1^+ et région O_1^-, que sont imposées les conditions aux limites en $+\infty$ et $-\infty$ respectivement (voir figure 2.3). Parmi les ondes WKBJ composant la solution formelle (2.60), seule l'onde de phase φ_0^- ne tend pas vers zéro, mais vers l'infini, lorsque X tend vers $+\infty$ ou $-\infty$ [8]. Ainsi dans les régions O_1^+ et O_1^- la solution $\phi_1^{(1)}$ qui doit tendre vers zéro à l'infini admet un développement asymptotique de la forme (2.60) avec un coefficient $\lambda(\varepsilon)$ nul dans chacune des régions O_1^+ et O_1^-. Nous reviendrons sur ce développement dans la section suivante sous des hypothèses supplémentaires dans le but de calculer le coefficient $\nu(\varepsilon)$ dans chacune de ces régions.

Pour l'instant, notons que dans les autres régions du plan complexe $\lambda(\varepsilon)$ et $\nu(\varepsilon)$ ne sont pas directement spécifiés par les conditions aux limites [9]. La détermination d'une approximation de la fonction $\phi_1^{(1)}$ sur l'axe réel nécessite donc, dès que X_s et X_1 sont éloignés de X_M, le calcul d'un grand nombre de coefficients $\nu(\varepsilon)$ et $\lambda(\varepsilon)$. Bien que ce calcul soit possible par raccordement successif des solutions de chaque région, il est difficilement envisageable de systématiser une telle procédure aux ordres suivants, si le nombre de régions augmente à chaque étape. De plus, il faut être conscient du fait que le calcul des constantes $L_m^{(k)}$ n'est pas aussi immédiat que celui des constantes $L_1^{(0)}$ et $L_1^{(1)}$. Il fait en effet intervenir des intégrales de fonctions dont on ne connaît plus d'approximations uniformes, et donc pour lesquelles la méthode

8. L'hypothèse de validité des développements WKBJ à l'infini est ici utilisée. Autrement, on devrait dire: seule l'onde de phase φ_0^- (à cause de son comportement exponentiellement grand lorsque $\varepsilon \to 0$ pour des grands X) se raccorde à une solution qui est exponentiellement grande lorsque $X \to \infty$.

9. Notez en particulier que la solution $\phi_1^{(1)}$ peut contenir l'onde WKBJ linéaire de phase φ_0^- dans son développement asymptotique sur un grand intervalle de l'axe réel. Ce résultat est assez surprenant d'un point de vue physique car la solution $\phi_1^{(1)}$ est la distribution spatiale d'une correction non linéaire de l'onde WKBJ linéaire de phase φ_0^+ et que les intéractions non linéaires de cette dernière ne résonnent pas nécessairement avec l'onde φ_0^- dans le domaine physique.

du col est délicate à mettre en oeuvre.

Dans le but d'obtenir (pour tout m et k) une approximation des fonctions $\phi_m^{(k)}$ pour tout X réel, ainsi qu'une approximation des constantes $L_m^{(k)}$, il apparaît finalement essentiel de bien contrôler à la fois la fragmentation des solutions, c'est-à-dire le nombre de régions contenant une partie de l'axe réel, et les types d'ondes intervenant dans le développement WKBJ des solutions dans chacune de ces régions. Dans la section suivante, nous introduisons les conditions supplémentaires sur le réseau de lignes de Stokes qui permettent effectivement de réaliser cet objectif à l'ordre 1.

2.3.4 Cas particulier de la résonance locale

Nous sommes maintenant à même de préciser la notion de résonance évoquée à la fin de la section 2.3.2. Les approximations WKBJ des constantes $L_1^{(0)}$ et $L_1^{(1)}$ et de la fonction $\phi_1^{(1)}$ ont permis de mettre en évidence le rôle joué par les points tournants X_s, X_M et X_1 définis par les relations

$$k^+(X_s,\omega_s^c) = k^-(X_s,\omega_s^c) \quad , \tag{2.64a}$$

$$\Im m[k^+])(X_M,\omega_s^c) = 0 \quad , \tag{2.64b}$$

$$(k^+ + 2i\Im m[k^+])(X_1,\omega_s^c) = k^-(X_1,\omega_s^c) \quad . \tag{2.64c}$$

Ces expressions peuvent toutes s'interpréter comme des conditions de **résonance** entre différents couples de nombres d'onde dont les fonctions de phase associées sont définies par les relations (2.59) et (2.61). Ainsi, X_s est le point de résonance des ondes de phases φ_0^+ et φ_0^-, X_M le point de résonance de φ_1^+ et φ_0^+, X_1 le point de résonance de φ_1^+ et φ_0^-. Dans cette section, on introduit tout d'abord une hypothèse supplémentaire de **résonance locale** : les 3 points tournants X_s, X_M et X_1 sont dans un même voisinage d'ordre $\sqrt{\varepsilon}$, c'est-à-dire

$$X_s = X_M + \sqrt{\varepsilon}\,\overline{\Delta X} \qquad avec \;\; \overline{\Delta X} = O(1) \quad , \tag{2.65a}$$

$$X_1 = X_M + \sqrt{\varepsilon}\frac{\overline{\Delta X}}{K_1} \qquad avec \;\; \frac{\overline{\Delta X}}{K_1} = O(1) \quad . \tag{2.65b}$$

En développant l'équation (2.64c) au voisinage de X_M, on obtient l'approximation dominante de K_1 :

$$K_1 \sim 1 + a\sqrt{\frac{\omega_{kk}^M}{\omega_{0XX}^M}} \quad , \tag{2.66}$$

avec

$$a \equiv \Im m[k_{0X}^M] + \Re e\left[\sqrt{\frac{\omega_{0XX}^M}{\omega_{kk}^M}}\right] \quad . \tag{2.67}$$

On a vu au chapitre 1 que le réseau de lignes de Stokes du point tournant X_s pouvait donner lieu à des configurations "tordues" ("twisted Stokes lines") comme l'illustre la figure 1.10b. Le même phénomène est suceptible de se produire pour le réseau associé à X_1, ce qui nécessiterait l'analyse d'un grand nombre de régions distinctes pour obtenir une approximation uniforme de $\phi_1^{(1)}$ sur l'axe réel. On choisit ici de limiter l'étude aux configurations "non-tordues" ("untwisted Stokes lines") représentées sur la figure 1.10d. On introduit donc l'hypothèse supplémentaire suivante :

Pour tout réel X tel que $|X - X_M| \gg \sqrt{\varepsilon}$, on a

$$\Im m\left[\int_{X_M}^{X} (k^+(r) - k^-(r))dr\right] \gg \varepsilon > 0 \quad . \tag{2.68}$$

Ainsi, aucune des lignes de Stokes associés aux ondes de phase φ_0^+ et φ_0^- ne coupe l'axe réel ailleurs que dans un voisinage de X_M d'ordre $\sqrt{\varepsilon}$. Le réseau de lignes de Stokes du problème linéaire est alors du type illustré sur la figure 1.10d avec X_s vérifiant (2.65a), En se reportant à la définition de X_M et à la configuration des lignes de Stokes associée de la figure 2.2, on constate que

$$\Re e\left[\int_{X_M}^{X} \Im m[k^+](r))dr\right] \geq 0 \quad .$$

L'hypothèse (2.68) implique aussi

$$\Im m\left[\int_{X_M}^{X} (k^+(r) - k^-(r) + 2i\Im m[k^+](r))dr\right] \gg \varepsilon > 0 \quad ,$$

pour tout réel X tel que $|X - X_M| \gg \sqrt{\varepsilon}$. Ainsi aucune ligne de Stokes associé aux ondes WKBJ de φ_1^+ et φ_0^- ne coupe l'axe réel ailleurs que dans le voisinage de X_M.

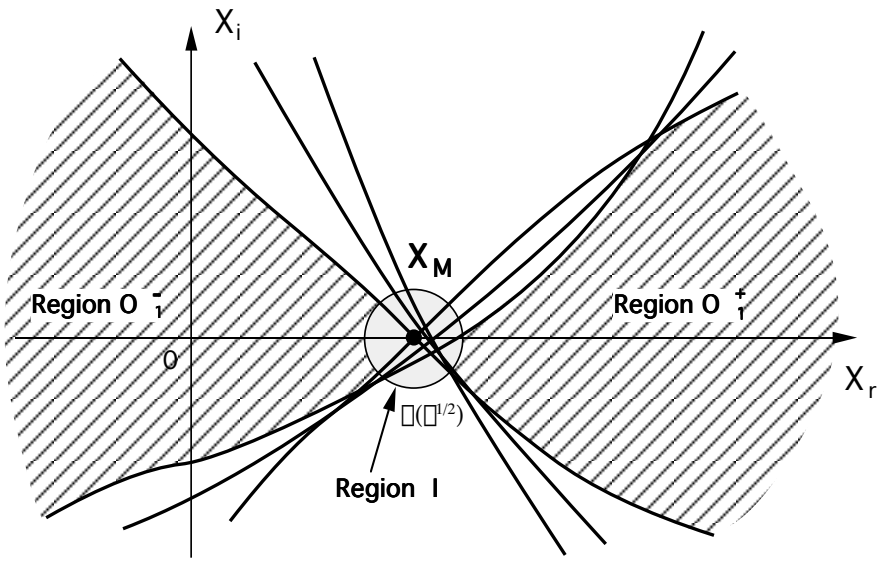

FIG. 2.4 - *Configuration du réseau de lignes de Stokes pour la correction $\phi_1^{(1)}$ sous les hypothèses supplémentaires introduites en section 2.3.4. Les régions extérieures O_1^+ et O_1^- et la région intérieure I couvrent entierement l'axe réel.*

En conséquence, on se ramène à la configuration de lignes de Stokes illustrée sur la figure 2.4. La détermination complète de la correction $\phi_1^{(1)}$ sur l'axe réel nécessite seulement l'étude de la région intérieure I et des régions extérieures O_1^+ et O_1^- (voir figure 2.4).

Valeurs des coefficients $L_1^{(0)}$ et $L_1^{(1)}$:

Les hypothèses supplémentaire introduites précedemment permettent d'évaluer au premier ordre les deux constantes $L_1^{(0)}$ et $L_1^{(1)}$. En utilisant les expressions (2.65a,b) reliant X_1 et X_s à X_M, les définitions (2.55a,b) de Θ et K deviennent

$$\Theta \sim -\frac{2a}{K_1}\overline{\Delta X}^2\varepsilon \quad ,$$
$$K \sim \frac{\gamma_M}{K_1} \quad .$$

On déduit immédiatement de (2.54b)

$$L_1^{(1)} \underset{\varepsilon\to 0}{\sim} \frac{\gamma_M}{K_1} e^{-\dfrac{2a\overline{\Delta X}^2}{K_1}} \quad , \tag{2.69}$$

où l'on rappelle que $\overline{\Delta X}$, K_1 et a sont respectivement définis par (2.65a), (2.66) et (2.67). De même, l'expression (2.54a) s'écrit sous la forme

$$L_1^{(0)} \underset{\varepsilon\to 0}{\sim} -\mathcal{L}_R(k_M^+, X_M; R_c) \quad . \tag{2.70}$$

Les deux coefficients $L_1^{(1)}(\varepsilon)$ et $L_1^{(0)}(\varepsilon)$ ont ainsi des limites non nulles quand $\varepsilon \to 0$. La condition physique (2.32) est donc bien vérifiée. La condition (2.34) s'écrit simplement $\mu \ll 1$ comme c'est le cas dans toute analyse faiblement non linéaire. La fonction de jauge $\delta(\varepsilon)$ calculée à l'aide de (2.29) dans la section 2.2.3 est d'ordre unité.

Approximation de la correction $\phi_1^{(1)}$ sur l'axe réel

Grâce aux hypothèses supplémentaires, on peut maintenant déterminer la forme du développement asymptotique de $\phi_1^{(1)}$ pour tout X réel. Compte tenu des résultats obtenus dans la section (2.3.3), on rappelle que le développement asymptotique de $\phi_1^{(1)}$ dans les régions O_1^+ et O_1^- est de la forme

$$\begin{aligned}\phi_1^{(1)\pm} = \quad & [a_0(X) + \varepsilon a_1(X) + \cdots] e^{i\varphi_1^+(X,\varepsilon)} - \frac{L_1^{(1)}(\varepsilon)}{\varepsilon}[b_0(X) + \varepsilon b_1(X) + \cdots] e^{i\varphi_0^+(X,\varepsilon)} \\ & + \nu^{\pm}(\varepsilon)[\alpha_0(X) + \varepsilon\alpha_1(X) + \cdots] e^{i\varphi_0^+(X,\varepsilon)} \ ,\end{aligned} \tag{2.71}$$

où les fonctions $a_r(X)$ et $b_r(X)$ sont données respectivement par les expressions (2.92) et (2.96) de l'annexe A.

Dans la région intérieure I, on recherche un développement de la fonction $\phi_1^{(1)}$ sous la forme

$$\tilde{\phi}_1^{(1)}(\tilde{X}, \varepsilon) = \frac{1}{\varepsilon}[\tilde{a}_0(\tilde{X}) + \sqrt{\varepsilon}\tilde{a}_1(\tilde{X}) + \cdots] e^{ik_M^+(x - x_M)} \tag{2.72}$$

Les fonctions $\tilde{a}_r(\tilde{X})$ sont déterminées de manière récursive en introduisant le développement (2.72) dans l'équation (2.22b) après avoir remplacé X par $X_M + \sqrt{\varepsilon}\tilde{X}$, développé les coefficients en séries de Taylor et identifié terme à terme les puissances de ε. La condition (2.22c) implique que $\tilde{a}_r(0) = 0$ pour tout r; couplée à la condition que les coefficients doivent être exponentiellement décroissant à l'infini[10] elle détermine de manière unique le développement (2.72).

Le raccordement des développements obtenus dans les régions O_1^+ et O_1^- avec celui obtenu dans la région intérieure I permet en principe de déterminer les coefficients $\nu^+(\varepsilon)$ et $\nu^-(\varepsilon)$. Nous nous contenterons ici de trouver l'équivalent de ces coefficients lorsque $\varepsilon \to 0$. La méthode consiste à réécrire les développement extérieurs (2.71) avec la variable intérieure $\tilde{X} = \frac{X - X_M}{\sqrt{\varepsilon}}$, et à comparer ensuite les expressions obtenues avec le développement intérieur (2.72). Elle nécessite la détermination du comportement de tous les coefficients a_r et b_r au voisinage de X_M. Ce calcul, bien que comportant peu de difficultés, est long et nous l'avons reporté en annexe B. Le résultat final [expressions (2.97a), (2.98a) et (2.100a,b) de l'annexe B] s'écrit

$$a_r(X_M + \sqrt{\varepsilon}\tilde{X}) \underset{\varepsilon\to 0}{\sim} \frac{\tilde{f}_r(\tilde{X})}{\varepsilon^{(r+1)}} \quad \forall r \geq 0 \quad , \tag{2.73a}$$

$$b_r(X_M + \sqrt{\varepsilon}\tilde{X}) \underset{\varepsilon\to 0}{\sim} \frac{\tilde{g}_r(\tilde{X})}{\varepsilon^{r}} \quad \forall r \geq 1 \quad , \tag{2.73b}$$

$$b_0(X_M + \sqrt{\varepsilon}\tilde{X}) \underset{\varepsilon\to 0}{\sim} [2i\partial_X(k^+ - k^-)(X_M)\omega_{kk}(X_M)]^{-1} \ln\varepsilon + \tilde{g}_0(\tilde{X}) \ . \tag{2.73c}$$

En utilisant le fait que les α_r ne sont pas singuliers en X_M, et $\alpha_0(X_M) = 1$, et

10. Cette deuxième condition provient de la condition de raccordement avec la solution dans les régions O_1^+ et O_1^-: le deuxième comportement possible des solutions est exponentiellement croissant, et il génère automatiquement des ondes WKBJ de phase φ_0^- dans les régions O_1^+ et O_1^-.

en exploitant les équivalents suivants

$$e^{i\phi_1^+} \underset{\varepsilon\to 0}{\sim} e^{ik_M^+(x-x_M)} e^{i\frac{\partial(k^+ + 2i\Im m[k^+])}{\partial X}(X_M)\frac{\tilde{X}^2}{2}} \quad ,$$
$$e^{i\phi_0^+} \underset{\varepsilon\to 0}{\sim} e^{ik_M^+(x-x_M)} e^{i\frac{\partial k^+}{\partial X}(X_M)\frac{\tilde{X}^2}{2}} \quad ,$$

le premier ordre de l'expression (2.71) écrite en variable intérieure devient :

$$\phi_1^{(1)\pm}(X_M + \sqrt{\varepsilon}\tilde{X}, \varepsilon) \underset{\varepsilon\to 0}{\sim} e^{ik_M^+(x-x_M)} \left[(P\frac{\ln\varepsilon}{\varepsilon} + \nu^{(\pm)}(\varepsilon)) e^{i\frac{\partial k^+}{\partial X}(X_M)\frac{\tilde{X}^2}{2}} + \frac{f(\tilde{X})}{\varepsilon} \right] \quad , \tag{2.74}$$

avec

$$P = -\frac{L_1^{(1)}}{2i\partial_X(k^+ - k^-)(X_M)\omega_{kk}(X_M)} \quad , \tag{2.75}$$

et

$$\tilde{f}(\tilde{X}) = \sum \tilde{f}_r(\tilde{X}) e^{i\frac{\partial(k^+ + 2i\Im m[k^+])}{\partial X}(X_M)\frac{\tilde{X}^2}{2}} + \sum \tilde{g}_r(\tilde{X}) e^{i\frac{\partial k^+}{\partial X}(X_M)\frac{\tilde{X}^2}{2}} \quad . \tag{2.76}$$

On suppose ici que $\tilde{f}$ définie par (2.76) a effectivement un sens. La condition de raccord avec l'expression (2.72) implique alors que $\tilde{f} = \tilde{a}_0$ et

$$\nu^{\pm}(\varepsilon) \underset{\varepsilon\to 0}{\sim} -P\frac{\ln\varepsilon}{\varepsilon} \quad . \tag{2.77}$$

Soulignons tout de même le fait suivant : bien que les fonctions ν^+ et ν^- aient le même équivalent, elles ne sont probablement pas égales. On pourrait d'ailleurs montrer que l'onde WKBJ de phase φ_1^+ dans l'équation (2.58) génère un saut d'ordre $O(1/\varepsilon)$ effectivement négligeable devant le terme $O(\ln\varepsilon/\varepsilon)$. L'expression (2.71) peut maintenant être simplifiée. Elle s'écrit au premier ordre

$$\phi_1^{(1)\pm} \underset{\varepsilon\to 0}{\sim} -P\frac{\ln\varepsilon}{\varepsilon}\phi_{g_0}^c \quad . \tag{2.78}$$

où l'on rappelle que $\phi_{g_0}^c$ représente le dernier terme de (2.71). La condition (2.35) écrite pour $m = 1$ et $k = 1$ implique ainsi

$$\mu \ll -\frac{\varepsilon}{\ln\varepsilon} \quad . \tag{2.79}$$

Sous les hypothèses supplémentaires de résonance locale au voisinage de X_M et de configurations "non-tordues" des lignes de Stokes (figure 2.4), nous avons donc pu calculer les deux coefficients $L_1^{(0)}$ et $L_1^{(1)}$ de l'équation de Landau ainsi que la correction $\phi_1^{(1)}$ sur l'axe réel. Contrairement au cas général considéré en section 2.3.2, la constante de Landau $L_1^{(1)}$ admet une limite bien définie permettent de déterminer la nature de la bifurcation. Alors que les écarts au seuil admissibles pouvaient être dans le cas général exponentiellement petits par rapport à ε, la condition nécessaire (2.79) exige seulement que l'écart au seuil μ soit très inférieur à $-\varepsilon/\ln\varepsilon$.

2.3.5 Interprétation de la condition de résonance locale sur un modèle simple.

Nous concluons cette étude par une interprétation des hypothèses supplémentaires de la section précédente pour un modèle simple d'opérateur $\mathcal{L}$. On suppose que les fonctions $\omega_{kk}(X;R)$, $k_0(X;R)$ et $\omega_0(X;R)$ apparaissant dans l'expression (2.2) de l'opérateur $\mathcal{L}$ admettent les variations particulières suivantes :

$$\omega_{kk}(X;R) = \omega_{kk}^s(R) \quad , \tag{2.80a}$$

$$k_0(X;R) = k_0^s(R) + k_{0X}^s(R)(X - X_s(R)) \quad , \tag{2.80b}$$

$$\omega_0(X;R) = \omega_s(R) + \frac{\omega_{0XX}^s(R)}{2}(X - X_s(R))^2 \quad . \tag{2.80c}$$

Le taux de croissance $\omega_i^{max}(X)$ défini par l'expression (1.13), ainsi que le taux de croissance absolu $\omega_{0,i}(X)$, sont donc des fonctions quadratiques de X qui tendent vers $-\infty$ en $\pm\infty$ dès que $\omega_{kk,i}^s < 0$ et $\omega_{0XX,i}^s - \frac{|\omega_{kk}^s|^2}{\omega_{kk,i}^s}[k_{0X,i}^s]^2 < 0$. Elles admettent un maximum unique, respectivement $\omega_{i,max}^{max}$ et $\omega_{0,i}^{max}$, et au plus deux zéros qui définissent les frontières de la région instable, et de la région instable absolue (voir figure 2.5). Nous désignerons par d_U et d_A la largeur de la région instable et de la région absolument instable respectivement. Chomaz *et al.* (1988) ont montré pour ce modèle qu'au seuil d'instabilité globale R_c, il existe une région absolument instable de largeur $d_A > 0$. Ceci implique nécessairement $\omega_{0,i}^{max} > 0$, $d_U > 0$ et $\omega_{i,max}^{max} > 0$.

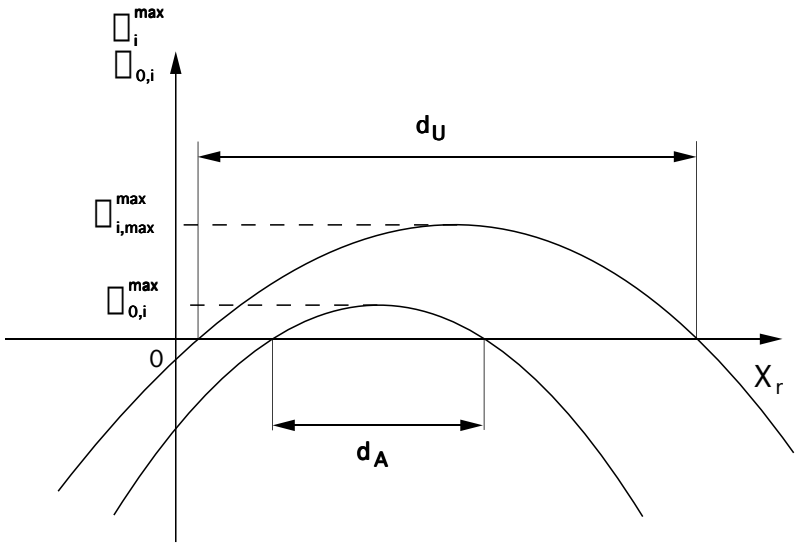

FIG. 2.5 - *Taux de croissance local maximum ω_i^{max} et taux de croissance local absolue $\omega_{0,i}$ en fonction de la position X au seuil d'instabilité globale R_c pour le modèle de Ginzburg-Landau quadratique défini en (2.2) et (2.80a,b,c). Le milieu contient une région localement instable de largeur d_U ainsi qu'une région localement absolument instable de largeur d_A.*

Nous allons montrer que les hypothèses supplémentaires introduites en section 2.3.4 entraînent des restrictions sur l'ordre de grandeur de ces quantités.

Dans cet exemple, le problème linéaire peut se résoudre pour des valeurs quelconques de ε. Les fréquences globales sont définies pour tout ε par les deux premiers ordres de l'expression (1.61). Ainsi, la fréquence globale ω_{g_0} est toujours la fréquence globale la plus instable. Les fonctions propres $\phi^c_{g_0}$ et $\phi^A_{g_0}$ ont des expressions particulièrement simples:

$$\phi^c_{g_0} = e^{\frac{i}{\varepsilon}\int_{X_M}^{X} k^+(r)dr} \quad , \tag{2.81a}$$

$$\phi^A_{g_0} = e^{\frac{i}{\varepsilon}\int_{X_M}^{X} [k^-(r)]^* dr} \quad , \tag{2.81b}$$

où

$$k^{\pm} = k_0^s - (k_{0X}^s + i\sqrt{\frac{\omega_{0XX}^s}{\omega_{kk}^s}})(X - X_s) \quad , \tag{2.82a}$$

$$X_M = \Re e[X_s] - \frac{\Im m[k_0^s] - \left(\Re e[k_{0X}^s] - \Im m\left[\sqrt{\frac{\omega_{0XX}^s}{\omega_{kk}^s}}\right]\right)\Im m[X_s]}{\Im m[k_{0X}^s] + \Re e\left[\sqrt{\frac{\omega_{0XX}^s}{\omega_{kk}^s}}\right]} \quad . \tag{2.82b}$$

Le calcul du point tournant X_1 peut se faire explicitement. La substitution de l'expression (2.82a) de k^+ dans l'équation (2.64c) conduit à

$$X_1 = X_M + \frac{X_s - X_M}{K_1^s} \quad , \tag{2.83}$$

avec

$$K_1^s = 1 + 2a_s\sqrt{\frac{\omega_{kk}^s}{\omega_{0XX}^s}} \quad , \tag{2.84a}$$

$$a_s \equiv \Im m[k_{0X}^s] + \Re e\left[\sqrt{\frac{\omega_{0XX}^s}{\omega_{kk}^s}}\right] \quad . \tag{2.84b}$$

L'hypothèse de résonance locale (2.65a,b) est alors équivalente à

$$|X_s - X_M| = O(\sqrt{\varepsilon}) \quad . \tag{2.85}$$

Compte tenu de l'expression (2.82b), elle est aussi équivalente à

$$\begin{cases} \Im m(X_s) = O(\sqrt{\varepsilon}) \quad , \\ \Im m(k_s) = O(\sqrt{\varepsilon}) \quad . \end{cases} \tag{2.86}$$

Les réseaux de lignes de Stokes associées aux couples d'ondes WKBJ de phases φ_0^+ et φ_0^-, de phases φ_1^+ et φ_0^+ et de phases φ_1^+ et φ_0^- sont composés de 2 droites se coupant respectivement en X_s, X_M et X_1. Aucun des réseaux de lignes de Stokes n'est donc "tordu", et les hypothèses supplémentaires (2.65a,b) et (2.68) se réduisent à la condition (2.85).

En calculant les quantités $\omega_{i,max}^{max}$ et d_U à l'aide des expressions (2.80a,b,c), on montre en particulier que la condition (2.85) est équivalente à l'une des conditions

suivantes

$$\omega_{i,max}^{max} = O(\varepsilon) \quad , \tag{2.87a}$$

$$d_U = O(\sqrt{\varepsilon}) \quad . \tag{2.87b}$$

Ces ordres de grandeurs s'appliquent également à $\omega_{0,i}^{max}$ et d_A : en utilisant (1.13), on montre qu'une quelconque des conditions (2.87a,b) entraîne

$$\omega_{0,i}^{max} = O(\varepsilon) \quad ,$$

$$d_A = O(\sqrt{\varepsilon}) \quad .$$

La réciproque est évidemment fausse.

Pour conclure, on peut aussi exprimer les conditions (2.87a,b) en fonction des paramètres critiques de déstabilisation du milieu. Le paramètre critique R_c de déstabilisation globale vérifie l'inégalité suivante

$$R_U \leq R_A \leq R_c \quad ,$$

où R_U et R_A sont respectivement les valeurs critiques associées à l'apparition d'une région instable (seuil d'instabilité locale), et d'une région absolument instable (seuil d'instabilité locale absolue). La condition (2.87b) sur la taille de la région instable signifie que R_U et R_c sont proches l'un de l'autre. Dans les cas non dégénérés, on aura ainsi

$$R_c - R_U = O(\varepsilon) \quad . \tag{2.88}$$

2.4 Conclusion

Ce chapitre a été consacré à l'extension dans le domaine faiblement non linéaire de l'analyse des modes globaux linéaires réalisée dans le chapitre 1. A cause de la présence d'un deuxième petit paramètre ε, les résultats classiques de l'analyse faiblement non linéaire ne s'appliquent pas de manière triviale. Nous avons obtenu

l'ensemble des conditions nécessaires et suffisantes pour qu'un mode global puisse avoir une amplitude décrite par l'équation de Landau au voisinage du seuil d'instabilité. On distingue deux types de conditions:

- la condition (2.32) qui est nécessaire pour pouvoir donner un sens physique à l'équation de Landau lorsque $\varepsilon \to 0$ et qui restreint de manière intrinsèque les modes globaux linéaires "acceptables".

- les conditions (2.34), (2.35) et (2.36) qui sont les limites de l'écart au seuil $\mu = R - R_c$.

Ces conditions ont été analysées pour le mode global avec un double point tournant (type 2) d'indice $n = 0$ obtenu au chapitre 1. La condition (2.32) a conduit au résultat surprenant suivant: l'équation de Landau n'a en général pas de sens physique, et plus précisément la nature de la bifurcation n'est pas définie à la limite $\varepsilon \to 0$. De plus, en raison de la condition (2.34), même lorsque l'équation de Landau a un sens, elle peut n'être valable que pour des écarts au seuil $R - R_c$ exponentiellement petits par rapport au paramètre ε. L'analyse faiblement non linéaire ne permet donc pas en général de décrire le comportement post-critique du mode global de type 2.

Nous pensons que les difficultés rencontrées proviennent du fait que les termes perturbatifs linéaires et non linéaires ont des contributions dominantes dans des régions éloignées du maximum X_M du mode global sur l'axe réel. A l'aide d'hypothèses supplémentaires sur le caractère local des premières résonances, nous avons étudié le cas où les effets perturbatifs proviennent à tous les ordres d'une région située au voisinage de X_M. L'équation de Landau a dans ces conditions un sens physique à la limite $\varepsilon \to 0$, et ses coefficients ne dépendent que des caractéristiques locales du milieu en X_M. Les conditions formelles (2.34), (2.35) impliquent nécessairement

$$R - R_c(\varepsilon) \ll -\frac{\varepsilon}{\ln \varepsilon} \quad .$$

Les hypothèses supplémentaires ont été interprétées en terme de caractéristiques locales d'instabilité sur le modèle de Ginzburg-Landau à coefficients quadratiques: les conditions (2.87a) ou (2.87b) signifient que le milieu doit être faiblement instable ou de manière équivalente instable dans une région très petite.

Le chapitre 1 a montré qu'il pouvait exister des situations pour lesquelles le mode global le plus instable est un mode de type 1. On peut appliquer les résultats de l'analyse développée dans la section 2.2 à condition de remplacer $\omega^c_{g_0}$ et $\phi^c_{g_0}$ par la fréquence $\omega^c_{g_{n(\varepsilon)}}$ et la distribution spatiale $\phi^c_{g_{n(\varepsilon)}}$ de ce mode. On obtient ainsi comme pour le mode global de type 2 avec $n = 0$, l'ensemble des conditions formelles garantissant la validité de l'équation de Landau au voisinage du seuil. En revanche, les modes de type 1 ayant deux points tournants distincts, l'hypothèse de résonance locale ne sera jamais vérifiée. Par conséquent, il est alors impossible de concentrer l'ensemble des effets perturbatifs linéaires et non linéaires au voisinage du maximum du mode global. Contrairement au cas du mode global avec double point tournant (type 2), l'équation de Landau n'est probablement jamais pertinente.

Nous avons considéré dans ce chapitre uniquement les modes globaux décrits par une équation de Ginzburg-Landau. Monkewitz *et al.* (1993) ont montré dans le cadre des écoulements cisaillés bidimensionnels, que l'addition d'une structure transverse non visqueuse ne modifiait pas la structure des modes globaux linéaires avec double point tournant (type 2). Les conditions de validité du régime faiblement non linéaire demeurent donc a priori inchangées. Sous les hypothèses de résonance locale, la détermination de l'équation de Landau nécessite cependant l'analyse des couches critiques visqueuses au voisinage de X_M (Le Dizès *et al.* 1991).

Il est essentiel de souligner que les difficultés rencontrées dans l'analyse faiblement non linéaire des modes globaux proviennent en totalité de l'hypothèse WKBJ de faible inhomogénéité du milieu. Rappellons que cette hypothèse a permis de définir et de relier les caractéristiques de l'instabilité locale et de l'instabilité globale

dans le régime linéaire. Dans les écoulements réels donnant lieu à un mode global amplifié tels que les jets et les sillages, la séparation entre l'échelle d'inhomogénéité du milieu et la longueur d'onde n'est pas nécessairement très marquée, ce qui pourrait expliquer le fait que l'équation de Landau semble expérimentalement vérifiée (Mathis *et al.* 1984).

Dans des études futures, il semblerait judicieux d'avoir recours à une approche fortement non linéaire où l'approximation dominante ne serait plus la fonction propre linéaire dans tout le domaine considéré. L'hypothèse WKBJ permettrait alors de conserver les notions d'instabilité locale et de mettre en évidence des effets **fortement** non linéaires dans certaines régions "intérieures" à définir. Dans ce cadre, la généralisation des concepts d'instabilité convective et absolue au régime non linéaire, récemment proposé par Chomaz (1992) pourrait s'avérer d'une grande utilité.

Annexe A : Calcul des coefficients $a_r(X)$ et $b_r(X)$ intervenant dans la correction $\phi_1^{(1)}$

Dans cette section, nous déterminons, par l'intermédiaire d'une relation de récurrence, l'ensemble des coefficients $a_r(X)$ et $b_r(X)$ apparaissant dans les expressions (2.60) et (2.71) de la fonction $\phi_1^{(1)}$. L'équation (2.58) est décomposée en deux parties correspondant aux deux ondes WKBJ du second membre :

$$[\omega_{g_0}^c + \mathcal{L}^c][a(X,\varepsilon)e^{i\varphi_1^+(X,\varepsilon)}] = [\alpha_0^{(1)}(X) + \varepsilon\alpha_1^{(1)}(X) + \cdots]e^{i\varphi_1^+(X,\varepsilon)} \quad (2.89a)$$

$$[\omega_{g_0}^c + \mathcal{L}^c][b(X,\varepsilon)e^{i\varphi_0^+(X,\varepsilon)}] = [\alpha_0(X) + \varepsilon\alpha_1(X) + \cdots]e^{i\varphi_0^+(X,\varepsilon)} \quad (2.89b)$$

où l'on a noté $a(X,\varepsilon) = \sum a_r(X)\varepsilon^r$ et $b(X,\varepsilon) = \sum b_r(X)\varepsilon^{r-1}$.

En vue d'évaluer $a_r(X)$, on décompose le premier membre de l'équation (2.89a) de la manière suivante:

$$\begin{aligned}[\omega_{g_0}^c + \mathcal{L}^c][a(X,\varepsilon)e^{i\varphi_1^+(X,\varepsilon)}] = e^{i\varphi_1^+(X,\varepsilon)} \quad & \Big[(\omega_s^c + \mathcal{L}^{c(1)+}(X)) \\ & +\varepsilon\left(\omega_2^c - i\mathcal{L}_k^{c(1)+}(X)\frac{\partial}{\partial X} - \frac{i}{2}\mathcal{L}_{kk}^{c(1)+}(X)\frac{\partial k_1^+}{\partial X}\right) \\ & +\varepsilon^2\left(\omega_4^c - \frac{1}{2}\mathcal{L}_{kk}^{c(1)+}(X)\frac{\partial^2}{\partial X^2}\right) \\ & +\varepsilon^3(\omega_6^c + \varepsilon\omega_8^c + \cdots)\Big]\, a(X,\varepsilon) \quad ,\end{aligned} \quad (2.90)$$

où

- ω_{2r}^c est la $r$ième correction de $\omega_{g_0}^c$: $\omega_{g_0}^c = \omega_s^c + \varepsilon\omega_2^c + \cdots$;
- $k_1^+ = k^+ + 2i\Im m[k^+]$;
- $\mathcal{L}^{c(1)+}(X) = \mathcal{L}(k_1^+, X, R_c)$;
- $\mathcal{L}_k^{c(1)+}(X) = \partial_k\mathcal{L}(k_1^+, X, R_c)$;
- $\mathcal{L}_{kk}^{c(1)+}(X) = \partial_{kk}\mathcal{L}(k_1^+, X, R_c) = -\omega_{kk}^c(X)$.

On peut alors simplifier par $e^{i\varphi_1^+}$ dans l'équation (2.89a). En identifiant terme à terme les développements en puissance de ε restants, on obtient

$$a_0(X) = \frac{\alpha_0^{(1)}}{\omega_s^c + \mathcal{L}^{c(1)+}(X)} \quad , \tag{2.91}$$

$$\begin{aligned} a_r(X) = \frac{1}{\omega_s^c + \mathcal{L}^{c(1)+}(X)} \Bigg\{ \alpha_r^{(1)} - \left(\omega_2^c - i\mathcal{L}_k^{c(1)+}(X)\frac{\partial}{\partial X} + \frac{i}{2}\omega_{kk}^c(X)\frac{\partial k_1^+}{\partial X} \right) a_{r-1}(X) \\ - \left(\omega_4^c + \frac{1}{2}\omega_{kk}^c(X)\frac{\partial^2}{\partial X^2} \right) a_{r-2}(X) - \omega_6^c a_{r-3}(X) - \cdots - \omega_{2r}^c a_0(X) \Bigg\} \quad . \end{aligned} \tag{2.92}$$

En vue d'évaluer $b_r(X)$, le premier membre de l'équation (2.89b) est décomposé d'une manière similaire :

$$\begin{aligned} [\omega_{g_0}^c + \mathcal{L}^c][b(X,\varepsilon)e^{i\varphi_0^+(X,\varepsilon)}] = e^{i\varphi_0^+(X,\varepsilon)} \quad & \Bigg[\varepsilon \left(\omega_2^c - i\mathcal{L}_k^{c+}(X)\frac{\partial}{\partial X} - \frac{i}{2}\mathcal{L}_{kk}^{c+}(X)\frac{\partial k^+}{\partial X} \right) \\ & + \varepsilon^2 \left(\omega_4^c - \frac{1}{2}\mathcal{L}_{kk}^{c+}(X)\frac{\partial^2}{\partial X^2} \right) \\ & + \varepsilon^3(\omega_6^c + \varepsilon\omega_8^c + \cdots) \Bigg] b(X,\varepsilon) \quad , \end{aligned} \tag{2.93}$$

où

$$\mathcal{L}_k^{c+}(X) = \partial_k \mathcal{L}(k^+, X, R_c) \qquad ; \qquad \mathcal{L}_{kk}^{c+}(X) = \partial_{kk}\mathcal{L}(k^+, X, R_c) = -\omega_{kk}^c(X) \ .$$

On en déduit alors l'équation satisfaite par $b_r(X)$:

$$\left(\omega_2^c - i\mathcal{L}_k^{c+}(X)\frac{\partial}{\partial X} + \frac{i}{2}\omega_{kk}^c(X)\frac{\partial k^+}{\partial X} \right) b_r(X) = h_r(X) \quad , \tag{2.94}$$

avec

$$h_0(X) = \alpha_0(X) \quad , \tag{2.95a}$$

$$h_r(X) = \alpha_r(X) - \left(\omega_4^c + \omega_{kk}^c(X)\frac{\partial^2}{\partial X^2} \right) b_{r_1}(X) - \omega_6^c b_{r_2}(X) + \cdots + \omega_{2r}^c b_0(X). \tag{2.95b}$$

Une solution particulière s'obtient ensuite facilement :

$$\begin{aligned} b_r(X) = \left[\int^X \frac{ih_r(u)}{\mathcal{L}^{c+}(u)} \exp\left(\int_{X_M}^u \frac{i\omega_2^c - (\partial_X k^+)(v)\omega_{kk}^c(v)/2}{\mathcal{L}_k^{c+}(v)} dv \right) du \right] \\ \times \exp\left(- \int_{X_M}^X \frac{i\omega_2^c - (\partial_X k^+)(v)\omega_{kk}^c(v)/2}{\mathcal{L}_k^{c+}(v)} dv \right) \quad . \end{aligned} \tag{2.96}$$

Annexe B : Comportement des coefficients $a_r(X)$ et $b_r(X)$ intervenant dans la correction $\phi_1^{(1)}$ au voisinage de X_M

On cherche à évaluer dans cette section les grandeurs $a_r(X_M + \sqrt{\varepsilon}\tilde{X})$ et $b_r(X_M + \sqrt{\varepsilon}\tilde{X})$ lorsque $\varepsilon \to 0$ sous les hypothèses supplémentaires introduites en section 2.3.4

L'expression $\omega_s^c + \mathcal{L}^{c(1)+}(X)$ apparaissant au dénominateur de (2.92) s'annule uniquement aux points $k_1^+ = k^+$ ou $k_1^+ = k^-$. Les zéros correspondants sont donc bien des points tournants associés aux couples d'ondes WKBJ de phases φ_1^+ et φ_0^+, et de phases φ_1^+ et φ_0^-.

L'hypothèse de résonance locale garantit alors que cette expression n'a que deux zeros X_1 et X_M et l'on peut écrire $\omega_s^c + \mathcal{L}^{c(1)+}(X) = g(X)(X - X_1)(X - X_M)$, avec $g(X)$ non nul et d'ordre unité en X_1 et X_M. La fonction $a_0(X)$ donnée par (2.91) admet ainsi un pôle simple au point X_1 et au point X_M et elle s'exprime sous la forme

$$a_0(X) = \frac{\alpha_0^{(1)}(X)}{g(X)(X - X_1)(X - X_M)} \quad .$$

Cette équation conduit, en utilisant la relation (2.65b) entre X_1 et X_M et le fait que $\alpha_0^{(1)}(X)$ et ses dérivées ne sont pas singuliers en X_M, à

$$a_0(X_M + \sqrt{\varepsilon}\tilde{X}) \sim \frac{\tilde{f}_0(\tilde{X})}{\varepsilon} \quad , \tag{2.97a}$$

$$\partial_X^l a_0(X_M + \sqrt{\varepsilon}\tilde{X}) \sim \frac{(\partial_{\tilde{X}}^l \tilde{f}_0)(\tilde{X})}{\varepsilon^{l/2+1}} \quad , \ \forall l > 0 \quad . \tag{2.97b}$$

On peut alors obtenir, par récurrence forte, les expressions suivantes de $a_r(X_M + \sqrt{\varepsilon}\tilde{X})$ et de ces dérivées

$$a_r(X_M + \sqrt{\varepsilon}\tilde{X}) \sim \frac{\tilde{f}_r(\tilde{X})}{\varepsilon^r} \quad , \tag{2.98a}$$

$$\partial_X^l a_r(X_M + \sqrt{\varepsilon}\tilde{X}) \sim \frac{(\partial_{\tilde{X}}^l f_r)(\tilde{X})}{\varepsilon^{l/2+r}} \quad , \ \forall l > 0 \quad . \tag{2.98b}$$

Démontrons ce résultat. On identifie pour cela la partie de la relation de récurrence (2.92) qui génère les singularités. Grâce au relations

$$k_1^+(X_M) = k^+(X_M) \;\; ; \quad \mathcal{L}_k(k^+(X_s), X_s, R_c) = 0 \;\; ; \quad X_s = X_M + \overline{\Delta X}\sqrt{\varepsilon} \;,$$

le coefficient de $\dfrac{\partial}{\partial X}$ dans la relation (2.92) s'écrit au voisinage de X_M :

$$\mathcal{L}_k^{c(1)+}(X_M + \sqrt{\varepsilon}\tilde{X}) \sim (c_1\tilde{X} + c_2)\sqrt{\varepsilon}$$

Les autres coefficients sont tous $O(1)$ ainsi que leurs dérivées. Si les relations (2.98a,b) sont vérifiées pour tout $l \leq r-1$, l'expression (2.92) devient

$$\begin{aligned} a_r(X_M + \sqrt{\varepsilon}\tilde{X}) \sim \Bigg(& (\omega_2^c - i\sqrt{\varepsilon}(c_1\tilde{X} + c_2)\frac{\partial}{\partial X} + \frac{i}{2}\omega_{kk}^c(X_M)\frac{\partial k_1^+}{\partial X_M})a_{r-1}(X_M + \sqrt{\varepsilon}\tilde{X}) \\ & + \frac{1}{2}\omega_{kk}^c(X_M)\frac{\partial^2 a_{r-2}}{\partial X^2}(X_M + \sqrt{\varepsilon}\tilde{X})\Bigg)\,[\varepsilon g(X_M)(\tilde{X} + \tfrac{\overline{\Delta X}}{K_1})\tilde{X}]^{-1} \quad . \end{aligned} \tag{2.99}$$

d'où on déduit (2.98a). Pour les dérivées, on reproduit le même raisonnement avec les dérivées de l'expression (2.92). L'équivalent obtenu est alors la dérivée du second membre de (2.99). La récurrence est ainsi établie.

On effectue le même type de raisonnement pour les fonctions $b_r(X)$. La fonction $b_0(X)$ a une singularité logarithmique en X_s et elle s'écrit

$$b_0(X) = g_0(X)\ln(X - X_s) \;,$$

avec g_0 non nul et d'ordre unité en X_s ainsi que ses dérivées. En utilisant [11]

- $\mathcal{L}_k^{c+}(X) \underset{X\to X_s}{\sim} \partial_X(k^+ - K^-)(X_s)\omega_{kk}^c(X_s)(X - X_s)$,
- $\dfrac{i\omega_2^c - (\partial_X k^+)(X)\omega_{kk}^c(X)/2}{\mathcal{L}_k^{c+}(X)} \underset{X\to X_s}{\sim} Cte$,

11. La deuxième expression est une propriété spécifique au mode global $n = 0$ qui s'obtient avec l'aide des expressions (1.61) des deux premiers ordres de $\omega_{g_0}^c$ et (1.8) de k^+. Elle est aussi démontrée dans Monkewitz *et al.* (1993).

on montre en particulier que

$$g_0(X_s) = i\frac{\alpha_0(X_s)}{\partial_X(k^+ - K^-)(X_s)\omega^c_{kk}(X_s)} \quad .$$

On déduit aussi facilement à l'aide des relations (2.95b) et (2.96), que pour tout $r \geq 1$, $b_r(X)$ a un pôle d'ordre $2r$ en X_s et s'écrit

$$b_r(X) = \frac{g_r(X)}{(X - X_s)^{2r}} \ ,$$

avec g_r non nul et d'ordre unité en X_s ainsi que ses dérivées. Par suite, l'équivalent de fonctions $b_r(X_M + \sqrt{\varepsilon}\tilde{X})$ est donné par

$$b_0(X_M + \sqrt{\varepsilon}\tilde{X}) \underset{\varepsilon\to 0}{\sim} i\frac{\alpha_0(X_s)}{\partial_X(k^+ - K^-)(X_s)\omega^c_{kk}(X_s)}[-\frac{1}{2}\ln\varepsilon + \ln\tilde{X}] \ , \quad (2.100a)$$

$$b_r(X_M + \sqrt{\varepsilon}\tilde{X}) \underset{\varepsilon\to 0}{\sim} \frac{\tilde{g}_r(\tilde{X})}{\varepsilon^r} \quad . \quad (2.100b)$$

Chapitre 3

VISCOUS STRUCTURE OF PLANE WAVES IN SPATIALLY-DEVELOPING SHEAR FLOWS

Stéphane Le Dizès*, Peter A. Monkewitz# and Patrick Huerre*

*Laboratoire d'Hydrodynamique (LadHyX)
Ecole Polytechnique, F-91128 Palaiseau cedex, France.

#Département de Mécanique, IMHEF,
Ecole Polytechnique Fédérale de Lausanne, ME-Ecublens,
CH-1015 Lausanne, Switzerland.

Abstract

This paper is concerned with the propagation of linear plane waves in incompressible, two-dimensional weakly nonparallel shear flows. These waves are analysed for arbitrary complex frequency and local wavenumber when the non-parallelism is assumed to be due to small viscous diffusion. The inviscid approximation correctly describes, at leading order, the cross-stream variations of local plane waves at all station where they are locally amplified in the frame of reference moving at the local phase speed $\omega_{,r}/k_{,r}$, i.e. when the growth rate $\sigma \equiv \omega_{,i} - k_{,i}\omega_{,r}/k_{,r}$ is positive. This result also holds when the local phase speed is outside the range of values reached by the basic velocity profile. By contrast, the inviscid approximation fails to represent cross-stream variations in the neighborhood of critical points when the waves are locally neutral ($\sigma = 0$), and in large viscous regions when they are damped ($\sigma < 0$). Uniform WKBJ approximations are obtained in these regions and the results are applied to the description of forced spatial waves and self-excited global modes.

3.1 Introduction

Most incompressible, two-dimensional unbounded shear flows are known to exhibit under certain conditions coherent large scale structures. The goal of this article is to describe these structures when they can be considered as local plane waves on a weakly non-parallel basic flow. Asymptotic approximations are obtained for arbitrary complex frequency and local wavenumber when the non-parallelism is induced by small viscous diffusion.

Since convectively unstable flows such as mixing layers and jets are known to be very sensitive to noise excitation, numerous experiments have been conducted to analyse the coherent structures that appear in response to a time-periodic excitation. Such structures have been found to be well-described by linear spatially-growing instability waves at their early stages of evolution. Using the multiple scale method by Bouthier (1972) in combination with WKBJ approximations, which takes into account the weak non-parallelism of the basic flow, Crighton & Gaster (1976) and Gaster *et al.* (1985) obtained good agreement with experimental results in jets and mixing layers respectively.

Due to viscous spreading of the basic flow, the local spatial growth rate of the instability wave typically becomes negative beyond some streamwise station. At least, two distinct types of streamwise evolution are then possible. If the maximum amplitude of the wave which is reached at the point of local neutral stability is sufficiently large, the critical layer is necessarily dominated by nonlinearities (Goldstein & Leib 1988, Goldstein & Hultgren 1988). By contrast, if it is sufficiently small, viscous diffusion dominates in the critical layer. In the present study, we are only concerned with the linear evolution of spatial waves in the viscous critical layer régime. In other words, local plane waves grow exponentially, reach neutral, and spatially decay as they propagate downstream.

In parallel flows, neutral eigenfunctions are known to exhibit critical layers in

which the inviscid approximation breaks down. For damped modes, the behavior of the eigenfunction is even more singular, since it involves large viscous regions in the limit of large Reynolds number (Tatsumi & Gotoh 1971). We then expect the inviscid approximation of Crighton & Gaster (1976) to become singular. One purpose of this article is to obtain WKBJ approximations in the region where the inviscid approximation breaks down.

Local plane waves are also essential ingredients of the global mode problem. Several shear-flows such as wakes (Karniadakis & Triantafyllou 1989), hot jets (Monkewitz *et al.* 1990), and counterflow mixing layers (Strykowski & Niccum 1991) exhibit self-excited oscillations. In such situations, the observed coherent structures are not created by external forcing but appear through a destabilization of the entire flow. Typically, they are represented in terms of global modes, i.e. linear time-harmonic perturbations of the basic flow satisfying homogeneous boundary conditions in all spatial directions. The complex global frequencies are then the result of an eigenvalue problem. If the basic flow is weakly non-parallel, global modes can be studied by the WKBJ method (Huerre & Monkewitz 1990). In this framework, a theory to determine the global frequencies has been developed (Chomaz *et al.* 1992, Le Dizès *et al.* 1993b) and recently applied to shear-flows by Monkewitz *et al.* (1993) and Pesenson & Monkewitz (1993) in an inviscid context. In particular, each global mode has been demonstrated to be locally a plane wave of complex global frequency and spatially varying complex wavenumber of the kind studied by Crighton & Gaster (1976). Knowing the critical point singularity that these modes may exhibit beyond the point of neutral stability, we may wonder if the inviscid limit process is valid everywhere.

Both the signaling and global mode problems address the same issues:

– For a given complex frequency and local wavenumber, what is the cross-stream scale of that wave, or equivalently in which regions does the inviscid analysis

of Crighton & Gaster (1976) apply?

– What is the local plane wave approximation in regions where the inviscid approximation breaks down?

The paper is organized as follows. The basic equations are given in section 3.2, where we show that the issue of finding the characteristic cross-stream scale (viscous or inviscid) of the plane wave is locally equivalent to the associated parallel flow problem. Classical results from temporal theory (k real) concerning the validity of the inviscid approach for parallel flows are extended to arbitrary complex wavenumbers in section 3.3. They are applied to local plane waves of arbitrary complex frequency and wavenumber in slowly varying flows in section 3.4. Viscous regions are shown to develop around any real critical point $(X_p, y_c(X_p))$ defined by

$$-i\omega + ik(\omega, X_p)U_0(y_c(X_p), X_p) = 0 \quad .$$

In section 3.5, a uniform approximation of local plane waves in the viscous region is constructed and matched with the inviscid approximation of Crighton & Gaster (1976). The application of the results to the signaling and global mode problems is discussed in the final section.

3.2 The basic equations

In the following, we consider a two-dimensional, incompressible, spatially-developing shear flow governed by the vorticity equation:

$$\left[\frac{\partial}{\partial t} + \frac{\partial \Psi_T}{\partial y}\frac{\partial}{\partial x} - \frac{\partial \Psi_T}{\partial x}\frac{\partial}{\partial y}\right]\nabla^2\Psi_T = \frac{1}{Re}\nabla^2\nabla^2\Psi_T \quad , \tag{3.1}$$

where Ψ_T is the total streamfunction. The streamwise and cross-stream coordinates x and y are normalized with respect to a typical instability wavelength λ or a characteristic vorticity thickness. Time t and all velocities are normalized by $\lambda/\overline{U}$ and $\overline{U}$ respectively, where $\overline{U}$ is a characteristic basic streamwise velocity.

The time-independent part $\Psi^{(0)}$ of Ψ_T satisfies:

$$\left[\frac{\partial\Psi^{(0)}}{\partial y}\frac{\partial}{\partial x}-\frac{\partial\Psi^{(0)}}{\partial x}\frac{\partial}{\partial y}\right]\nabla^2\Psi^{(0)}=\frac{1}{Re}\nabla^2\nabla^2\Psi^{(0)} \quad . \tag{3.2}$$

As long as no body forces are present, the weakly non-parallel assumption is equivalent to assuming that the leading-order approximation $\Psi_0^{(0)}$ of $\Psi^{(0)}$ varies on the slow viscous scale x/Re with $Re \gg 1$. The small parameter ε defined by λ/L, where L is a characteristic scale of the inhomogeneity is another measure of the degree of nonparallelism, and it is directly linked to the Reynolds number through

$$Re=\frac{R}{\varepsilon}\ where\ R=O(1) \quad . \tag{3.3}$$

Variations of $\Psi_0^{(0)}$ thus occur on the slow scale $X=\varepsilon x$ and equation (3.2), up to order $O(\varepsilon^2)$, becomes a boundary layer equation for $\Psi_0^{(0)}$:

$$[\frac{\partial\Psi_0^{(0)}}{\partial y}\frac{\partial^3\Psi_0^{(0)}}{\partial X\partial y^2}-\frac{\partial\Psi_0^{(0)}}{\partial X}\frac{\partial^3\Psi_0^{(0)}}{\partial y^3}]=\frac{1}{R}\frac{\partial^4\Psi_0^{(0)}}{\partial y^4} \quad . \tag{3.4}$$

If the vorticity equation is linearized around the time-independent solution $\Psi^{(0)}$, the perturbation $\Psi=\Psi_T-\Psi^{(0)}$ of the basic flow satisfies

$$\left[(\frac{\partial}{\partial t}+U_0\frac{\partial}{\partial x})\nabla^2-U_{0yy}\frac{\partial}{\partial x}+\varepsilon[V_0\nabla^2\frac{\partial}{\partial y}-V_{0yy}\frac{\partial}{\partial y}-\frac{1}{R}\nabla^2\nabla^2]+O(\varepsilon^2)\right]\Psi=0 \quad , \tag{3.5}$$

where the functions $(U_0(y,X),\varepsilon V_0(y,X))=(\frac{\partial\Psi_0^{(0)}}{\partial y},-\varepsilon\frac{\partial\Psi_0^{(0)}}{\partial X})$ are the leading-order streamwise and cross-stream basic flow velocities, and $\nabla^2=\frac{\partial^2}{\partial x^2}+\frac{\partial^2}{\partial y^2}$.

We shall only consider local plane wave solutions of (3.5). For this purpose, Ψ is assumed to be a time-harmonic function of frequency ω and local wavenumber k defined by

$$k=-\frac{i}{\Psi}\frac{\partial\Psi}{\partial x} \quad , \tag{3.6}$$

which is, at leading order, a function $k(\omega,X)$ depending continuously on space variables only through the slow scale X. Furthermore, Ψ is subject to boundary conditions in the cross-stream y direction at infinity.

A leading-order expression for plane waves of frequency ω and wavenumber $k(\omega, X)$ is obtained in the form

$$\Psi = \Phi(x, y, \varepsilon) e^{\frac{i}{\varepsilon}\int_{X_m}^{X} k(\omega,r)dr} e^{-i\omega t} \quad , \tag{3.7}$$

where Φ satisfies the conditions

$$\frac{1}{\Phi}\frac{\partial \Phi}{\partial x} \ll 1 \; for \; all \; X \; and \; y \quad , \tag{3.8}$$

and

$$\lim_{y\to\infty} |\Phi| = 0 \quad . \tag{3.9}$$

The reference point in the integral is a constant that can be fixed by a local normalization condition. Note that no boundary conditions have been applied in the streamwise direction.

These solutions are the starting point in the WKBJ approach to describe instabilities of weakly non-parallel flows. In that framework, all solutions are **locally** decomposed into local plane waves at any streamwise station X. The frequency ω is either a given real number in the forced case, where the response to an oscillating source is sought or, an unknown complex number in the global mode case that is determined by an eigenvalue problem in the streamwise direction. To cover both instances, we shall consider an arbitrary complex frequency ω in the subsequent analysis.

The equation satisfied by $\Phi(x, y, \varepsilon)$ is immediately obtained by inserting the function Ψ given by expression (3.7) into equation (3.5). Its leading-order expression depends on the characteristic cross-stream scale of the local plane wave. If this scale is the typical wavelength λ used to non-dimensionalise equation (3.1), Φ is found to satisfy the Rayleigh equation

$$\left[(-i\omega + ik(\omega, X)U_0(y, X))(\frac{\partial^2}{\partial y^2} - k^2(\omega, X)) - iU_{0yy}(y, X)k(\omega, X)\right] \Phi = 0 \quad . \tag{3.10}$$

The function $\Phi(x, y, \varepsilon)$ is in this case a solution of the inviscid parallel flow instability problem on the local basic flow $U_0(y, X)$. The reduction at leading order to the inviscid equation (3.10) is indeed justified in the signaling problem (ω real) in regions where the local plane wave is spatially amplified (Crighton & Gaster 1976). However, when the local plane wave is spatially damped or when the frequency is complex, such a reduction is not guaranteed everywhere. There is a priori then no reason to assume that the characteristic scale is everywhere inviscid.

If variations in the cross-stream direction are for instance faster, the viscous term may become dominant. With a balance between viscous and inviscid effects, the cross-stream scale is viscous in character and given by $y_v = y/\sqrt{\varepsilon}$, and the leading-order equation obtained from (3.5) takes the form

$$\left[(-i\omega + ik(\omega, X)U_0(y, X))\frac{\partial^2}{\partial y_v^2} - \frac{1}{R}\frac{\partial^4}{\partial y_v^4}\right]\Phi = 0 \quad . \tag{3.11}$$

One can easily show that for scales other than y and y_v, the leading-order equation for Φ can always be obtained from either equation (3.10) or (3.11) : if Φ varies faster than the inviscid scale, the governing leading-order equation can be deduced from (3.11); if the variations are slower, they can be deduced from the Rayleigh equation (3.10).

One notes that (3.10) and (3.11) are also the only two possible leading-order expressions for $Re \to \infty$ that can be deduced from the Orr-Sommerfeld equation of the equivalent parallel flow problem :

$$\begin{aligned}\Big[(-i\omega + ik(\omega; X)U_0(y; X))(\frac{\partial^2}{\partial y^2} - k^2(\omega; X)) - iU_{0yy}(y; X)k(\omega; X) \\ -\frac{1}{Re}(\frac{\partial^2}{\partial y^2} - k^2(\omega; X))^2\Big]\Phi = 0.\end{aligned} \tag{3.12}$$

This implies that, for any fixed X and $Re \to \infty$, the cross-stream variations of Φ are described by equation (3.12). As a consequence, one immediately deduces that the problem of finding the leading-order equation satisfied by Φ can indeed be resolved in

the context of parallel flow analysis and be formulated as follows : For given complex eigenvalues ω and $k = k(\omega; X)$ and a given streamwise basic velocity profile $U_0(y; X)$, what are the regions in which the function Φ of the parallel instability problem (3.12) with homogeneous boundary conditions at ∞ satisfies at leading order the Rayleigh equation (3.10) when $Re \to \infty$? The main results relating to this issue are presented in the next section.

3.3 Stability analysis of parallel shear flows

The justification of the inviscid approach is an old issue that has been resolved during the 40's and 50's. The major results have been obtained in the temporal framework where k is assumed real. Extensions of these results are given for arbitrary complex ω and k.

We first need to introduce two quantities σ and δ defined by

$$\sigma = \omega_{,i} - \frac{\omega_{,r}}{k_{,r}} k_{,i} \quad , \tag{3.13a}$$

$$\delta = \left[\frac{\omega_{,r}}{k_{,r}} - U_{0,min} \right] \left[\frac{\omega_{,r}}{k_{,r}} - U_{0,max} \right] \quad . \tag{3.13b}$$

The parameter σ represents the temporal growth rate of the instability wave of frequency ω and wavenumber k in a frame of reference moving at the phase speed $\omega_{,r}/k_{,r}$ where the subscript r denotes the real part. The parameter δ characterises the value of the phase speed relative to the range of basic flow velocities : δ is negative (resp. positive) when there exists (resp. does not exist) a location on the real y-axis where $U_0(y; X) = \omega_{,r}/k_{,r}$.

The following statements will be proven :

(a) $\delta > 0$ **or** $\sigma > 0$: The inviscid eigenfunction is the asymptotic limit of the Orr-Sommerfeld eigenfunction for $Re \to \infty$; the Rayleigh equation (3.10) is the leading-order equation satisfied by Φ for all real y.

(b) $\delta \leq 0$ **and** $\sigma = 0$: Real points where U_0 equals the phase speed $\omega_{,r}/k_{,r}$ are critical points around which the Rayleigh equation (3.10) is not the leading-order equation.

(c) $\delta \leq 0$ **and** $\sigma < 0$: There may exist large viscous regions in which the Orr-Sommerfeld eigenfunction does not reduce to a solution of the Rayleigh equation (3.10) when $Re \to \infty$.

Note that each statement corresponds to a classical result of temporal theory when k is real, which may be found in Lin (1955), for instance.

Statement (a) is proven using the following result of Lin (1955) (itself deduced from Wasow 1948): there exist four formal independent solutions ϕ_j , $j \in \{1,2,3,4\}$ of the Orr-Sommerfeld equation that admit the following expansions

$$\phi_1 = \phi_1^{(0)} + \frac{1}{Re}\phi_1^{(1)} + \cdots \quad , \tag{3.14a}$$

$$\phi_2 = \phi_2^{(0)} + \frac{1}{Re}\phi_2^{(1)} + \cdots \quad , \tag{3.14b}$$

$$\phi_3 = e^{\int^y \sqrt{Re(ikU_0 - i\omega)}}[\phi_3^{(0)} + \frac{1}{\sqrt{Re}}\phi_3^{(1)} + \cdots] \quad , \tag{3.14c}$$

$$\phi_4 = e^{-\int^y \sqrt{Re(ikU_0 - i\omega)}}[\phi_4^{(0)} + \frac{1}{\sqrt{Re}}\phi_4^{(1)} + \cdots] \quad . \tag{3.14d}$$

The two functions ϕ_1 and ϕ_2 are commonly called the "inviscid" solutions of the Orr-Sommerfeld equation. Their leading-order approximations $\phi_1^{(0)}$ and $\phi_2^{(0)}$ satisfy equation (3.10) and viscous effects only appear as correction terms at order $1/Re$. The two other functions ϕ_3 and ϕ_4 are purely "viscous" solutions. Their leading-order approximations satisfy equation (3.11). Lin (1955) has demonstrated that the four **formal** functions (3.14a,b,c,d) represent **asymptotic** solutions of the Orr-Sommerfeld equation when $Re \to \infty$, which are **uniformly valid** in any domain D where any two points can be connected by a curve along which $\Re e[\int^y \sqrt{Re(ikU_0 - i\omega)}]$ changes monotonically.

Under the assumption (a), the square root $\sqrt{Re(ikU_0 - i\omega)}$ can be chosen such that $\Re e[\sqrt{Re(ikU_0 - i\omega)}]$ remains strictly positive on the entire real axis. The exponent $\Re e[\int^y \sqrt{Re(ikU_0 - i\omega)}]$ is then a strictly increasing function on the entire real axis and the above theorem applies. The boundary conditions applied to

$$\phi = a_1\phi_1 + a_2\phi_2 + a_3\phi_3 + a_4\phi_4 \tag{3.15}$$

imply that $a_3 = a_4 = 0$ since ϕ_3 and ϕ_4 are exponentially large in $+\infty$ and $-\infty$, respectively. Thus, the leading-order approximation for ϕ reduces to $a_1\phi_1^{(0)} + a_2\phi_2^{(0)}$ and thus satisfies equation (3.10). This proves statement (a)[1].

Note that when k is real and equation (3.10) is asymptotically valid on the real axis, Howard's semi-circle theorem guarantees that $\omega_{,r}/k_{,r}$ is always in the range of U_0, i.e. $\delta \leq 0$. No such theorem can be derived when k is complex; therefore, configurations for which $\omega_{,r}/k_{,r}$ is outside the range of U_0, and σ is positive, may a priori exist.

The proof of statements (b) and (c) is similar to their equivalent in temporal theory. Its principle is based on the analysis of Orr-Sommerfeld solutions in the limit $Re \to \infty$ near a critical point y_c, defined by $-i\omega + ikU_0(y_c) = 0$. The Orr-Sommerfeld solutions are known to have no uniform decomposition into formal solutions (3.14a,b,c,d) in a full complex neighborhood of critical points. The vicinity of y_c is in fact partitioned into Stokes sectors delimited by Stokes lines defined by $\Re e[\int_{y_c}^y \sqrt{Re(ikU_0 - i\omega)}] = 0$. Close to a first-order critical point y_c, the direction of Stokes lines is given by

$$arg(y - y_c) = \pi/6 + arg(k) + arg(U_{0y}(y_c)) + 2l\pi/3 \ , \ l = 0, 1, 2 \ , \tag{3.16}$$

which means that three Stokes sectors of equal angle $2\pi/3$ emanate from y_c. An important result, first proven by Wasow (1948) is the following: if in one sector the

1. Note that no assumptions have to be made concerning the number of critical points involved in the problem. In a certain sense, it generalizes also the results of temporal theory found in text books which usually treat problems involving only one or two critical points.

solution is approximated by an "inviscid" solution that becomes singular[2] at y_c, say ϕ_1 is non singular and ϕ_2 is singular, it is necessarily asymptotic to a dominant viscous solution ϕ_3 or ϕ_4 in at least one of the 2 other Stokes sectors. It follows that, if the real axis crosses the 3 sectors, a region of the physical domain may be viscous.

This is indeed what happens when σ evolves from positive to slighty negative values with $\omega_{,r}/k_{,r}$ in the range of U_0 ($\delta \leq 0$). In such a case one critical point (at least) moves onto the real axis at a point y_c where $U_0(y_c) = \omega_{,r}/k_{,r}$. This critical point crosses the real axis when σ evolves towards negative values as soon as $U_{0y}(y_c)$ is nonzero[3] for $\sigma = 0$. The evolution of the Stokes line network in the neighborhood of such a critical point is illustrated in figure 3.1. When $\sigma > 0$, the real axis cuts only one Stokes line: both Stokes sectors containing the real axis are inviscid at leading order and the Orr-Sommerfeld eigenfunction can be expanded as $a_1\phi_1 + a_2\phi_2$ as established above. If one excludes the exceptional case where the coefficient a_2 of the singular "inviscid" solution ϕ_2 is zero, the Orr-Sommerfeld eigenfunction becomes viscous in the third sector and in the neighborhood of the critical point y_c: one obtains the asymptotic behavior illustrated on figure 3.1a. When σ evolves continuously towards negative values, the Stokes sectors as well as the asymptotic behavior of the Orr-Sommerfeld eigenfunction are expected to vary in a continuous manner. The decomposition of ϕ into $a_1\phi_1 + a_2\phi_2$ should still be possible in the two Stokes sectors which contained the real axis when σ was positive. As long as the coefficient of the singular solution is not identically zero during the process, the Orr-Sommerfeld eigenfunction ϕ is viscous in the third sector and in the critical layer as illustrated in figure 3.1b,c. In figure 3.1b, only the critical layer is cut by the real axis: the viscous region is localized in a neighborhood of the critical point.

2. At least one of the 2 independent "inviscid" solutions has a singular expansion at y_c. If $U_{0yy}(y_c) \neq 0$, that logarithmic singularity appears at leading order in the expansion in powers of $1/Re$.

3. Note that if $U_{0y}(y_c) = 0$ for $\sigma = 0$, y_c is a double critical point: two critical points from opposite sides of the real axis have then collided to give the configuration illustrated on figure 3.4a.

In figure 3.1c, the viscous Stokes sector is cut by the real axis and a large region of the real axis is viscous. Statements (b) and (c) are then established.

On figure 3.1b the Stokes lines network near a real critical point in temporal theory are shown in dashed lines [see figure 8.2 of Lin (1955) for instance]. One notices that the Stokes lines limiting the viscous sector do not necessarily correspond to the angles $+\pi/6$ and $+5\pi/6$ but are subject to an additional rotation of amount $arg(k)$ according to equation (3.16). If $arg(k) = \pi/6 + l\pi/3,\ l \in \{0,1,2,3,4,5\}$, one of the Stokes lines delimiting the viscous region is asymptotic to the real axis near y_c. In this case, the viscous region is not confined to the critical layer [as illustrated in figure 3.1b] but spreads along the real axis as far as the Stokes line is within a distance of order ε from the real axis.

We have shown that the existence of viscous regions is guaranteed if these modes can be obtained by a continuous process from amplified modes ($\sigma > 0$) with $\omega_{,r}/k_{,r}$ remaining in the range of U_0. As illustrated in figure 3.1, the viscous regions are then determined by studying the evolution of complex critical points and Stokes lines in the complex y plane as a function of σ. If this is not the case, viscous regions do not necessarily exist for modes satisfying the assumptions (c).

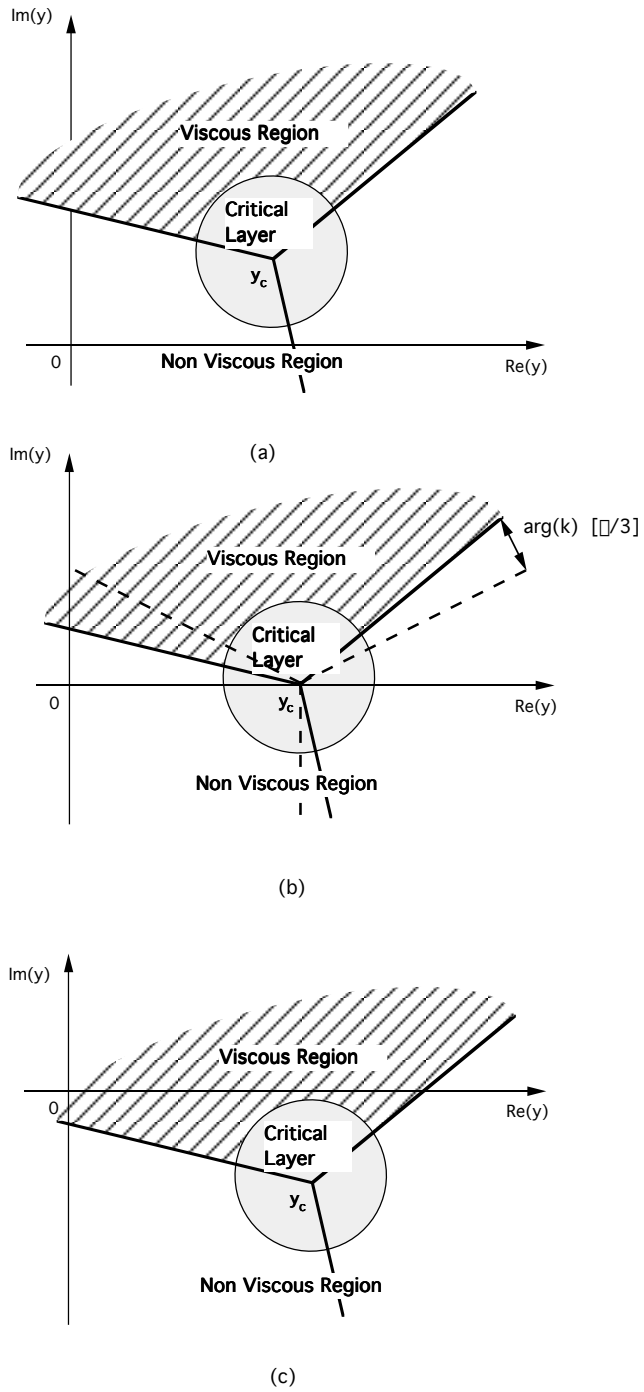

FIG. 3.1 - *Viscous and inviscid behavior of the Orr-Sommerfeld eigenfunctions in the complex y plane in the limit* $Re \to \infty$ *in the neighborhood of a first-order critical point* y_c*; (a):* $\sigma > 0$*, (b):* $\sigma = 0$*, (c):* $\sigma < 0$*.*

3.4 Viscous structure of local plane waves in weakly non-parallel flows

By analogy with (3.13a,b), the following quantities for weakly non-parallel flows are defined :

$$\sigma(X) = \omega_{,i} - k_{,i}(\omega, X)\omega_{,r}/k_{,r}(\omega, X) \quad , \tag{3.17a}$$

$$\delta(X) = \left[\frac{\omega_{,r}}{k_{,r}(\omega, X)} - U_{0,min}\right]\left[\frac{\omega_{,r}}{k_{,r}(\omega, X)} - U_{0,max}\right] \quad . \tag{3.17b}$$

From the conclusions of section 3.2 and statement (a) of the last section, we know that at any point X where $\sigma(X) > 0$ or $\delta(X) > 0$, the characteristic cross-stream scale of the local plane wave is everywhere inviscid and the approach of Crighton & Gaster (1976) is justified. By contrast, if there is no such point in the entire flow, nothing can be said regarding the characteristic scale of the local plane wave at any point in the flow[4]. Furthermore, if there is no region where $\sigma(X)$ evolves from positive to negative values with $\delta(X) < 0$, nothing can be said concerning the viscous regions since the analysis of the former section cannot be applied. We therefore exclude these situations and assume that **there exists a point X_p in the flow where $\delta(X)$ is negative and $\sigma(X)$ changes sign**. The variations of $k(\omega, X)$ being continuous with respect to X, one is sure that the evolution of $\sigma(X)$ from positive to negative values is continuous as well and that $\delta(X)$ remains negative in at least a neighborhood of X_p. The analysis of the former section used to prove statement (b) and (c) can then be directly applied. It follows that there exists a critical point $y_c(X)$ satisfying

$$-i\omega + ik(\omega, X)U_0(y_c(X), X) = 0 \quad , \tag{3.18}$$

which crosses the real y axis for $X = X_p$ provided that $U_{0y}(y_c(X_p), X_p) \neq 0$. Figure 3.1 of the last section thus correctly shows the evolution with respect to X of the

4. Except perhaps near $y = \pm\infty$ where the local plane wave is inviscid in order to satisfy the boundary conditions.

critical point and the viscous Stokes sector, figure 3.1b representing the situation at X_p. A large viscous region develops on the side of X_p where $\sigma(X) \leq 0$ (figure 3.1c). with an extent in the real (X, y) plane near $(X_p, y_c(X_p))$ illustrated in figure 3.2. On

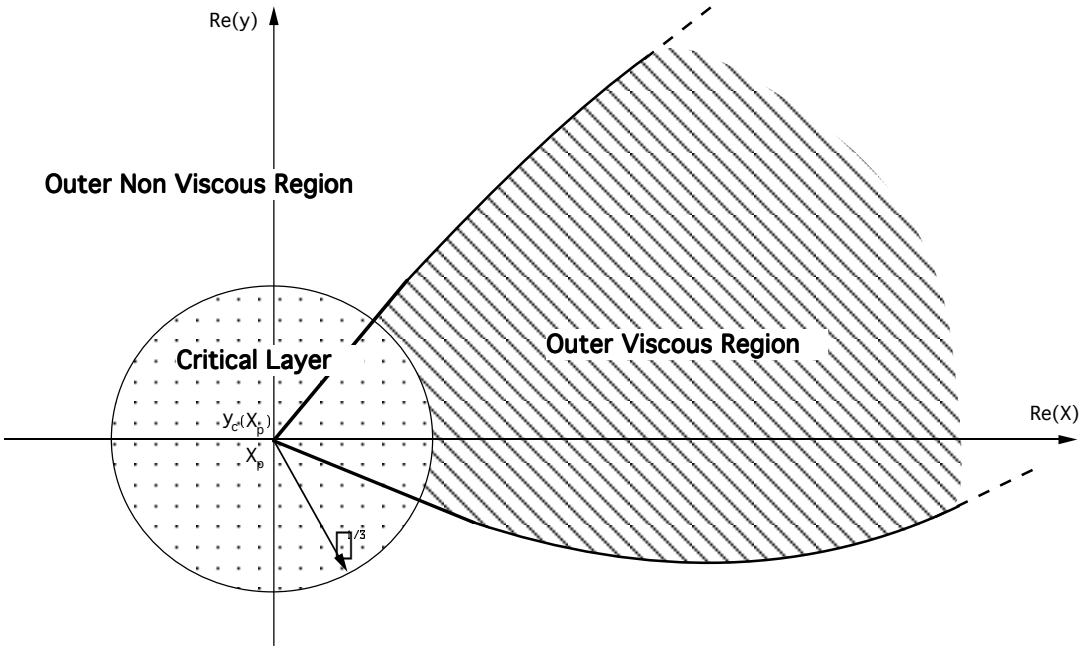

FIG. 3.2 - *Viscous structure of the local plane wave near a (first order) critical point* $(X_p, y_c(X_p))$ *in the real* (X, y) *plane. The side with respect to* X_p *under which the viscous region develops correspond to locations such that* $\sigma(X) < 0$.

the locally amplified side ($\sigma(X) > 0$), the cross-stream characteristic scale of the local plane wave is inviscid as argued above. Viscous regions first appear in a real critical layer region near $(X_p, y_c(X_p))$. On the side where $\sigma(X) < 0$, a large viscous region develops in a sector originating from the real critical point $(X_p, y_c(X_p))$.

The angle of the viscous sector and its position with respect to the X and y axes near $(X_p, y_c(X_p))$ can be directly obtained from the definition (3.18) of $y_c(X)$ and equation (3.16). The particular case in which the viscous sector leaves the real critical point $(X_p, y_c(X_p))$ parallel to the real y axis occurs when

$$arg(k(\omega, X_p)) = \pi/6 + l\pi/3, \; l = 0, 1, 2, 3, 4, 5 \quad .$$

In this paragraph, we address the particular case of a temporally neutral wave ($\omega_{,i} = 0$). When $\omega_{,i} = 0$, the locations where the change of local behavior occurs are easily identified as the points, say X_p, where $k_{,i}(\omega, X)$ changes sign and the plane wave therefore corresponds to a neutral mode of temporal theory. According to a classical result of temporal theory (Foote & Lin 1950), $\omega/k(\omega, X_p)$ is in the range of $U_0(y, X_p)$. Furthermore, any maximum of the wave amplitude $|\Psi|$ occurs at a station (y_m, X_m) which satisfies

$$k_{,i}(\omega, X_m) = 0 \quad . \tag{3.19}$$

Hence $k_{,i}(\omega, X)$ must change sign at X_m and the analysis that has led to the structure displayed on figure 3.2 is readily applicable to any temporally neutral wave at the location where it reaches a maximum[5]. Note also that in this case the Stokes lines limiting the viscous region cannot be parallel to the real y axis since $arg(k(\omega, X_p)) = \pm\pi \neq \pi/6 + l\pi/3$.

To close this section, we again emphasize the fact that the continuity of the local wavenumber with respect to X is fundamental in the present analysis. If this assumption is violated (one could think of a flow with a step change in stability properties induced by heat addition, for instance), one cannot "follow" the evolution of critical points and Stokes lines, and the appearance of viscous regions cannot be predicted. However, the local wavenumber does not have to be differentiable. The analysis of this section therefore remains valid at branch points of the dispersion relation[6]. The reader is however reminded that the local plane wave approximation is generally different at those points (Monkewitz *et al.* 1993).

5. Recall that several other properties have been proven for a local neutral plane wave at X_p. In particular, the local basic flow profile $U_0(y, X_p)$ is known to have an inflexion point. For monotone or symmetric profiles, the phase speed corresponds to the basic flow velocity at the inflexion point which is a regular critical point ($U_{0yy} = 0$). For more complicated profiles, there exist at least one singular critical point ($U_{0yy} \neq 0$). At each critical point, a discontinuity of the Reynolds stress is created but the sum of all Reynolds stress jumps is zero which yields a condition for the phase speed (Foote & Lin 1950).

6. At branch points, the local wavenumber $k(X, \omega)$ exhibits square-root-type singularities.

3.5 The evolution of planes waves on weakly non-parallel flows

In this section, the leading-order approximation for the evolution of a local plane wave is given in each region of the neighborhood of a real critical point $(y_c(X_p), X_p)$ displayed on figure 3.2. For each X the matching between inviscid and viscous approximations is carried out in the complex y plane through the complex critical layer around $y_c(X)$. In the following, we shall only consider streamwise locations that are not branch points of the dispersion relation, which will allow us to obtain uniform approximations with respect to X. The implications of this assumption are discussed in the final section 3.6.

3.5.1 Outer inviscid region

The characteristic cross-stream scale of the plane wave is then the inviscid scale y. The amplitude $\Phi(x, y, \varepsilon)$ of the plane wave (3.7) satisfies, at leading order, equation (3.10) and may be written as

$$\Phi(x, y, \varepsilon) = \phi(y, X) A(x, \varepsilon) \quad , \tag{3.20}$$

where $\phi(y, X)$ satisfies

$$[(-i\omega + ik(\omega, X)U_0(y, X))(\frac{\partial^2}{\partial y^2} - k^2(\omega, X)) - iU_{0yy}(y, X)k(\omega, X)]\phi = 0 \quad , \tag{3.21}$$

and $A(x, \varepsilon)$ is an arbitrary amplitude which is unambiguously defined if the normalization of $\phi(y, X)$ is specified for all X. In order to match with the viscous region, it is convenient to fix the normalization for any X at the complex critical point $y_c(X)$ such that

$$A(x, \varepsilon) = \Phi(x, y_c(X), \varepsilon) \quad . \tag{3.22}$$

The characteristic scale of $A(x, \varepsilon)$ is unknown and the only information comes from (3.8) which tells us that it is slower than x.

If there exists a path C (generally in the complex y plane) from $-\infty$ to $+\infty$ which remains in regions where the characteristic scale is inviscid , the amplitude $A(x,\varepsilon)$ can be obtained from the second-order equation by a solvability condition involving only the inviscid approximation. As shown by Crighton & Gaster (1976), this yields, at a location X which is not a branch point of the local dispersion relation, an equation of the form

$$b(X)\frac{\partial A}{\partial X} + p(X)A = 0 \quad . \tag{3.23}$$

In such a case, the amplitude A is only dependent on X and is written as $A(X)$. The first correction of the amplitude (3.20) is easily evaluated as being of order ε. So, with (3.7) and (3.20), the inviscid approximation of the local plane wave is

$$\Psi = [\phi(y,X)A(X) + O(\varepsilon)]e^{\frac{i}{\varepsilon}\int_{X_m}^{X} k(\omega,r)dr}e^{-i\omega t} \quad . \tag{3.24}$$

The path C is the real axis at locations where $\sigma(X) > 0$. At locations where $\sigma(X) \leq 0$, it is a complex contour that avoids the viscous regions as shown on figure 3.3. One must keep in mind that no solvability condition can be obtained with only the inviscid approximation if it is no longer possible to find such a path. This may occur as soon as two critical points are involved even for $\sigma(X) = 0$ when two critical points or two Stokes lines collide in one of the two configurations shown on figure 3.4. The viscous approximation in the viscous region crossed by the path C then intervenes explicitly in the solvability condition leading to the amplitude equation for $A(x,\varepsilon)$. In the present case, the existence of a path C that stays in inviscid regions is guaranteed for locations close to X_p, if the real critical points are all simple at X_p to avoid the situation of figure 3.4a, and if $arg(k(X_p,\omega)) \neq \pi/6 + l\pi/3$ to avoid the situation of figure 3.4b. In the following, these conditions are assumed to be satisfied.

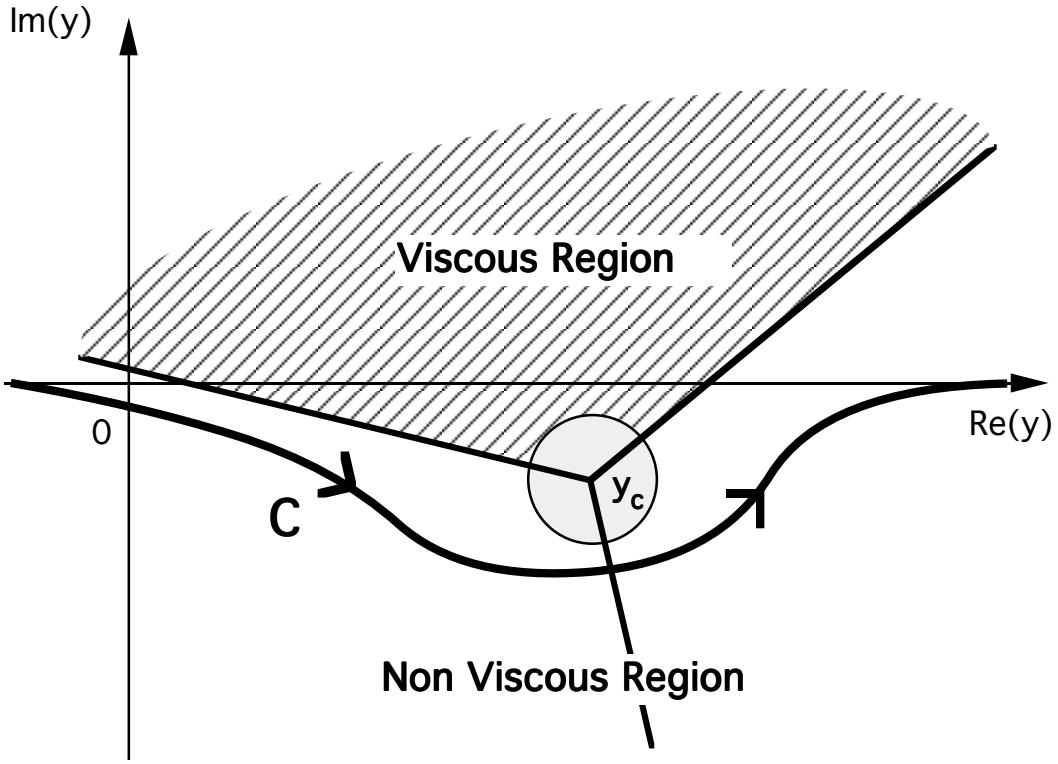

FIG. 3.3 - *Example of contour C avoiding viscous regions in the complex y plane along which the solvability condition is applied.*

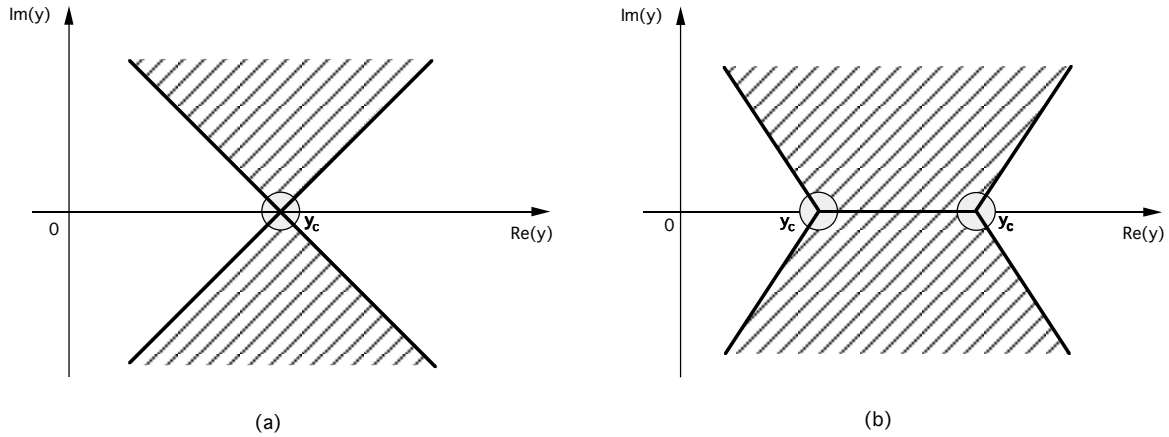

FIG. 3.4 - *Particular situations at $\sigma = 0$ for which no contour C avoiding viscous regions exists; (a): Two critical points collapse at a real location, (b): Two Stokes lines limiting the viscous region associated to two critical points collide.*

3.5.2 The complex critical layer

The study of this region in the complex plane is necessary in order to match viscous and inviscid regions. By using the WKBJ expression (3.7), we obtain a uniform approximation with respect to X in the X-dependent complex critical layer.

At any location X, the inviscid approximation (3.20) becomes singular at the complex critical point $y_c(X)$. Its expansion near $y_c(X)$ is commonly obtained by representing the Rayleigh eigenfunction $\phi(y,X)$ in terms of Frobenius series. Using the normalisation of $\phi(y,X)$ at $y_c(X)$, this gives

$$\begin{aligned}\phi(y,X) = \quad & 1 + (b_\phi(X) - \alpha_\phi(X)\ln(y - y_c(X)))(y - y_c(X)) \\ & + c_\phi(X)(y - y_c(X))^2 + o((y - y_c(X))^2) \quad ,\end{aligned} \tag{3.25}$$

where $c_\phi(X)$, $\alpha_\phi(X)$ are defined by

$$\left\{\begin{array}{l} c_\phi(X) = k(\omega,X)^2 + \dfrac{U^c_{0y^3}(X)}{U^c_{0y}(X)} \quad , \\ \alpha_\phi(X) = \dfrac{U^c_{0yy}(X)}{U^c_{0y}(X)} \quad . \end{array}\right. \tag{3.26}$$

If $\alpha_\phi(X)$ is zero at the location considered, i.e. if the critical point is regular, the singularity appears at higher order but it does not fundamentally modify the following analysis.

In the critical layer, one introduces the cross-stream scale (Lin 1955, Drazin & Reid 1981)

$$\check{y} = \frac{y - y_c(X)}{\varepsilon^{1/3}} \quad .$$

The inviscid approximation (3.20) is reduced to (3.25) which, in terms of $\check{y}$, reads

$$\Phi(y_c,X) = [1 + \varepsilon^{1/3}\ln(\varepsilon^{1/3})\alpha_\phi(X)\check{y} + \varepsilon^{1/3}(b_\phi(X) - \alpha_\phi(X)\ln\check{y})\check{y} + O(\varepsilon^{2/3})]A(X) \quad . \tag{3.27}$$

Accordingly, the critical layer expansion is sought in the form

$$\check{\Phi} = [\check{\Phi}_0 + \varepsilon^{1/3}\ln(\varepsilon^{1/3})\check{\Phi}_1 + \varepsilon^{1/3}\check{\Phi}_2 + \cdots] \quad . \tag{3.28}$$

The functions $\check{\Phi}_0$ and $\check{\Phi}_1$ can directly be obtained from expression (3.27) as

$$\begin{cases} \check{\Phi}_0(\check{y}, X) = A(X) \quad , \\ \check{\Phi}_1(\check{y}, X) = A(X)\alpha_\phi(X)\check{y} \quad . \end{cases} \tag{3.29}$$

The third term in (3.27) is singular and is not directly a solution of the critical layer equation. The function $\check{\Phi}_2$ is obtained by solving

$$[\lambda(X)\frac{\partial^4}{\partial \check{y}^4} - i\check{y}\frac{\partial^2}{\partial \check{y}^2}]\check{\Phi}_2 = i\alpha_\phi(X)A(X) \quad ,$$

where

$$\lambda(X) = \frac{1}{k(X)RU_0(y_c(X), X)} \quad ,$$

with the matching condition $\check{\Phi}_2 \sim A(X)[b_\phi(X) - \alpha_\phi(X)\ln\check{y}]\check{y}$ as $|\check{y}| \to +\infty$ in the inviscid region. This equation can be integrated in terms of generalized Airy functions as

$$\check{\Phi}_2(\check{y}, X) = A(X)[b_\phi(X)\check{y} + \alpha_\phi(X)(\lambda(X)/i)^{1/3}B_{j_0}((i/\lambda(X))^{1/3}\check{y}, 2, 1)] \quad . \tag{3.30}$$

The function $B_j(z, 2, 1)$ for any $j \in \{1, 2, 3\}$ has been defined by Reid (1972) and in the appendix of Drazin & Reid (1981) as the solution of

$$[\frac{\partial^4}{\partial z^4} - z\frac{\partial^2}{\partial z^2}]f = 1 \quad ,$$

which is balanced in the sector S_j of the complex z-plane (figure 3.5). As demons-

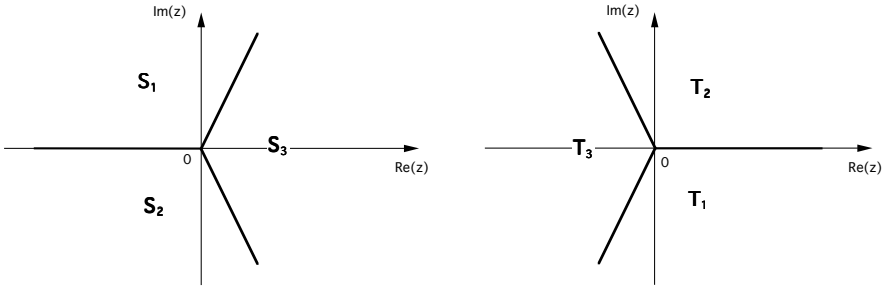

FIG. 3.5 - *Sectors S_j and T_j, $j = 1, 2, 3$ in the complex y plane.*

trated by Reid (1972), the functions $B_j(z,p,q)$ appear systematically in the critical layer to represent solutions which are "inviscid" in two Stokes sectors and admit a logarithmic singularity at the critical point [function ϕ_2 defined by (3.14b)]. More explicitly, the approximation in the critical layer obtained in terms of the function B_j can be matched to the singular "inviscid" solution ϕ_2 of the Orr-Sommerfeld equation in the outer continuation[7] of both sectors T_k where $k \in \{1,2,3\}$ and $k \neq j$. By contrast, in the third sector T_j, the function B_j is dominant, i.e. it is exponentially large when $|z| \to \infty$ and can only be matched to a dominant outer viscous solution. It is by this kind of reasoning that the existence of viscous regions can in fact be proven. A more comprehensive account for strictly parallel flows can be found in Drazin & Reid (1981).

In expression (3.30), j_0 is chosen such that the sector T_{j_0}, after a rotation of angle $arg[(i/\lambda(X))^{1/3}]$, corresponds to the inner expression of the viscous sector drawn in figures 3.1a,b,c.

Using (3.7), (3.28), (3.29) and (3.30), the approximation in the complex critical layer is finally found to be

$$\check{\Psi} = A(X)e^{\frac{i}{\varepsilon}\int_{X_m}^{X} k(\omega,r)dr} e^{-i\omega t} \Big\{ 1 + \alpha_\phi(X)\check{y}\varepsilon^{1/3}\ln\varepsilon^{1/3} + \varepsilon^{1/3}[b_\phi(X)\check{y} + \alpha_\phi(X)(\lambda(X)/i)^{1/3} B_{j_0}((i/\lambda(X))^{1/3}\check{y},2,1)] + O(\varepsilon^{2/3}) \Big\} \ . \tag{3.31}$$

In order to obtain the approximation of the local plane wave in the real critical layer sketched in figure 3.2, expression (3.31) has to be expanded near X_p with respect to the inner scale

$$\tilde{X} = \frac{X - X_p}{\varepsilon^{1/3}} \ .$$

This task presents no difficulty and is left to the reader.

7. One easily shows that the boundaries of the sector T_k are given by the critical layer expression of the Stokes lines defined in section 3.3.

3.5.3 Viscous approximations

In this section the outer viscous approximation of the local plane wave is obtained. The cross-stream characteristic scale is then viscous, in view of relation (3.3) between Reynolds number and ε, can be written $y_v = y/\sqrt{\varepsilon}$.

The leading-order equation governing the amplitude $\Phi^{(v)}$ in the outer viscous region is given by (3.11). It admits four independent solutions which correspond to the leading-order approximations of (3.14a,b,c,d). The solution is dominated by viscous diffusion and can be written, after normalisation at $y_c(X)$, as

$$\Phi^{(v)} = \phi^{(v)}(x, y, \varepsilon) e^{\frac{1}{\sqrt{\varepsilon}} \int_{y_c(X)}^{y} \sqrt{(-i\omega + ikU_0)R} dy} \quad , \tag{3.32}$$

where the square root is defined such that $\Re e[\int_{y_c(X)}^{y} \sqrt{(-i\omega + ikU_0)R} dy] > 0$ for any y in the viscous sector. The scales of variation of the function $\phi^{(v)}$ in the x and y directions are a priori unknown but from condition (3.8) and the integration of (3.11) one immediately obtains the restrictions $O(\varepsilon) \leq \dfrac{1}{\phi^{(v)}} \dfrac{\partial \phi^{(v)}}{\partial x} \ll 1$ and $O(1) \leq \dfrac{1}{\phi^{(v)}} \dfrac{\partial \phi^{(v)}}{\partial y} \ll 1/\sqrt{\varepsilon}$.

The equation for $\phi^{(v)}$ can be derived by inserting expressions (3.7) and (3.32) into equation (3.5), thereby leading to

$$\begin{aligned} &-\frac{RU_0}{\sqrt{\varepsilon}} \frac{\partial \phi^{(v)}}{\partial x} - 2\sqrt{(-i\omega + ikU_0)R} \frac{\partial \phi^{(v)}}{\partial y} - 5\partial_y \left[\sqrt{(-i\omega + ikU_0)R} \right] \phi^{(v)} \\ &\quad + RV_0 \sqrt{(-i\omega + ikU_0)R} \phi^{(v)} + RU_0 \partial_X \left[\int_{y_c(X)}^{y} \sqrt{(-i\omega + ikU_0)R)} \right] \phi^{(v)} = 0 \quad . \end{aligned} \tag{3.33}$$

This equation must be integrated and the solution matched with its inviscid counterpart. Since matching between the complex critical layer and the inviscid region has already been accomplished in section 3.5.2, it is convenient to match through the complex critical layer.

Considering the following expansion of $B_{j_0}(z, 2, 1)$ for large parameters in T_{j_0} (Drazin & Reid 1981)

$$B_3(z, 2, 1) \sim i\pi^{1/2} z^{-5/4} e^{\frac{2}{3} z^{3/2}} \ , \ z \in T_{j_0} \ and \ |z| \to \infty \quad , \tag{3.34}$$

the behavior of the complex critical layer amplitude $\check{\Phi}$ given by (3.28)-(3.30) is easily obtained in the outer viscous region as

$$\begin{aligned}\check{\Phi} \sim\ & i\varepsilon^{5/2}A(X)\alpha_\phi(X)\pi^{1/2}(\lambda(X)/i)^{3/4}(y-y_c(X))^{-5/4} \\ & \times e^{\frac{2}{3\sqrt{\varepsilon}}(\frac{i}{\lambda(X)})^{1/2}(y-y_c(X))^{3/2}}(1+O(\varepsilon^{1/3}))\ .\end{aligned} \tag{3.35}$$

Since

$$e^{\frac{1}{\sqrt{\varepsilon}}\int_{y_c(X)}^{y}\sqrt{(-i\omega+ikU_0)R}dy} \sim e^{\frac{2}{3\sqrt{\varepsilon}}(\frac{i}{\lambda(X)})^{1/2}(y-y_c(X))^{3/2}} \quad when\ y\to y_c(X)\ ,$$

the matching between expressions (3.32) and (3.35) implies the following condition as $y \to y_c(X)$:

$$\phi^{(v)} \sim \varepsilon^{5/12} iA(X)\alpha_\phi(X)\pi^{1/2}(\lambda(X)/i)^{3/4}(y-y_c(X))^{-5/4}\ . \tag{3.36}$$

The function $\phi^{(v)}$ must therefore be sought in the form:

$$\phi^{(v)}(x,y,\varepsilon) = \varepsilon^{5/12}\xi(y,X)\ . \tag{3.37}$$

By inserting this "ansatz" in equation (3.33), one immediately finds that the first term in (3.33) is negligible with respect to the others. Hence the leading-order equation for $\xi(y,X)$ reads

$$\begin{aligned}\frac{1}{\xi}\frac{\partial\xi}{\partial y} = & -\frac{5}{2}\frac{\partial_y[\sqrt{(-i\omega+ikU_0)R}]}{\sqrt{(-i\omega+ikU_0)R}} + \frac{RV_0}{2} \\ & + \frac{\sqrt{(-i\omega+ikU_0)R}}{2ik}\partial_X[\int_{y_c(X)}^{y}\sqrt{(-i\omega+ikU_0)R})]\ .\end{aligned} \tag{3.38}$$

Its solution is

$$\begin{aligned}\xi = & B(X)(-i\omega+ik(X)U_0(X,y))^{-5/4} \\ & \times e^{\frac{1}{2}\int_{y_c(X)}^{y}\left[RV_0+\sqrt{(-i\omega+ikU_0)R}\partial_X(\int_{y_c(X)}^{y}\sqrt{(-i\omega+ikU_0)R})\right]dy}\ ,\end{aligned} \tag{3.39}$$

with $B(X)$ given by condition (3.36) and expression (3.37) as

$$B(X) = i\pi^{1/2} A(X)\alpha_\phi(X)(\lambda(X)/i)^{1/3} \quad . \tag{3.40}$$

Collecting the results (3.32), (3.37), (3.39), (3.40) and using (3.7), the leading-order approximation of the local plane wave amplitude $\psi^{(v)}$ in the viscous region is finally obtained as

$$\psi^{(v)} = \varepsilon^{5/12} i\pi^{1/2} A(X)\alpha_\phi(X)(\lambda(X)/i)^{1/3}(-i\omega + ik(X)U_0(X,y))^{-5/4}$$
$$\times e^{\frac{1}{2}\int_{y_c(X)}^{y}\left[RV_0+\sqrt{(-i\omega+ikU_0)R}\partial_X\left\{\int_{y_c(X)}^{y}\sqrt{(-i\omega+ikU_0)R}\right\}\right]dy} e^{\frac{1}{\sqrt{\varepsilon}}\int_{y_c(X)}^{y}\sqrt{(-i\omega+ikU_0)R}dy} \quad . \tag{3.41}$$

The term $(-i\omega + ik(X)U_0(X,y))^{-5/4} e^{\frac{1}{\sqrt{\varepsilon}}\int_{y_c(X)}^{y}\sqrt{(-i\omega+ikU_0)R}dy}$ in the above expression is the WKBJ approximation of the viscous solution in parallel flows as obtained by Tatsumi *et al.* (1971). The additional terms are due to nonparallel effects: the exponential $e^{\frac{R}{2}\int_{y_c(X)}^{y} V_0 dy}$ is an amplitude correction induced by the $\sqrt{\varepsilon}$ correction of the leading-order operator and may be seen as a two-dimensional effect. The second exponential $e^{\frac{R}{2}\int_{y_c(X)}^{y}\left[\sqrt{(-i\omega+ikU_0)R}\partial_X\left\{\int_{y_c(X)}^{y}(\sqrt{(-i\omega+ikU_0)R})\right\}\right]dy}$ is due to the X dependence of the local cross-stream wavenumber $l = \sqrt{(-i\omega + ikU_0)R}$. The last amplitude factor $i\pi^{1/2}A(X)\alpha_\phi(X)(\lambda(X)/i)^{1/3}$ is fixed by the matching condition with the outer inviscid region. It is important to notice here that the X dependence of the local wavenumber l in the y direction has induced an $O(\sqrt{\varepsilon})$ correction of the streamwise wavenumber which is not present in the outer inviscid region.

Upon inspection of the results at a given station X, one immediately sees that the amplitude in the viscous region is exponentially larger with respect to its counterpart in the inviscid region and exhibits fast oscillations (figure 3.6). This peculiar behavior is due to the dominant viscous WKBJ factor $e^{\frac{1}{\sqrt{\varepsilon}}\int_{y_c(X)}^{y}\sqrt{(-i\omega+ikU_0)R}dy}$. One notes however that in the limit $\varepsilon \to 0$, the strength of the damping factor $e^{\frac{i}{\varepsilon}\int_{X_m}^{X} k(\omega,r)dr}$ in the streamwise direction remains much more important than the amplifying viscous factor in the cross-stream direction. The location of maximum amplitude therefore

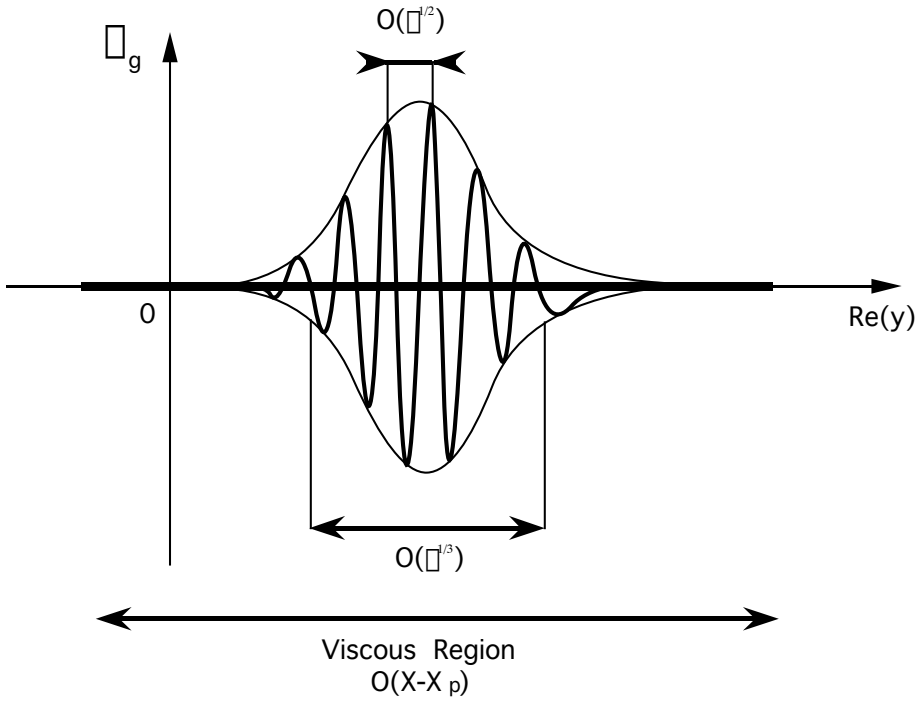

FIG. 3.6 - *Cross-Stream variation of a local plane wave in the viscous region at a location where* $\sigma < 0$.

remains at the streamwise station where $e^{\frac{i}{\epsilon}\int_{X_m}^{X} k(\omega,r)dr}$ displays a maximum, where the wave is spatially neutral.

3.6 Discussion

Approximations for linear local plane waves in two-dimensional weakly non-parallel shear flows have been obtained. The characteristic cross-stream scale of local plane waves has been determined for arbitrary complex frequency ω and local wavenumber $k(\omega, X)$ by extending classical parallel flow results for real k. The inviscid approximation at a given location X is asymptotically valid for any y if the local plane wave is amplified in a frame of reference moving with the local phase speed $\omega_{,r}/k_{,r}$, i.e. if $\sigma = \omega_{,i} - k_{,i}(\omega, X)\omega_{,r}/k_{,r}(\omega, X) > 0$, or if the phase speed is not

within the range of the streamwise velocity $U_0(y;X)$. As soon as the local behavior is damped ($\sigma < 0$) with $\omega_{,r}/k_{,r}$ in the range of $U_0(y;X)$, the existence of viscous regions has been demonstrated.

The development of the viscous region in the neighborhood of a critical point $(y_c(X_p), X_p)$ satisfying

$$-i\omega + ik(\omega, X_p)U_0(y_c(X_p), X_p) = 0 \tag{3.42}$$

has been analysed and proven to generically display the structure sketched in figure 3.2. In the process, the leading-order approximation of local plane waves has been calculated everywhere.

These results are readily applicable to both the signaling and global mode problems. In the signaling case, local plane waves represent the flow response to an oscillating source at a given real frequency. As outlined in Huerre & Monkewitz (1990), for instance, this problem is physically relevant only in convectively unstable systems. In free shear flows it has so far only been studied in regions where the wave is amplified, i.e. for $\sigma > 0$, thereby allowing the use of an inviscid approach. As shown by Crighton & Gaster (1976) for jets and by Gaster (1985) for mixing layers, expression (3.20) for the streamfunction perturbation explains the observed variations of individual physical quantities, such as growth rate and wavelength. A consistent description of local plane wave evolution has now been obtained around and beyond the point of maximum amplitude. We have shown in particular, that variations of quantities such as the local streamfunction wavenumber are more important in viscous regions than in inviscid regions as a consequence of the different order of the correction terms in each region. One can also expect an improvement in comparing relative gains as a result of a better localisation of maximum amplitudes.

It must be said that, to our knowledge, no linear viscous waves have so far been detected in free shear flows because, in most cases, non linear effects become important well before the wave reaches its maximum amplitude. In fact, one has

to keep in mind that theoretically the condition $|\Psi|_{max} \ll 1$ is not sufficient for neglecting nonlinear effects. As soon as $|\Psi_{max}|$ is $O(1/\sqrt{Re}) = O(\sqrt{\varepsilon})$, nonlinear terms come into play in the neighborhood of the critical point at the streamwise location of maximum amplitude and one has to proceed to a nonlinear critical layer analysis (Goldstein & Leib 1988, Goldstein & Hultgren 1988). In boundary layers, on the other hand, linear viscous waves are a common occurence in the form of Tollmien-Schlichting waves (Drazin & Reid 1981), for instance. But since the T-S instability is of the weak viscous type, the inviscid approximations considered in this paper are inappropriate.

The results obtained apply also to the problem of linear global modes which has been reviewed by Huerre & Monkewitz (1990) and analysed for free shear flows by Monkewitz *et al.* (1993). In the limit of slow streamwise evolution of the basic flow, they can be described locally in terms of plane waves oscillating at the global frequency ω_g, and for each wave the analysis of sections 3.4 and 3.5 directly applies.

The real issue is in fact to determine local plane waves that approximate the global mode. Neglecting the cross-stream structure and using a Ginzburg-Landau model with two turning points in the streamwise direction, Chomaz *et al.* (1991) and Le Dizès *et al.* (1993) have obtained two types of global modes. Global modes with distant turning points (type 1) have been found to be approximated by a single local plane wave everywhere except in the neighborhood of the Stokes line that connects both turning points. Global modes with a double turning point (type 2) are approximated by a single local plane wave everywhere.

Double-turning-point global modes have also been obtained in shear flows using an inviscid approach (Monkewitz *et al.* 1993). The global frequency is determined in that case by matching two subdominant WKBJ waves at the double turning point X_s. The inviscid approximations of the global modes in both the outer region and the inner double turning point regions have been calculated. The results obtained

in the present article guarantee that at any location where $\omega_{g,r}/k_{,r}(\omega_g, X)$ is not in the range of $U_0(y, X)$ or $\sigma(X)$ is positive, these approximations are asymptotically valid for all y. We have also proven that they break down in the neighborhood of any critical point $(y_c(X_p), X_p)$ satisfying (3.42) in the viscous regions displayed on figure 3.2 and that if this occurs at a streamwise location different from the double-turning-point X_s, the approximations of section 3.5 can be used.

Note finally that the appearence of viscous regions in physical space does not necessarily affect the inviscid determination of the global frequency ω_g as obtained by Monkewitz *et al.* (1993). Even if there exist viscous regions at the locations X_s, one can still apply the matching condition at X_s that yields ω_g, using inviscid approximations provided that, at the streamwise location X_s, there is a path from $-\infty$ to $+\infty$ in the complex y plane which remains in the inviscid regions.

This work is supported by DRET under grant #92-098 (SLD,PH), AFOSR under grant #F49620-92-J-0471 (PAM) and SNECMA (SLD).

Chapitre 4

CONCLUSION

Dans cette dernière section, nous rappelons l'ensemble des résultats obtenus dans les trois chapitres de cette thèse, en insistant sur le rôle essentiel joué par les lignes de Stokes et les points tournants, et en proposant un certain nombre d'extensions possibles de ces résultats.

Afin de relier les propriétés globales et locales de l'instabilité de l'écoulement, nous nous sommes intéressés dans le premier chapitre, au mécanisme **linéaire** de déstabilisation globale des écoulements faiblement non parallèles. Cette étude nous a amenés à élaborer sur le modèle de Ginzburg-Landau, une méthode basée d'une part sur l'analyse des réseaux de lignes de Stokes, et d'autre part sur l'utilisation d'approximations uniformes dues à Lynn & Keller (1972). Appliquée au cas de deux points tournants, cette méthode a permis de montrer que les fréquences globales sont discrétisées, et qu'elles sont effectivement reliées aux caractéristiques d'instabilité locale. En particulier, nous montrons qu'une région absolument instable est nécessaire pour entraîner la déstabilisation globale de l'écoulement.

Il est par ailleurs apparu lors de l'étude que ces fréquences globales correspondent à deux types de modes globaux, caractérisés par la géométrie de leurs lignes de Stokes. Les modes globaux de type 1 possèdent un double point tournant; ceux de type 2 ont deux points tournants reliés par une ligne de Stokes. Le critère de sélection

de fréquence obtenu généralise ainsi les études antérieures de Chomaz *et al.* (1991), qui n'avaient pris en compte que les modes globaux ayant un double point tournant (type 2).

Il serait maintenant souhaitable d'étendre l'analyse, dans un premier temps au cas de plusieurs points tournants, puis à des équations d'ordre supérieur (i.e. ayant plus de deux branches spatiales), afin de vérifier si ces modes peuvent être obtenus dans un contexte plus général.

Le chapitre 2 aborde l'extension de l'analyse des modes globaux, dans le domaine faiblement non linéaire. La non linéarité a été introduite par l'adjonction d'un terme cubique au modèle de Ginzburg-Landau du chapitre 1. Dans ce cadre, nous avons montré que l'équation de Landau associée à la bifurcation d'un mode global de type 2 n'a généralement pas de sens physique, et qu'en particulier, la nature de la bifurcation n'est pas toujours définie. Ce résultat a priori surprenant peut néanmoins s'interpréter de la façon suivante: les effets perturbatifs linéaires et non linéaires générés au-dessus du seuil d'instabilité, ont des contributions importantes en des régions situées loin du point X_M (point d'amplitude maximale du mode global). En conséquence, il se crée entre tous ces effets, un déphasage singulier qui empêche leur comparaison sous la forme d'une équation de Landau. Il faut toutefois noter que cette situation déplaisante ne se produit pas lorsque il y a **résonance locale**, c'est-à-dire lorsque les points tournants entre les ondes WKBJ générées par l'interaction du mode global avec lui-même, et les ondes WKBJ linéaires, sont au voisinage de X_M. Ceci fournit une condition suffisante simple de validité physique de l'équation de Landau. Sous l'hypothèse supplémentaire que les lignes de Stokes coupent l'axe réel uniquement au voisinage de X_M, nous avons montré que le critère faiblement non linéaire de sélection de fréquence alors obtenu n'est plus valable dès que les écarts au seuil sont de l'ordre de $-\varepsilon/\ln\varepsilon$, ε étant le paramètre WKBJ d'inhomogénéité de l'écoulement. Dans un cas particulier (équation de Ginzburg-Landau à

coefficients quadratiques), la condition de résonance locale peut s'interpréter à partir des caractéristiques d'instabilité locale, et elle stipule les ordres de grandeur de la région localement instable, et du taux maximal d'amplification locale (ε et $\sqrt{\varepsilon}$ respectivement).

Dans le chapitre 3, nous avons considéré la situation réelle des écoulements plans cisaillés faiblement non-parallèles. Nous nous sommes plus particulièrement attachés à l'étude de la structure transverse des perturbations qui se décomposent localement en ondes planes. Nous avons étendu les résultats classiques de la théorie temporelle (k réel) des écoulements parallèles, en montrant que l'approximation non visqueuse d'une onde plane de fréquence ω et de nombre d'onde k (tous deux complexes) est valable pour tout y (direction transverse) dans les deux cas suivants:

- l'onde est localement amplifiée ($\sigma = \omega_{,i} - \omega_{,r} k_{,i}/k_{,r} > 0$);
- la vitesse de phase locale $\omega_{,r}/k_{,r}$ n'est jamais égale à la vitesse moyenne longitudinale de l'écoulement.

Dans les autres cas, l'apparition d'un point critique et le développement d'une région visqueuse à des positions longitudinales où $\sigma \leq 0$, ont pu être mis en évidence. Ce résultat a été obtenu par l'étude dans le plan complexe en y, de l'évolution le long de la direction longitudinale, du réseau de lignes de Stokes associé aux ondes WKBJ visqueuses. Nous avons de plus donné les approximations de l'onde plane dans la couche critique visqueuse et dans les régions visqueuses, complétant ainsi l'approximation non visqueuse de Crighton & Gaster (1976) dans les régions où elle n'est plus valable.

Naturellement, le prochain objectif est maintenant de combiner les analyses des chapitres 2 et 3, et de réaliser l'analyse faiblement non linéaire du mode global de type 2, en incluant sa structure transverse. Actuellement, la première étape a été réalisée (Le Dizès *et al.* 1991) : sous la condition que le double point tournant

est proche de X_M, nous avons obtenu formellement l'équation de Landau par une analyse fine de la couche critique visqueuse au voisinage du double point tournant. La justification asymptotique complète, ainsi que la détermination des limites de validité de ce résultat, sont en cours d'élaboration.

Les études réalisées dans les couches de mélange forcées (Goldstein & Leib 1988, Goldstein & Hulgren 1988) laissent entrevoir une nouvelle approche des modes globaux dans les écoulements cisaillés. Dans un régime d'amplitude élevé, la couche critique n'est plus visqueuse mais non linéaire. Son étude en régime libre pourrait donner de nouveaux types de modes globaux. Cette approche **fortement non linéaire** permettrait de court-circuiter l'analyse faiblement non linéaire et d'apporter peut être un critère de sélection de fréquence ayant un champ d'application plus étendu.

Il est essentiel de souligner l'importance de l'hypothèse WKBJ dans l'étude réalisée. Sans cette hypothèse, l'on ne peut pas interpréter les modes globaux en terme d'ondes d'instabilité locales ni même définir les propriétés d'instabilité locale. Le problème est dans ce cas inévitablement bidimensionnel et l'utilisation d'un modèle unidimensionnel de type Ginzburg-Landau ne peut pas être justifié. Dans les écoulements réels tels que le sillage donnant lieu à un mode global décrit par une équation de Landau, le paramètre WKBJ est une constante fixée qui n'est pas nécessairement proche de zéro au seuil d'instabilité globale. L'application du modèle développé dans cette thèse nécessite donc une grande prudence. Il est en particulier difficile de savoir si la validité expérimentale de l'approximation de Landau provient du fait que l'on est effectivement dans le cadre des conditions restrictives obtenues au chapitre 2 ou du fait que l'hypothèse WKBJ n'est pas valable.

Pour répondre à cette question sur un cas concret, il serait intéressant de concevoir une expérience où le paramètre WKBJ peut être contrôlé indépendamment des propriétés d'instabilité locale de sorte que l'on puisse effectivement faire tendre le

paramètre WKBJ vers zéro au voisinage du seuil d'instabilité globale.

Signalons pour finir, qu'il serait aussi intéressant de mettre en évidence la structure visqueuse des ondes d'instabilité des écoulements cisaillés que prédit la théorie asymptotique réalisée au chapitre 3. Une étude numérique des ondes d'instabilité paraît bien adaptée car elle devrait permettre d'analyser la limite des grands nombres de Reynolds tout en restant dans un régime laminaire.

REFERENCES

Anyanwu, D. U. & Keller, J. B. 1975 Asymptotic solutions of eigenvalue problems for second-order ordinary differential equations. *Comm. Pure Appl. Math.* **28**, 753-763.

Bar-Sever, Y. & Merkine, L. O. 1988 Local instabilities of weakly non-parallel large scale flows : WKB analysis. *Geophys. Astrophys. Fluid Dyn.* **41**, 233-286.

Batchelor, G. K. 1967 An Introduction to Fluid Dynamics. Cambridge University Press.

Bender, C. M. & Orszag, S. A. 1978 *Advanced Mathematical Methods for Scientists and Engineers.* New York : McGraw-Hill.

Bergé, P., Pomeau, Y. & Vidal, C. 1984 L'ordre dans le chaos, vers une approche déterministe de la trubulence. Hermann, Paris.

Bers A. 1983 Space-time evolution of plasma instabilities –absolute and convective. In *Handbook in Plasma Physics* (ed. M. N. Rosenbluth and R. Z. Sagdeev), vol. 1, 451-517, Amsterdam : North-Holland.

Bouthier, M. 1972 Stabilité linéaire des écoulements presque parallèles. *J. Méc.* **11**, 599-621.

Chomaz, J. M., Huerre, P. & Redekopp, L. G. 1988 Bifurcations to local and global modes in spatially developing flows. *Phys. Rev. Lett.* **60**, 25-28.

Chomaz, J. M., Huerre, P. & Redekopp, L. G. 1990 Effect of nonlinearity and forcing on global modes. In *Proceedings of the Conference on New Trends in Nonlinear Dynamical Systems and Pattern-forming Phenomena : The Geometry of Nonequilibrium* (ed. P. Coullet & P. Huerre), NATO ASI Series B : Physics, vol. 37, 259-274, New York : Plenum Press.

Chomaz, J. M., Huerre, P. & Redekopp, L. G. 1991 A frequency selection criterion in spatially-developing flows. *Stud. Appl. Math.* **84**, 119-144.

Chomaz, J. M. 1992 Absolute and Convective Instabilities in Nonlinear Systems. *Phys. Rev. Lett.* **69**, 1931-34.

Crighton, D. G. & Gaster, M. 1976 Stability of slowly diverging jet flow. *J. Fluid Mech.* **77**, 397-413.

DiPrima, R. C. & Stuart, J. T. 1972 Non-local effects in the stability of flow between eccentric rotating cylinders. *J. Fluid Mech.* **54**, 393-415.

Drazin, P. G. 1974a On a model of instability of a slowly-varying flow. *Quart. J. Mech. Appl. Math.* **27**, 69-86.

Drazin, P. G. 1974b Kelvin-Helmholtz instability of a slowly varying flow. *J. Fluid Mech.* **65**, 781-797.

Drazin, P. G. & Reid, W. H. 1981 Hydrodynamic stability, Cambridge University Press.

Eckelmann, H., Graham, J. M. R., Huerre, P. & Monkewitz, P. A. 1993 Bluff-Body Wakes, Dynamics and Instabilities, IUTAM Symposium, Berlin : Springer-Verlag.

Foote, J. R. & Lin, C. C. 1950 Some recent investigations in the theory of hydrodynamic stability. *Quart. Appl. Math.* **8**, 265-280.

Gaster, M., Kit, E. & Wygnanski, I. 1985 Large scale structures in a forced turbulent mixing layer. *J. Fluid Mech.* **150**, 23-39.

Gent, P. R. 1976 Baroclinic instability of a slowly varying zonal flow. *J. Atm. Sci.* **31**, 1983-1994.

Gent, P. R. & Leach, H. 1976 Baroclinic instability in an eccentric annulus. *J. Fluid Mech.* **77**, 769-788.

Goldstein, M. E. & Hultgren, L. S. 1988 Nonlinear spatial evolution of a externally excited instability wave in a free shear layer. *J. Fluid Mech.* **197**, 295-330.

Goldstein, M. E. & Leib, S. J. 1988 Nonlinear roll-up of externally excited free shear layers. *J. Fluid Mech.* **188**, 481-515.

Guckenheimer, J. & Holmes, P. 1983 Nonlinear Oscillations, Dynamical Systems, and Bifurcations of Vector Fields. *Applied Mathematical Sciences* **42**, New-York : Springer-Verlag.

Hannemann, K. & Oertel, H. Jr. 1989 Numerical simulation of the absolutely and convectively unstable wake. *J. Fluid Mech.* **199**, 55-88.

Homann, F. 1936 *Forsch. Ing.-Wes.* **7**,1.

Huerre, P. & Monkewitz, P. A. 1990 Local and global instabilities in spatially developing flows. *Annu. Rev. Fluid Mech.* **22**, 473-537.

Hunt, R. E. 1993 An everywhere locally absolutely unstable, globally stable flow. To be published in *Proc. R. Soc. Lond.* A.

Hunt, R. E. & Crighton, D. G. 1991 Instability of flows in spatially developing media. *Proc. R. Soc. Lond.* A **435**, 109-128.

Karniadakis, G. E. & Triantafyllou, G. S. 1989 Frequency selection and asymptotic states in laminar wakes. *J. Fluid Mech.* **199**, 441-469.

Koch, W. 1985 Local instability characteristics and frequency determination of self-excited wake flows. *J. Sound Vib.* **99**, 53-83.

Langer, R. E. 1949 The asymptotic solutions of ordinary linear differential equations of the second-order, with special reference to a turning point. *Trans. Amer. Math. Soc.* **67**, 461-490.

Landau, L. D. 1944 On the problem of turbulence. *C. R. Acad. Sci. U.R.S.S.* **44**, 311-314.

Le Dizès, S., Monkewitz, P. A. & Huerre, P. 1991 Weakly nonlinear analysis of spatially-developing shear flows. *Bull. Am. Phys. Soc.* **36**, 2675.

Le Dizès, S., Huerre, P., Chomaz, J. M. & Monkewitz, P. A. 1993a Nonlinear stability analysis of slowly-diverging flows : Limitations of the weakly nonlinear approach. In *Proceedings of the IUTAM Symposium on Bluff-Body Wakes, Dynamics and Instabilities* (ed. H. Eckelmann, J. M. R. Graham, P. Huerre & P. A. Monkewitz), Berlin : Springer-Verlag, 147-152.

Le Dizès, S., Huerre, P., Chomaz, J. M. & Monkewitz, P. A. 1993b Linear global modes in spatially-developing media. Submitted to *Phil. Trans. R. Soc. Lond.* A.

Lin, C. C. 1955 The Theory of Hydrodynamic Stability. Cambridge University Press.

Lynn, R. Y. S. & Keller, J. B. 1970 Uniform asymptotic solutions of second-order linear ordinary differential equations with turning points. *Comm. Pure Appl. Math.* **23**, 379-408.

Manneville, P. 1991 Structures dissipatives, chaos et turbulence. Aléa-Saclay, Gif-sur-Yvette.

McKelvey, R. N. 1955 The solutions of second-order linear ordinary differential equations about turning points of order two. *Trans. Amer. Math. Soc.* **79**, 103-123.

Maslowe, S. A. 1986 Critical layers in shears flows. *Ann. Rev. Fluid Mech.* **18**, 405-432.

Mathis, C., Provansal, M. & Boyer, L. 1984 The Bénard-von Kármán instability : an experimental study near the threshold. *J. Phys. (Paris) Lett.* **45**, 483-491.

Monkewitz, P. A. 1988 The absolute and convective nature of instability in two-dimensional wakes at low Reynolds numbers. *Phys. Fluids* **31**, 999-1006.

Monkewitz, P. A. 1990 The role of absolute and convective instability in predicting the behavior of fluid systems. *Eur. J. Mech.* B/Fluids **9**, 395-413.

Monkewitz, P. A., Bechert, D. W., Lehmann, B. & Barsikow, B. 1990 Self-excited oscillations and mixing in heated round jets. *J. Fluid Mech.* **213**, 611-639.

Monkewitz, P. A., Huerre, P. & Chomaz, J. M. 1993 Global linear stability analysis of weakly non parallel shear flows, *J. Fluid Mech.*, **251**, 1-20.

Monkewitz, P. A. & Sohn, K. D. 1988 Absolute instability in hot jets. *AIAA J.* **26**, 911-916.

Nayfeh, A. H. 1973 Perturbation methods. New-York : Wiley.

Papageorgiou, O. 1987 Stability of the unsteady viscous flow in a curved pipe. *J. Fluid Mech.* **182**, 209-233. Pierrehumbert, R. T. 1984 Local and global baroclinic instability of zonally varying flow. *J. Atmos. Sci.* **41**, 2141-2162.

Pesenson, M. Z. & Monkewitz, P. A. 1993 Frequency Selection and Global Instabilities in Three-Dimensional Weakly Nonparallel Flows. *Phys. Rev. Lett.* **70**, 2722-5.

Pokrovskii, V. L. & Khalatnikov, I. M. 1961 On the problem of above-barrier reflection of high-energy particles. *Sov. Phys. JETP* **13**, 1207-1210.

Reid, W. H. 1972 Composite Approximations of the Solutions of the Orr-Sommerfeld Equation. *Stud. Appl. Math.* **51**, 341-368.

Schär, C. & Smith, R. B. 1993 Shallow-Water Flow past Isolated Topography. Part II : Transition to Vortex Shedding. *J. Atmos. Sci.* **50**, 1401-1428.

Sibuya, Y. 1975 Global theory of a second order linear ordinary differential equation with a polynomial coefficient. *Mathematics Studies*, vol. 18, Amsterdam : North-Holland.

Soward, A. M. & Jones, C. A. 1983 The linear stability of the flow within narrow gap between two concentric rotating spheres. *Quart. J. Mech. Appl. Math.* **36**, 19-42.

Soward, A. M. 1992 Thin disc kinematic $\alpha\omega$-dynamo models II. Short length scale modes. *Geophys. Astrophys. Fluid Dyn.* **64**, 201-225.

Sreenivasan, K. R., Raghu, S. & Kyle, D. 1989 Absolute instability in variable density round jets. *Exp. Fluids* **7**, 309-317.

Strykowski, P. J. & Sreenivasan, K. R. 1990 On the formation and suppression of vortex "shedding" at low Reynolds numbers. *J. Fluid Mech.* **218**, 71-107.

Strykowski, P. J. & Niccum, D. L. 1991 The stability of countercurrent mixing layers in circular jets. *J. Fluid Mech.* **227**, 309-343.

Stuart, J. T. 1960 On the nonlinear mechanics of wave disturbances in stable and unstable parallel flows. Part 1. The basic behavior in plane Poiseuille flow. *J. Fluid Mech.* **9**, 353-70.

Tatsumi, T. & Gotoh, K. 1971 The Structure of the Damping Disturbances in the Stability of Unbounded Laminar Flows, *Proceedings of the IUTAM Symposium on Instability of Continuous Systems*, Editor H. Leipholz, Springer Verlag, 368-375.

Triantafyllou, G. S., Triantafyllou, M. S. & Chryssostomidis, C. 1986 On the formation of vortex streets behind stationary cylinders. *J. Fluid Mech.* **170**, 461.

Wasow, W. 1948 The complex asymptotic theory of a fourth order differential equation of hydrodynamics. *Ann. Math.* **49**, 852-871.

Wasow, W. 1985 Linear turning point theory. New-York : Springer-Verlag.

Watson, J. 1960 On the nonlinear mechanics of wave disturbances in stable and unstable parallel flows. Part 2. The development of a solution for plane Poiseuille flow and for plane Couette flow. *J. Fluid Mech.* **9**, 371-89.